1-1-2013

Oligospermines For Non-Viral Sirna Delivery

Maha Elsayed
Wayne State University,

Recommended Citation

OLIGOSPERMINES FOR NON-VIRAL SIRNA DELIVERY

by

MAHA ELSAYED

THESIS

Submitted to the Graduate School

of Wayne State University,

Detroit, Michigan

in partial fulfillment of the requirements

for the degree of

MASTER OF SCIENCE

2013

MAJOR: PHARMACEUTICAL SCIENCES

APPROVED BY:

_____

Advisor   Date

DEDICATION

To my beloved family

ACKNOWLEGMENT

Merci Beaucoup! Thank you Dr. Denise Conti for your help with AFM imaging. My helpful labmetes, Yuran Xie and Steven Jones, thanks for all your help.

Thank you Dr. David Oupicky for introducing me to the field, your advice and help. Thank you Dr. Na Hyung Kim and Dr. Venkatareddy Nadithe for all the advice and guidance you gave me. You introduced me to the lab, taught me a great deal in the field and have been always there to answer my questions whenever I needed help. Thanks a lot! Thanks Dr. Back for flowcytometry assisatance and Dr. Mike for TEM imaging. Also I would like to gratefully acknowledge all my professors back home in Egypt, College of Pharmacy, Misr University for Sciences and Technology (MUST) for their help and support.

List of Publications

This thesis is based on the following publications:

1. Inhaled delivery of siRNA, **Maha Elsayed[1]**, Olivia M. Merkel[1, 2]accepted for publication in Future Medicine as eBook chapter

2. The influence of oligospermine architecture on their suitability for siRNA delivery, ***Maha Elsayed[1]**, Vincent Corrand[1,3], Yuran Xie[1], Denise Conti[5], Sandro da Rocha[5], Rohit Kolhatkar[4], Olivia M Merkel[1,2]*, in preparation for submission to Biomacromoles

3. Nanoimprinting of topographical and 3D cell culture scaffolds, **Maha Elsayed[1]**, Olivia M. Merkel[1, 2], accepted for publication in Nanomedicine

[1]Department of Pharmaceutical Sciences, Eugene Applebaum College of Pharmacy and Health Sciences, Wayne State University, 259 Mack Ave, Detroit, MI 48201

[2] Molecular Therapeutics Program, Barbara Ann Karmanos Cancer Institute, Detroit, MI 48201, United States

[3]Ecole Nationale Supérieure de Chimie, Rennes, France

[4]Department of Biopharmaceutical Sciences, College of Pharmacy, University of Illinois, 1601 Parkview Ave, Rockford, IL 61107

[5]Department of Chemical Engineering, College of Engineering, Wayne State University, 5050 Anthony Wayne Drive, Detroit, MI 48201

Table of Contents

List of Tables

List of Figures

Chapter 1. Introduction - Inhaled delivery of siRNA

Maha Elsayed[1], Olivia M. Merkel[1, 2]

[1]Department of Pharmaceutical Sciences, [2]Department of Oncology, Wayne State University, Detroit, MI 48201

1.1.   Abstract

Inhaled delivery of siRNA using non-viral vectors is a promising tool for the treatment of diseases associated with overexpressed genes, however many barriers exist in the lung which need to be overcome. In this chapter, we discuss various types of siRNA carriers and successful delivery systems for pulmonary delivery *in vivo*. A few clinical trials targeting the lung exist at the present time. Therapeutic applications are developing by identifying new target genes in various lung diseases.

1.2.   siRNA delivery

RNA interference (RNAi) is a sequence-specific post-transcriptional gene silencing mechanism that occurs naturally in the cell to disrupt double stranded RNA (dsRNA) and regulate RNA expression. RNAi has been artificially utilized in the past two decades to silence the expression of disease-associated genes and hence has been applied in many versatile areas of research. RNAi holds the most promise for the treatment of diseases that are caused by overproduction of certain genes or expression of mutated genes such as cancer [1]. RNAi was first discovered by Fire and Mello in *C.elegans* worms in 1998 [2] for which the two scientists received the Nobel Prize in Physiology and Medicine in 2006. In 2001, RNAi was shown to

knock down target genes in mammalian cells without triggering immune responses; [3] which was a very favorable outcome. RNAi can be artificially achieved in three ways: (i) Introducing plasmid DNA to the cell that encodes for short hairpin RNA (shRNA) which is cleaved to short (21-26 nucleotides) interfering RNA (siRNA) in the cell by the enzyme complex Dicer which contains endoribonuclease activity. The resulting siRNA will lead to the cleavage and degradation of the target mRNA. (ii) Introducing long double stranded RNA (dsRNA) which is endogenously processed inside the cell by Dicer to siRNA. (iii) Directly introducing synthetic siRNA to achieve mRNA degradation. The latter approach is of great interest and will be further discussed in this chapter. When siRNA is internalized in the cell, the double stranded siRNA binds to the RNA-induced silencing complex (RISC) and is unwound into two single strands; the sense and anti-sense strand. The sense strand is removed and degraded by nucleases. The anti-sense strand directs the RISC to the complementary sequence of the mRNA to induce cleavage by a catalytic component, Argonaute, and to post-transcriptionally silence the gene as shown in

Figure 1.1.

siRNA delivery: Introducing short interfering RNA (siRNA, 21-26 nucleotides) with a specific sequence to the cell in order to induce RNA interferenace (RNAi), and to silence a specific target gene. siRNA delivery is used to silence overexpressed genes in various diseases including lung diseases.

Small interfering RNA
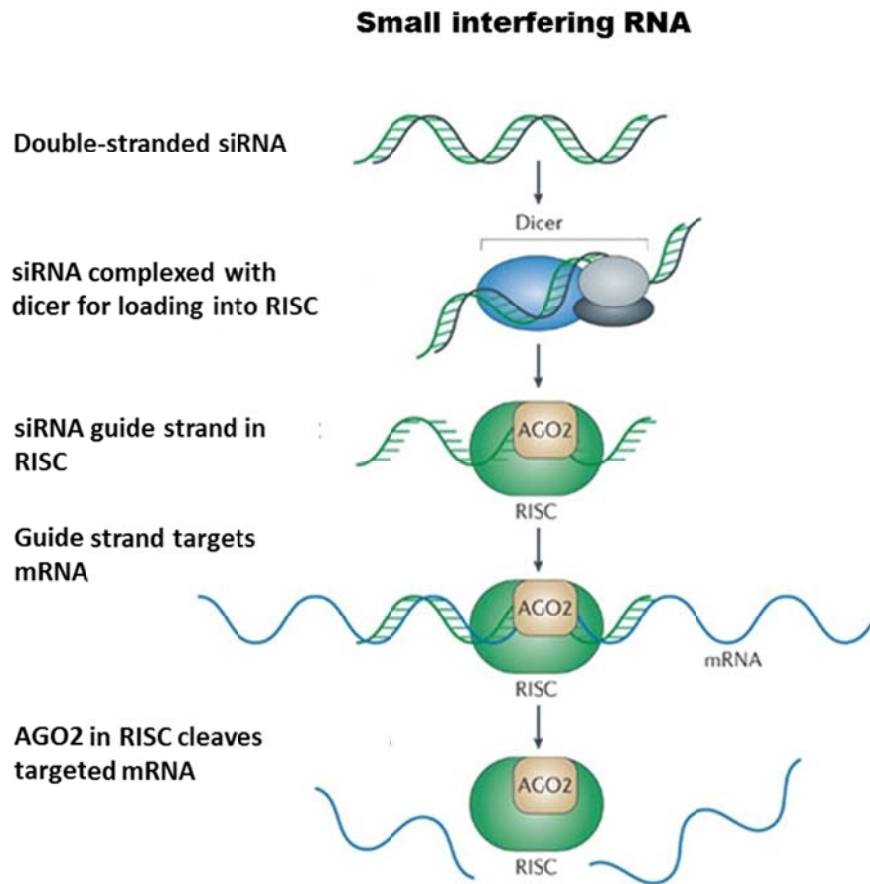
Figure 1.1. Schematic representation of RNA interference (RNAi) mechanism. Adapted from [4] with permission from copyright holder.

1.3. siRNA delivery to the lung

The lung is prone to many diseases because of its physiological function, location and exposure to various pollutants which may cause diseases such as influenza, asthma or fatal diseases such as tuberculosis that are transmitted by airborne pathogens [5, 6]. As a result, the lung has received special attention as a target for siRNA-based therapy. The anatomy of the lung is divided into two different zones; first, the conducting zone i.e. mouth, nasal cavity, pharynx, larynx, trachea, bronchi, and bronchioles which are responsible for air conduction and transport.

The second zone is the respiratory zone where the gas exchange occurs. It consists of the respiratory bronchioles and alveoli [7]. Pulmonary delivery of siRNA presents many advantages compared to the systemic route such as the localized effect on lung epithelial cells with lower administered doses of siRNA, reduced undesired systemic effects, and higher stability due to negligible nuclease activity in the lung compared to the blood stream. In addition, the lungs can function as a remarkable site of absorption for systemic effects with a rapid and effective delivery due to the large alveolar surface area with high vascularization and thin air-blood-barrier. Such advantages have promoted pulmonary delivery to be an attractive route of administration. However, pulmonary delivery also needs to overcome the barriers associated with many parts of the respiratory airways. Coughing and dissolution are important parts of the lung's defense against inhaled particles but can prove to be difficult barriers to overcome. The ciliated epithelial cells in the lung perform a rapid mucociliary clearance action to remove any deposited particles which are eventually swallowed or coughed out. The presence of the mucus layer and surfactant proteins is another barrier for uptake. In addition, macrophages present in the respiratory airways tend to phagocytose particles between 1 and 3 μm in size and to degrade them. Therefore, the lung possesses several anatomical, physiological, and physiochemical barriers that can be impaired or more prominent in a disease state and alter the efficiency of the delivered agent to the lung [8, 9].

> Mucociliary clearance: a host defense clearing mechanism of the airways which is performed by coordinated cilia movement to clear particles deposited in mucus covering the respiratory epithelium.

For efficient siRNA delivery, a therapeutic agent is required to overcome those barriers and successfully reach the lower respiratory tract where the cell layer and the mucus layer are significantly thinner than in the upper airways. The site of the particle deposition in the lung depends on the size, expressed as aerodynamic diameter, of the administered particle as well as the patient's pulmonary function [10-12]. Large particles with aerodynamic diameters larger than 6 μm are usually deposited at the back of the pharynx or throat due to their high momentum. Thus, they are not suitable for the delivery to lower respiratory sites. Therefore, smaller droplet or particle sizes are required to maximize the siRNA deposition in the lung. However, particles smaller than 1 μm in aerodynamic diameter were believed to be exhaled during normal breathing as their movement is controlled by Brownian motion [10-12]. For efficient deposition in the lung, the optimal hydrodynamic diameter has been reported to range between 1 and 5 μm. Newer studies show that as the size of the particles decreases below 100nm, the diffusional mobility of the particles increases and hence their deposition in the lung increases. Nanoparticles (<100nm) can successfully reach and settle in the alveolar site with 55 % and higher fractional deposition depending on the particle diameter [13] and pulmonary function in healthy and asthmatic subjects [14, 15].

1.4. Routes of administration for pulmonary siRNA delivery

Several ways are used to administer siRNA to lung. Inhalation is the easiest and most common method used; where siRNA can be formulated in a liquid formulation (aerosol) or a dry powder aerosol. Currently available inhalation devices which can be used for inhaled siRNA delivery with some adjustment and optimization include nebulizers, metered dose inhalers (MDI) and dry powder inhalers (DPIs) [16, 17]. Although inhaled administration is clinically the most common method used, very limited studies chose the route of inhalation for siRNA delivery in animal models. This disparity may be due to the difficulty of preserving the biological and physicochemical stability of siRNA in inhalers. In order to preserve the properties of siRNA during the inhalation process, particles can be spray-dried and inhaled in a dry-powder aerosol. Excellair^{TM} (ZaBeCor, Bala Cynwyd, PA, USA), is an inhaled siRNA-based treatment that has entered phase II of clinical trials for treatment of asthma. The intranasal route is another non-invasive and easily accessible route of administration in which siRNA is administered to the airways as a nasal suspension in the nasal cavity. It is simple and adaptable; however, some amount of the administered siRNA can be wasted in the nasal cavity or swallowed [18, 19]. siRNA-based clinical trials include the successful study of ALN-RSV01 for respiratory syncytial virus (RSV) treatment which is currently in Phase IIb. The third administration route is the intra-tracheal one, which is more invasive than the others. Thus, it is only employed in animal studies and has not been utilized in clinical trials. By far, most animal *in vivo* studies use either intra-tracheal or intra-nasal administration. The advantage of the intratracheal route, however, can ensure more quantitative delivery of siRNA to the lung at reduced risk of swallowing the dose.

1.5. Intracellular barriers to pulmonary siRNA delivery

Double strands of siRNA are hydrophilic, negatively charged macromolecules. The cell membrane on the other hand is hydrophobic and negatively charged which causes electrostatic repulsion of siRNA molecules. Due to this electrostatic repulsion, siRNA is incapable of crossing the cell membrane on its own in order to reach its target site [20]. Therefore, siRNA carriers are used to facilitate cell uptake [20, 21]. Internalization of siRNA delivery systems is mainly mediated via endocytosis [22]. Particles intended for delivery should be smaller than 150 nm in size in order to be endocytosed and to avoid macrophage phagocytosis [23]. Among the many endocytotic pathways, clathrin-mediated endocytosis is the best characterized pathway in mammalian cells. Particles are bounded in clathrin-coated vesicles and transported to early endosomes which fuse with late endosomes and finally into lysosomes where the pH gradually drops to 5. At this low pH, nuclease enzymes are present which rapidly degrade siRNA molecules. From a designing perspective, it is desired that the nanocarrier escapes the endosomal trafficking to lysosomes and is released from the endosomes to the cytosol to protect the siRNA from enzymatic degradation. One strategy to escape endosomal degradation is to exploit the "proton sponge effect" that employs a polymer with high buffering capacity. During ripening of an endosome to a lysosome, the polymer can thus buffer the pH by being protonated. The buffering of the pH leads to an increased influx of protons and chloride counter ions. This also provides an osmotic influx of water into the endosomes and subsequently leads to endosomal rupture and release of siRNA into the cytosol [24]. Another strategy is to use fusogenic peptides such as INF7 [25], GALA [26], and KALA [27, 28] with pH-dependant structures . At low pH,

such peptides experience a structural conformational change that disrupts the endosomal membrane and enables the release of the siRNA [29, 30].

1.6.   siRNA carriers for pulmonary delivery

Over the last years, researchers developed many successful formulations of siRNA delivery that aim to overcome the delivery challenges described above. An ideal siRNA formulation is desired to be biocompatible, biodegradable, efficient at condensing siRNA and able to avoid clearance by macrophages [31]. Once delivered to the cell surface, the siRNA carrier should facilitate the internalization and cellular uptake into the cell. Afterwards, the carrier should escape the endosome and release the siRNA to the cytoplasm, where the mRNA is cleaved after binding to the antisense strand in the activated RISC [32, 33]. Carriers are also desired to have minimal toxicity and off-target effects. In order to achieve all these parameters, researchers optimize siRNA carriers in terms of the size, chemistry, surface charge, shape, and biocompatibility. In addition, it is necessary that the siRNA carrier would be well-incorporated and compatible with the excipients of an aerosol formulation, i.e. propellants or lyoprotectants [34, 35]. During further formulation, the siRNA integrity and stability needs to be maintained so that it may be protected from degradation and the forces generated by aerosolization.

> Off-target effects are non-specific responses which arise when siRNA interacts with RISC and silence un-intended target genes resulting in measurable phenotypes and unwanted toxicities. It is essential to understand the mechanism behind the off-target effect to minimalize it.

Two main approaches have been developed for delivery of siRNA. The first approach is the chemical modification of naked siRNA at the sugar, at the ribose backbone or at the base of

the oligoribonucleotides which is pursued mainly to increase the nuclease resistance. In addition, chemical modification of siRNA is aimed to increase siRNA specificity and potency as well as to reduce the off-targeting and immune response without impairing the ability of siRNA to knock down the target gene [36, 37]. Chemically modified siRNA therapeutics succeeded in clinical trials. One example is Alynam's ALN-RSV-01 siRNA which is modified by cholesterol attachment to the sense strand. The second approach may also employ modified siRNA but additionally enhances the siRNA protection by using carrier systems which are divided into viral vectors and non-viral vectors. Viral vectors take advantage of the penetration ability of viruses through cellular membranes. Examples for viral vectors are retroviruses, adenoviruses, and lentiviruses which can transfect cells very effectively. However, they present some safety concerns such as toxicity, immunogenicity, tumorigenicity as well as uncontrolled virus replication [38]. Despite their toxicity, viral vectors are still considered in clinical trials due to their high transfection efficacy. In order to overcome these side effects, however, non-viral vectors have gained great interest. They are subdivided into:

> Non-viral vectors possess low host immunogenicity, however lower transfection efficiency compared to viruses. Various strategies are followed to design and develop non-viral vectors with enhanced transfection efficiency.

i. Lipid-based delivery vectors, such as liposomes and lipid particles. Positively-charged lipids, for example, can interact with negatively charged siRNA oligonucleotides by spontaneous electrostatic interaction to form lipoplexes. When aerosolized, lipoplexes may underdo structural changes that may lead to premature release of siRNA from the lipoplexes

[20, 39]. The drawbacks of these vectors are their toxicity and non-selective activation of immune response [40, 41]. Many of the commercially available siRNA transfection agents that are engaged in pulmonary delivery are lipid-based, such as lipofectamine® and oligofectamine[TM].

ii. Polymer-based delivery vectors, such as synthetic poly (lactic-co-glycolic acid) (PLGA), polyethylenimine (PEI), and natural chitosan. This class of vectors can easily be chemically modified to avoid the induction of immune responses. In addition polymer-based vectors are generally cheap, versatile and easy to modify to gain desirable characteristics such as biodegradability and cell- specific targeting effect [42-44]. Polymeric vectors can be further subdivided into polycations for electrostatic self-assembly and polymeric solid nanoparticles which encapsulate their load. Polycations react with negatively charged siRNA to form polyelectrolyte complexes, so called polyplexes. The main concern with polycations is their toxicity generated from their charge. Examples for polycations widely used for siRNA delivery are polyamide amine (PAMAM) dendrimers [45], PEI [24], and chitosan [46]. The characteristics of the delivery system depend on the charge ratio, molecular weight of the polymer and method of preparation [47]. Solid polymeric nanoparticles such as PLGA nanoparticles encapsulate siRNA. The siRNA can be encapsulated and dispersed completely in the nanoparticle core or surrounded by a polymeric shell.

iii. Peptide transduction domains (PTDs) or cell-penetrating peptides are small positively charged molecules (10-30 amino acids). They usually contain arginine and lysine to provide positive charges which electrostatically interact with siRNA and enhance the permeability of the vector across the cell membrane.

A summary of non-viral vectors used in pulmonary siRNA delivery *in vivo* is presented in **Table 1.1**.

Table 1.1: Examples of in vivo studies of siRNA delivery systems in the lung grouped according to the type of delivery system

Type of siRNA delivery	SiRNA/ Targeted gene	Route of administration	Animal model	Delivery system/ Polymer used	Outcome	Re|22 22222 22222 22222 22222 22222
Naked siRNA	HO-1	Intra-nasal	C57BL/6 mice	Unmodified siRNA	Knock down of endogenous gene expression	[48]
	RSV-P	Intra-nasal	BALB/c mice	Unmodified siRNA	Inhibition of RSV infection	[49]
	SiRNA-cy3	Intra-nasal	C57BL/6 mice	Unmodified siRNA	Low distribution of siRNA in lung	[50]
	PAI-1	Intra-nasal	C57BL/6 mice	Unmodified siRNA	Inhibition of PAI-1 level in broncho-alveolar fluid	[51]
	PAI-1	Intra-tracheal	Bleomycin-treated Male	Naked siRNA	Inhibition of alveolitis and pulmonary fibrosis	[52]

			Wistar rats			
	Fas Caspase 8	Intra-tracheal	C57BL/6 mice	Unmodified siRNA	Significant reduction in expression of Fas and caspase 8 in lung	[53]
	XCL1	Intra-tracheal	C57BL/6 mice	Unmodified siRNA	Suppression of XCL1 mRNA and protein expression by 40-50%	[54]
	KC-MIP-2	Intra-tracheal	C57BL/6 mice	Unmodified siRNA	Suppression of mRNA expression of KC and MIP-2 in lung by ~40% Reduction of IL-6 and MPO activity	[55]
	siSC2-5	Intra-nasal	Rhesus macaque	Unmodified siRNA	Diminished SARS coronavirus (SCV) levels in monkey respiratory tract Decreased acute diffuse alveoli damage	[56]
	EHV-1	Intra-nasal	BALB/c mice	Unmodified siRNA	significantly reduced viral replication and clinical signs	[57]

	Ang2	Intra-nasal	C57BL/6 mice	Naked siRNA	Ang2 increases inflammation and cell death during hyperoxia	[58]
	SiRNA-cy3 (2′O-methyl modification)	Intra-tracheal	C57BL/6 mice	Modified siRNA	High distribution of siRNA- cy3 in lung ~21% knock down of E-cadherin but no significant reduction of endothelial VE-cadherin	[50]
Lipid	RSV-P	Intra-nasal	BALB/c mice	Lipid (TransIT-TKO)	Inhibition of RSV infection	[49]
	E-cadherin VE-cadherin	Intra-tracheal	C57BL/6 mice	Liposomes (AtuFECT01/DPhyPE/DSPE-PEG)	Enhanced transfection efficiency of lipoplex-siRNA compared to naked siRNA Lipoplex caused cellular inflammation in lung	[50]
	P38 MAP kinase	Intra-tracheal	BALB/c mice	Lipid (cholesterol)	Knock down effect not enhanced Extended duration of knock down compared to	[59]

					naked siRNA	
	SiGLO red	Intra-tracheal	nude mice with orthotopic model of human lung cancer	Liposomes (DOTAP)	Higher peak concentrations Abundant longer retention of liposomes in the lungs compared with systemic administration	[60]
	SiGLO Green/SPARC	Intra-tracheal	C57BL/6 mice	Lipid (DharmaFECT)	SPARC siRNA significantly reduced gene and protein expression	[61]
Polymer	WT1	Intra-nasal	Mice with B16F10 lung metastasis	PEI-WT1 complexes	Significant reduction in tumor foci Reduction in size and number of tumor blood vessels	[62]
	EGFP	Intra-nasal	C57BL/6 mice	Chitosan	Effective (~37%) EGFP knock down in bronchiole epithelial cells of mice	[63]
	GAPDH	Intra-nasal	BALB/c mice C57BL/6 mice	Imidazole-modified chit-osan	Significant (~45) knockdown of GAPDH enzyme in lung	[64]

	Akt1	Inhalation-aerosol	K-rasLA1 mice	Poly(ester amine)	Inhibition of Akt-related signals and cell cycle Significant suppression of lung tumor progression	[65]
	NS1	Intra-nasal	BALB/c mice	Naonogene NG042 (chitosan)	Enhanced transfection efficiency compared to high MW chitosan Attenuate RSV infection	[66]
	EGFP	Intra-tracheal	C57BL/6 mice	PEI and PEI-PEG	PEI-PEG formulations caused ~42 knock down efficiency	[67]
	Luc	Dry powder Inhalation	mouse lung met astasis model	Chitosan	Specific gene silencing effect against tumor cells	[68]
Peptide	P38 MAP kinase	Intra-tracheal	BALB/c mice	*CPP (TAT and penetratin)	No increase in gene knock down effect compared to naked siRNA and provoked inflammatory reaction	[59]2

2

*2CPP: Cell Penetrating Peptide and MW: Molecular weight

Schematic illustrations of non-viral siRNA carriers are illustrated in **Figure 1.2**. As discussed later, nanocarriers can be chemically modified in a modular fashion to design multi-functional particles which unite therapeutic and diagnostic properties that are target specific.
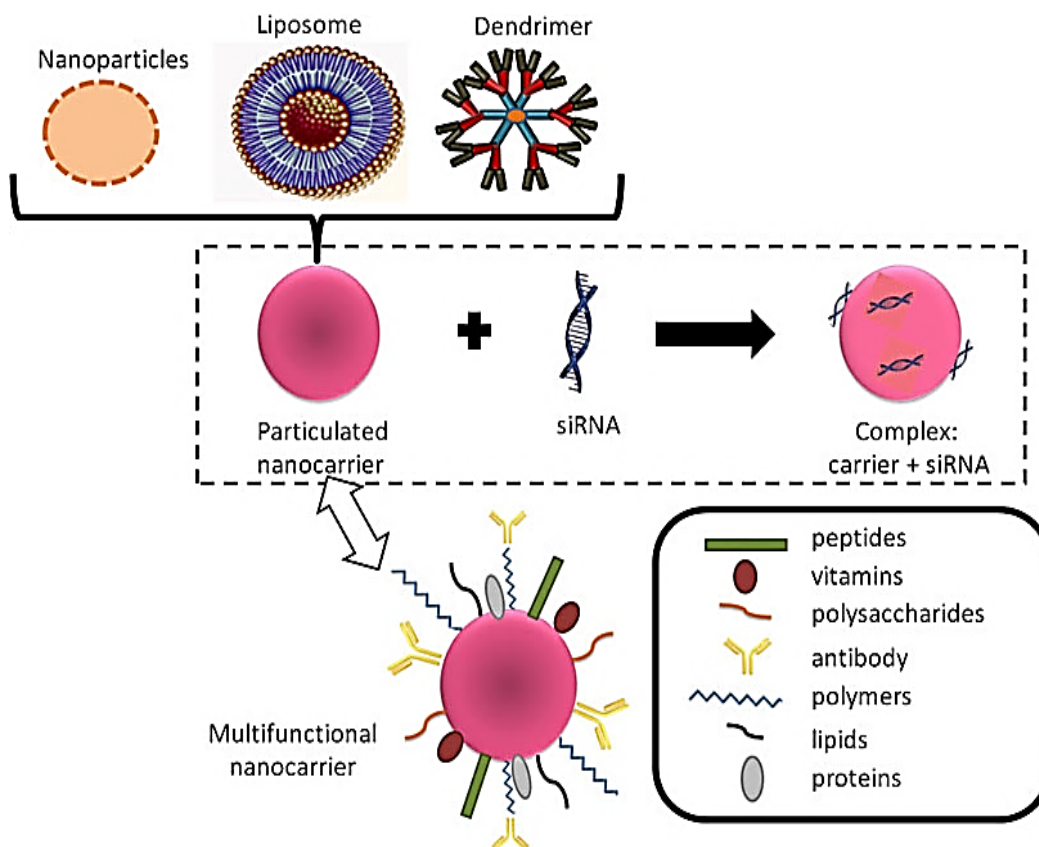
Figure 1.2: Schematic illustration of three classes of siRNA delivery systems; Polymer-, lipid-, or dendrimer-based vectors form complexes with negatively charged siRNA via electrostatic interaction. siRNA can be encapsulated in the core of the particle or attached to the particle surface. Multi-functional nanocarriers can be engineered with multiple components to unite multiple functions and to optimize siRNA delivery. Reproduced from [69] with permission from copyright holder.

1.7. Targeted pulmonary siRNA delivery

2Targeted siRNA delivery aims to reach the target cell types while minimizing the potential side effects on non-targeted cell populations. Targeted siRNA delivery via cell surface receptors is achieved by receptor-mediated endocytosis [70]. For example, the overexpression of transferrin receptors on a majority of cancer cells renders the receptor a good target for siRNA delivery [71]. In the lung, active targeted delivery can improve the distribution and pharmcokinetics of siRNA by engineering the surface of the nanocarrier with targeting moieties that have high affinity to their identified receptors and consequently enhance the uptake of the targeted delivery systems [72]. Furthermore, targeted nanocarriers can be complemented with imaging probes which can be used for detection of the targeted tissue concurrently, termed "theragnostics" [69]. By combining multiple functions in one carrier, so-called multi-functional nanocarriers can be obtained, as shown in Figure 2.

1.8. Therapeutic applications

The major advances in the pulmonary delivery of siRNA leading towards clinical research hold a great potential for treating many lung diseases. siRNA delivery to the lung started in the early 2000s addressing three lung diseases: severe acute respiratory syndrome (SARS) [73], respiratory syncytial virus (RSV) [66, 74], and influenza [75]. Subsequently, this work expanded, and additional endogenous target genes in pulmonary fibrosis [51], lung cancer [76-79], asthma [80-82], tuberculosis [6, 54], and acute lung injury (ALI) [53, 83] were identified. Given the growing number of studies proposing siRNA delivery systems, identifying new target genes besides the already known targets will prove to be invaluable in disease treatment and

prevention. Discovering these new target genes will eventually open new opportunities for therapeutic siRNA delivery strategies. Pulmonary siRNA-based therapeutics are heading towards fulfilling therapeutic effects in the lung by exploiting smart delivery systems. The development of these systems requires a critical understanding of the numerous pulmonary barriers and stringent optimization of the carriers in order to achieve maximum results.

Despite being a new field, reports on siRNA delivery in the literature increase steadily. Therapeutics based on siRNA technology have entered clinical trials. Their success in terms of safety and efficacy is currently being investigated at different stages. Many trials exploit local delivery, including inhaled or intranasally delivered siRNA (**Table 1.2**).

Table 1.2: Examples of current siRNA-based clinical trials [84]

SiRNA Delivery agent	Delivery agent	Route of administration	Sponsor	Disease	Status
ALN-RSV01	Naked siRNA	Intranasal spray	Alnylam Pharmaceuticals	*RSV infection	Phase II
Excellair^{TM}	unknown	Inhalation	ZaBeCor Pharmaceuticals	Asthma	Phase II
TKM-ApoB	Lipid nanoparticles	IV	Tekmira Pharmaceuticals	Hypercholesterolmia	Phase I
CALAA-01	Cyclodextrin	IV	Calando	Solid tumors	Phase I

	nanoparticles		Pharmaceuticals		
TD101	Naked siRNA	Intradermal Injection	Pachyonychia Congenita Project	Pachyonychia congenita	Phase Ib
QPI-1007	Naked siRNA	IVT	Quark Pharmaceuticals	Chronic optic nerve atrophy	Phase I
PF-655	Naked siRNA	IVT	Quark Pharmaceuticals	AMD and diabetic macular edema	Phase II
AGN-745	Naked siRNA	IVT	Allergan	AMD	Phase II
QPI-1002	Naked siRNA	IV	Quark Pharmaceuticals	Acute Kidney injury	Phase II
Bevasiranib	Naked siRNA	IVT	Opko Health	AMD	Phase III

*RSV: Respiratory syncytial virus; IV: Intravenous injection; IVT: Intravitreal injection; AMD:

Age-related degeneration.

1.9.   Summary

- Pulmonary siRNA delivery is a powerful tool to silence any target gene, thus, it can be used for treatment of diseases associated with over expression of genes.

- Pulmonary delivery is associated with many advantages, yet there are many barriers that challenge successful delivery to the lung.

- siRNA is delivered to the lung by either inhaled, intra-nasal or intra-tracheal administration.

- siRNA faces several intracellular barriers in order to reach the target site of action.

- Non-viral delivery of siRNA provides a wide variety of options and opportunities.

- Identifying new target genes, especially in cancer, will open new potentials for siRNA treatments.

1.10.   Acknowledgments

1.11.   References

1.   Wu W, Sun M, Zou Gm, Chen J: MicroRNA and cancer: Current status and prospective. *Int J Cancer* 120(5), 953-960 (2007).

2.   Fire A, Xu S, Montgomery Mk, Kostas Sa, Driver Se, Mello Cc: Potent and specific genetic interference by double-stranded RNA in Caenorhabditis elegans. *Nature* 391(6669), 806-811 (1998).

3.   Elbashir S, M. , Harborth J, Lendeckel W, Yalcin A, Weber K, Tuschl T: Duplexes of 21-nucleotide RNAs mediate RNA interference in cultured mammalian cells. *Nature* 411(6836), 494-498 (2001).

4.   Ryszard K, Adrian Rk, Sidney A: RNA therapeutics: beyond RNA interference and antisense oligonucleotides. *Nature Reviews Drug Discovery* 11(2), 125-140 (2012).

5.   Thomas M, Lu Jj, Chen J, Klibanov Am: Non-viral siRNA delivery to the lung. *Advanced Drug Delivery Reviews* 59(2–3), 124-133 (2007).

6.   Misra A, Hickey Aj, Rossi C *et al.*: Inhaled drug therapy for treatment of tuberculosis. *Tuberculosis (Edinb)* 91(1), 71-81 (2011).

7.   Patton Js, Byron Pr: Inhaling medicines: delivering drugs to the body through the lungs. *Nat Rev Drug Discov* 6(1), 67-74 (2007).

8.   Van Der Schans Cp: Bronchial mucus transport. *Respir Care* 52(9), 1150-1156; discussion 1156-1158 (2007).

9.   Groneberg Da, Eynott Pr, Lim S *et al.*: Expression of respiratory mucins in fatal status asthmaticus and mild asthma. *Histopathology* 40(4), 367-373 (2002).

10.   Heyder J: Deposition of inhaled particles in the human respiratory tract and consequences for regional targeting in respiratory drug delivery. *Proc Am Thorac Soc* 1(4), 315-320 (2004).

11.   Carvalho Tc, Peters Ji, Williams Ro, 3rd: Influence of particle size on regional lung deposition--what evidence is there? *Int J Pharm* 406(1-2), 1-10 (2011).

12.   Hussain M Mp, Khan A: Lung deposition predicoins of airborne particles and the emergence of contemporary diseases Part-I. . *theHealth* 2(2), 51-59 (2011).

13.   Daigle Cc, Chalupa Dc, Gibb Fr *et al.*: Ultrafine particle deposition in humans during rest and exercise. *Inhal Toxicol* 15(6), 539-552 (2003).

14. Pietropaoli Ap, Frampton Mw, Hyde Rw *et al.*: Pulmonary function, diffusing capacity, and inflammation in healthy and asthmatic subjects exposed to ultrafine particles. *Inhal Toxicol* 16 Suppl 1, 59-72 (2004).

15. Frampton Mw, Utell Mj, Zareba W *et al.*: Effects of exposure to ultrafine carbon particles in healthy subjects and subjects with asthma. *Res Rep Health Eff Inst* (126), 1-47; discussion 49-63 (2004).

16. Chow Al, Tong Hy, Chattopadhyay P, Shekunov B: Particle Engineering for Pulmonary Drug Delivery. *Pharm Res* 24(3), 411-437 (2007).

17. Al-Hallak Mh, Sarfraz Mk, Azarmi S, Roa Wh, Finlay Wh, Lobenberg R: Pulmonary delivery of inhalable nanoparticles: dry powder inhalers. *Ther Deliv* 2(10), 1313-1324 (2011).

18. Kublik H, Vidgren Mt: Nasal delivery systems and their effect on deposition and absorption. *Advanced Drug Delivery Reviews* 29(1–2), 157-177 (1998).

19. Mclean Ja, Bacon Jr, Mathews Kp *et al.*: Distribution and clearance of radioactive aerosol on the nasal mucosa. *Rhinology* 22(1), 65-75 (1984).

20. Lam Jk-W, Liang W, Chan H-K: Pulmonary delivery of therapeutic siRNA. *Advanced Drug Delivery Reviews* 64(1), 1-15 (2012).

21. Wolff Ja, Rozema Db: Breaking the bonds: Non-viral vectors become chemically dynamic. *Molecular Therapy* 16(1), 8-15 (2008).

22. Khalil Ia, Kogure K, Akita H, Harashima H: Uptake pathways and subsequent intracellular trafficking in nonviral gene delivery. *Pharmacological Reviews* 58(1), 32-45 (2006).

23. Lebhardt T, Roesler S, Beck-Broichsitter M, Kissel T: Polymeric nanocarriers for drug delivery to the lung. *Journal of Drug Delivery Science and Technology* 20(3), 171-180 (2010).

24. Boussif O, Lezoualc'h F, Zanta Ma *et al.*: A versatile vector for gene and oligonucleotide transfer into cells in culture and in vivo: polyethylenimine. *Proc Natl Acad Sci U S A* 92(16), 7297-7301 (1995).

25. Oliveira S, Van Rooy I, Kranenburg O, Storm G, Schiffelers Rm: Fusogenic peptides enhance endosomal escape improving siRNA-induced silencing of oncogenes. *Int J Pharm* 331(2), 211-214 (2007).

26. Hatakeyama H, Ito E, Akita H *et al.*: A pH-sensitive fusogenic peptide facilitates endosomal escape and greatly enhances the gene silencing of siRNA-containing nanoparticles in vitro and in vivo. *J Control Release* 139(2), 127-132 (2009).

27. Lee Sh, Kim Sh, Park Tg: Intracellular siRNA delivery system using polyelectrolyte complex micelles prepared from VEGF siRNA-PEG conjugate and cationic fusogenic peptide. *Biochem Biophys Res Commun* 357(2), 511-516 (2007).

28. Choi Sw, Lee Sh, Mok H, Park Tg: Multifunctional siRNA delivery system: polyelectrolyte complex micelles of six-arm PEG conjugate of siRNA and cell penetrating peptide with crosslinked fusogenic peptide. *Biotechnol Prog* 26(1), 57-63 (2010).

29. Kichler A, Mason Aj, Bechinger B: Cationic amphipathic histidine-rich peptides for gene delivery. *Biochim Biophys Acta* 1758(3), 301-307 (2006).

30. Liang W, Lam Jkw: Endosomal Escape Pathways for Non-Viral Nucleic Acid Delivery Systems. (2012).

31. Nguyen J, Steele Twj, Merkel O, Reul R, Kissel T: Fast degrading polyesters as siRNA nano-carriers for pulmonary gene therapy. *Journal of Controlled Release* 132(3), 243-251 (2008).

32. Dehousse V, Garbacki N, Colige A, Evrard B: Development of pH-responsive nanocarriers using trimethylchitosans and methacrylic acid copolymer for siRNA delivery. *Biomaterials* 31(7), 1839-1849 (2010).

33. Fernandez Ca, Rice Kg: Engineered nanoscaled polyplex gene delivery systems. *Mol Pharm* 6(5), 1277-1289 (2009).

34. Patil Js, Sarasija S: Pulmonary drug delivery strategies: A concise, systematic review. *Lung India* 29(1), 44-49 (2012).

35. Yadava P, Gibbs M, Castro C, Hughes Ja: Effect of lyophilization and freeze-thawing on the stability of siRNA-liposome complexes. *AAPS PharmSciTech* 9(2), 335-341 (2008).

36. Ui-Tei K, Naito Y, Zenno S *et al.*: Functional dissection of siRNA sequence by systematic DNA substitution: modified siRNA with a DNA seed arm is a powerful tool for mammalian gene silencing with significantly reduced off-target effect. *Nucleic Acids Res* 36(7), 2136-2151 (2008).

37. Bramsen Jb, Laursen Mb, Nielsen Af *et al.*: A large-scale chemical modification screen identifies design rules to generate siRNAs with high activity, high stability and low toxicity. *Nucleic Acids Res* 37(9), 2867-2881 (2009).

38. Thomas Ce, Ehrhardt A, Kay Ma: Progress and problems with the use of viral vectors for gene therapy. *Nature Reviews Genetics* 4(5), 346-358 (2003).

39. Gaspar Mm, Bakowsky U, Ehrhardt C: Inhaled liposomes - Current strategies and future challenges. *Journal of Biomedical Nanotechnology* 4(3), 245-257 (2008).

40. Fenske Db, Chonn A, Cullis Pr: Liposomal Nanomedicines: An Emerging Field. *Toxicologic Pathology* 36(1), 21-29 (2008).

41. Wu Sy, Mcmillan Na: Lipidic systems for in vivo siRNA delivery. *AAPS J* 11(4), 639-652 (2009).

42. Merdan T, Kopecek J, Kissel T: Prospects for cationic polymers in gene and oligonucleotide therapy against cancer. *Adv Drug Deliv Rev* 54(5), 715-758 (2002).

43. Han S, Mahato Ri, Sung Yk, Kim Sw: Development of biomaterials for gene therapy. *Mol Ther* 2(4), 302-317 (2000).

44. Pack Dw, Hoffman As, Pun S, Stayton Ps: Design and development of polymers for gene delivery. *Nat Rev Drug Discov* 4(7), 581-593 (2005).

45. Bielinska A, Kukowska-Latallo Jf, Johnson J, Tomalia Da, Baker Jr, Jr.: Regulation of in vitro gene expression using antisense oligonucleotides or antisense expression plasmids transfected using starburst PAMAM dendrimers. *Nucleic Acids Res* 24(11), 2176-2182 (1996).

46.   Lai Wf, Lin Mc: Nucleic acid delivery with chitosan and its derivatives. *J Control Release* 134(3), 158-168 (2009).

47.   Wang J, Lu Z, Wientjes Mg, Au Jl: Delivery of siRNA therapeutics: barriers and carriers. *AAPS J* 12(4), 492-503 (2010).

48.   Zhang X, Shan P, Jiang D *et al.*: Small interfering RNA targeting heme oxygenase-1 enhances ischemia-reperfusion-induced lung apoptosis. *J Biol Chem* 279(11), 10677-10684 (2004).

49.   Bitko V, Musiyenko A, Shulyayeva O, Barik S: Inhibition of respiratory viruses by nasally administered siRNA. *Nature Medicine* 11(1), 50-55 (2005).

50.   Gutbier B, Kube Sm, Reppe K *et al.*: RNAi-mediated suppression of constitutive pulmonary gene expression by small interfering RNA in mice. *Pulmonary Pharmacology & Therapeutics* 23(4), 334-344 (2010).

51.   Senoo T, Hattori N, Tanimoto T *et al.*: Suppression of plasminogen activator inhibitor-1 by RNA interference attenuates pulmonary fibrosis. *Thorax* 65(4), 334-340 (2010).

52.   Zhang Yp, Li Wb, Wang Wl *et al.*: siRNA against plasminogen activator inhibitor-1 ameliorates bleomycin-induced lung fibrosis in rats. *Acta Pharmacol Sin* 33(7), 897-908 (2012).

53.   Perl M, Chung Cs, Lomas-Neira J *et al.*: Silencing of Fas, but not caspase-8, in lung epithelial cells ameliorates pulmonary apoptosis, inflammation, and neutrophil influx after hemorrhagic shock and sepsis. *Am J Pathol* 167(6), 1545-1559 (2005).

54.   Rosas-Taraco Ag, Higgins Dm, Sanchez-Campillo J, Lee Ej, Orme Im, Gonzalez-Juarrero M: Intrapulmonary delivery of XCL1-targeting small interfering RNA in mice chronically infected with Mycobacterium tuberculosis. *Am J Respir Cell Mol Biol* 41(2), 136-145 (2009).

55.   Lomas-Neira Jl, Chung Cs, Wesche De, Perl M, Ayala A: In vivo gene silencing (with siRNA) of pulmonary expression of MIP-2 versus KC results in divergent effects on hemorrhage-induced, neutrophil-mediated septic acute lung injury. *J Leukoc Biol* 77(6), 846-853 (2005).

56. Li Bj, Tang Q, Cheng D *et al.*: Using siRNA in prophylactic and therapeutic regimens against SARS coronavirus in Rhesus macaque. *Nature Medicine* 11(9), 944-951 (2005).

57. Fulton A, Peters St, Perkins Ga *et al.*: Effective treatment of respiratory alphaherpesvirus infection using RNA interference. *PLoS One* 4(1), e4118 (2009).

58. Bhandari V, Choo-Wing R, Lee Cg *et al.*: Hyperoxia causes angiopoietin 2-mediated acute lung injury and necrotic cell death. *Nat Med* 12(11), 1286-1293 (2006).

59. Moschos Sa, Jones Sw, Perry Mm *et al.*: Lung delivery studies using siRNA conjugated to TAT(48-60) and penetratin reveal peptide induced reduction in gene expression and induction of innate immunity. *Bioconjug Chem* 18(5), 1450-1459 (2007).

60. Garbuzenko Ob, Saad M, Betigeri S *et al.*: Intratracheal versus intravenous liposomal delivery of siRNA, antisense oligonucleotides and anticancer drug. *Pharm Res* 26(2), 382-394 (2009).

61. Wang Jc, Lai S, Guo X *et al.*: Attenuation of fibrosis in vitro and in vivo with SPARC siRNA. *Arthritis Res Ther* 12(2), R60 (2010).

62. Zamora-Avila De, Zapata-Benavides P, Franco-Molina Ma *et al.*: WT1 gene silencing by aerosol delivery of PEI-RNAi complexes inhibits B16-F10 lung metastases growth. *Cancer Gene Ther* 16(12), 892-899 (2009).

63. Howard Ka, Rahbek Ul, Liu X *et al.*: RNA interference in vitro and in vivo using a novel chitosan/siRNA nanoparticle system. *Mol Ther* 14(4), 476-484 (2006).

64. Ghosn B, Singh A, Li M *et al.*: Efficient gene silencing in lungs and liver using imidazole-modified chitosan as a nanocarrier for small interfering RNA. *Oligonucleotides* 20(3), 163-172 (2010).

65. Xu Cx, Jere D, Jin H *et al.*: Poly(ester amine)-mediated, aerosol-delivered Akt1 small interfering RNA suppresses lung tumorigenesis. *Am J Respir Crit Care Med* 178(1), 60-73 (2008).

66. Zhang W, Yang H, Kong X *et al.*: Inhibition of respiratory syncytial virus infection with intranasal siRNA nanoparticles targeting the viral NS1 gene. *Nat Med* 11(1), 56-62 (2005).

67. Merkel Om, Beyerle A, Librizzi D *et al.*: Nonviral siRNA delivery to the lung: investigation of PEG-PEI polyplexes and their in vivo performance. *Mol Pharm* 6(4), 1246-1260 (2009).

68. Okuda T, Kito D, Oiwa A, Fukushima M, Hira D, Okamoto H: Gene silencing in a mouse lung metastasis model by an inhalable dry small interfering RNA powder prepared using the supercritical carbon dioxide technique. *Biol Pharm Bull* 36(7), 1183-1191 (2013).

69. Vicentini F, Borgheti-Cardoso L, Depieri L *et al.*: Delivery Systems and Local Administration Routes for Therapeutic siRNA. *Pharm Res* 30(4), 915-931 (2013).

70. Liu Y, Tao J, Li Y *et al.*: Targeting hypoxia-inducible factor-1alpha with Tf-PEI-shRNA complex via transferrin receptor-mediated endocytosis inhibits melanoma growth. *Mol Ther* 17(2), 269-277 (2009).

71. Tros De Ilarduya C, Duzgunes N: Delivery of therapeutic nucleic acids via transferrin and transferrin receptors: lipoplexes and other carriers. *Expert Opin Drug Deliv*, (2013).

72. Zhu Q, Feng C, Liao W, Zhang Y, Tang S: Target delivery of MYCN siRNA by folate-nanoliposomes delivery system in a metastatic neuroblastoma model. *Cancer Cell Int* 13(1), 65 (2013).

73. Li Bj, Tang Q, Cheng D *et al.*: Using siRNA in prophylactic and therapeutic regimens against SARS coronavirus in Rhesus macaque. *Nat Med* 11(9), 944-951 (2005).

74. Devincenzo J, Cehelsky Je, Alvarez R *et al.*: Evaluation of the safety, tolerability and pharmacokinetics of ALN-RSV01, a novel RNAi antiviral therapeutic directed against respiratory syncytial virus (RSV). *Antiviral Res* 77(3), 225-231 (2008).

75. Ge Q, Mcmanus Mt, Nguyen T *et al.*: RNA interference of influenza virus production by directly targeting mRNA for degradation and indirectly inhibiting all viral RNA transcription. *Proc Natl Acad Sci U S A* 100(5), 2718-2723 (2003).

76. Tong Aw: Small RNAs and non-small cell lung cancer. *Current Molecular Medicine* 6(3), 339-349 (2006).

77. Li Sd, Huang L: Targeted delivery of antisense oligodeoxynucleotide and small interference RNA into lung cancer cells. *Molecular Pharmaceutics* 3(5), 579-588 (2006).

78. Jere D, Xu Cx, Arote R, Yun Ch, Cho Mh, Cho Cs: Poly(β-amino ester) as a carrier for si/shRNA delivery in lung cancer cells. *Biomaterials* 29(16), 2535-2547 (2008).

79. Xu Cx, Jere D, Jin H *et al.*: Poly(ester amine)-mediated, aerosol-delivered Akt1 small interfering RNA suppresses lung tumorigenesis. *American Journal of Respiratory and Critical Care Medicine* 178(1), 60-73 (2008).

80. Kim N, Batton D, Thakur A, Lum L, Bassett D, Merkel O: *Targeted siRNA Delivery to Activated T Cells for Anti-Inflammatory Therapy of Asthma*. In: *Journal of Aerosol Medicine and Pulmonary Drug Delivery*. 2013.

81. Huang Hy, Chiang Bl: siRNA as a therapy for asthma. *Curr Opin Mol Ther* 11(6), 652-663 (2009).

82. Popescu Fd: Antisense- and RNA interference-based therapeutic strategies in allergy. *J Cell Mol Med* 9(4), 840-853 (2005).

83. Bardita C, Predescu D, Justice Mj, Petrache I, Predescu S: In vivo knockdown of intersectin-1s alters endothelial cell phenotype and causes microvascular remodeling in the mouse lungs. *Apoptosis* 18(1), 57-76 (2013).

84. Http://Www.Clinicaltrials.Gov/: The US National Institutes of Health. ClinicalTrials.gov.,

Chapter 2. The influence of oligospermine architecture on their suitability for siRNA delivery

2.1.   Abstract

Spermines are naturally abundant polyamines which condense and stabilize helical nucleic acids. They can therefore condense DNA or RNA as non-viral vectors for intracellular nucleic acid delivery. In this study, we synthesized bis- and tetraspermines with different molecular architecture to yield linear bisspermine, linear tetraspermine, and dendritic tetraspermine. Self-assembled polyplexes of oligospermines and siRNA were formed. The structure-activity relationship of these carriers was evaluated in terms of their efficiency to deliver siRNA in a non-small cell lung carcinoma cell line (H1299/LUC). Oligospermines displayed minimal cytotoxicity but efficient siRNA condensation capacity with better stability against polyanions than polyethylenimine at neutral and acidic pH. The morphology of the polyplexes was strongly affected by the oligospermine architecture. Linear tetraspermine/siRNA polyplexes showed the best gene silencing efficiency among the oligospermines tested on both the mRNA and protein expression levels. In conclusion, the linear tetraspermine had the most favorable structure and is a promising siRNA delivery vector.

2.2.   Introduction

RNA interference (RNAi) is a post-transcriptional gene silencing mechanism (PTGS) that occurs naturally in the cell in a sequence-specific manner to break down double stranded RNA (dsRNA) and to regulate RNA expression.[1] RNAi-based therapeutics have rapidly progressed

from basic research to clinical trials. In 1998, RNAi was discovered in C. elegans worms by Fire and Mello, for which they received the Nobel Prize in Physiology and Medicine in 2006.[2] Small interfering RNA (siRNA) is an intermediate in the RNAi process and is double stranded RNA with 21-25 nucleotides in length. Synthetic siRNA can be used to achieve RNAi and to down-regulate overexpressed genes.[3] In 2001, siRNA was reported to induce RNAi in mammalian cells.[4] To the present day, only a few human clinical trials for siRNA therapeutics are ongoing. Among which, two therapeutics are targeting the lung, i.e. ALN-RSV01 and ExcellairTM.[5]

The primary challenge of siRNA therapeutics, however, is the hurdle of intracellular delivery. siRNA cannot cross a biological membrane due to being a hydrophilic, negatively charged macromolecule and highly prone to nuclease degradation.[3b] Viral vectors achieve high transduction but are associated with many safety problems at the clinical level such as immune responses and carcinogensis.[6] Therefore, safe and effective non-viral siRNA carriers are required for pulmonary delivery of siRNA.[7]
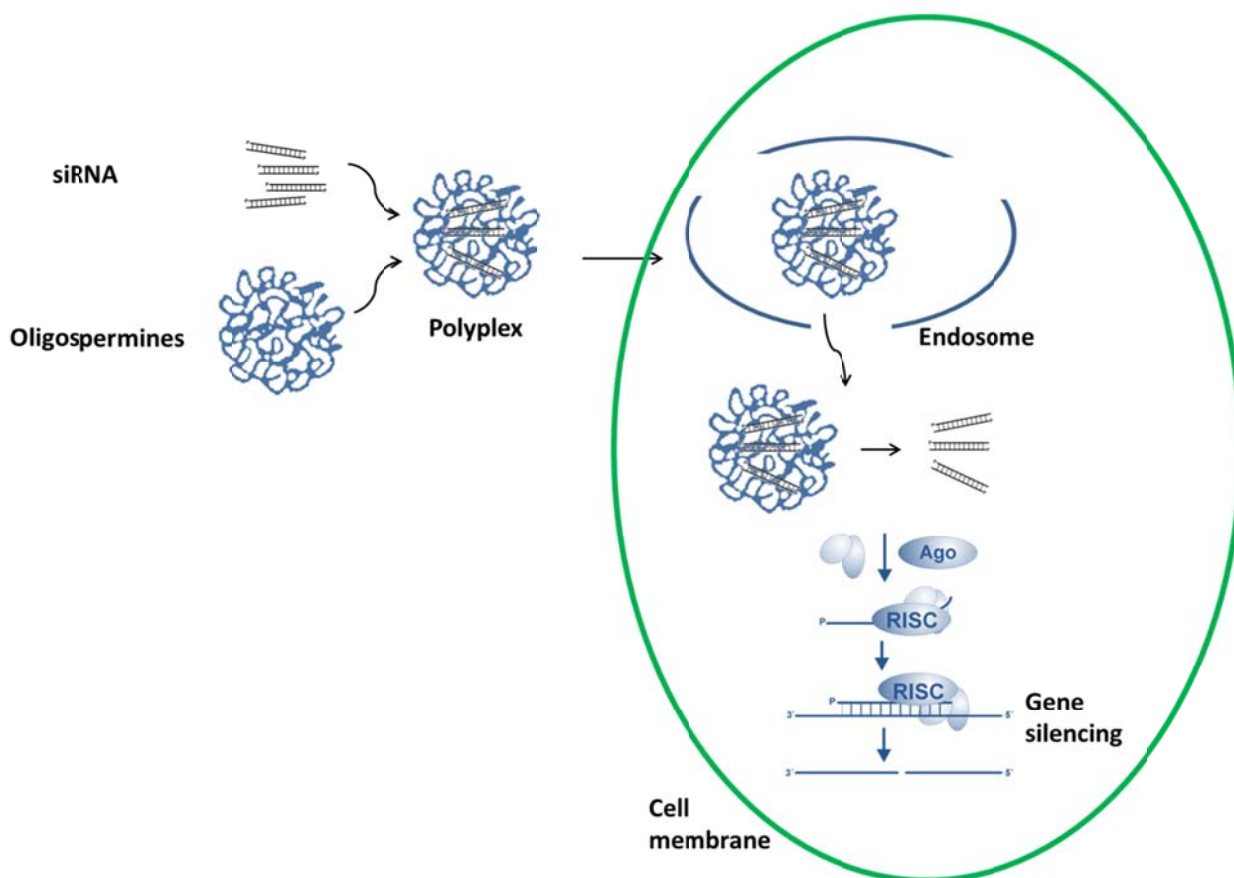
Figure 2.1. Schematic illustration of oligospermine/siRNA polyplex formation, cellular entry, endosomal escape, and gene silencing.

Cationic polymers interact with negatively charged oligonucleoutides via charge complexation to form poly-electrolyte complexes.[8] Spermines (SPE) are safe, naturally-occurring, small linear tetraamines with two primary amines and two secondary amines that aid to package cellular DNA into a compact state.[9]. The polyamine structure is required for stable DNA binding. The interaction between a single cationic amine and anionic phosphate groups of nucleic acids is relatively week and is further weakened by copetition of salt binding in biological conditions.[10] Exogenous spermine poorly condenses and transfects nucleic acids to cells which could be due to its low molecular weight (~200 Da).[11] In addition, spermines yield

limited endosomal escape despite their good proton-buffering capacity.[11b] It is hypothesized that the maximum interaction of siRNA with cations consists of four carbon-bridges. However the low molecular weight of spermine limits its siRNA complexation ability.[12] Therefore, it was necessary that spermine polyamines be modified to increase their molecular weight in order to act as building blocks for nucleic acid delivery systems.[11a, 13] This suggests that polymerized spermines could be capable of condensing siRNA and of disassembling at the target site.[14] Polyspermines showed high buffering capacity.[15] Many studies described the linkage of spermines through their amino groups by different cleavable linkers such as disulfide bonds or esters.[11a, 15-16] When polyspermines are degraded to release spermine monomers, sometimes fragments of the linker are still attached to spermine monomers which affects their transfection properties.[17] Very recently, Du et al. compared three polymerized spermines to show that linkage structures play an important role in the activity of the polyspermine-based nucleic acid carriers.[8b]

Moreover, spermine polymerization allows for multi-step intracellular degradation of a biocompatible polymeric platform.[14]. Several groups have studied spermine-based carriers for DNA,[18] [19] [11a] siRNA,[11a, 20] and short RNA delivery.[21] Gene silencing efficiency was shown specifically via aerosol delivery.[21-22]. Spermines have been incorporated in many delivery systems such as lipoplexes,[20b, 23] conjugates,[20a] and nanoparticles[24] for siRNA delivery to enhance the transfection efficiency. Vijayanathan et al. synthesized a series of spermine homologues with different methylene chain length separating the secondary amino groups of the polyamines. The lower homologues were more efficacious in DNA condensation than the higher analogues. These results showed the importance of the regiochemical distribution of the positive charge in the polyamines presented by the varying distance of the methylene spacing which affected the polyamine ability to provoke structural changes in the DNA and hence strongly

affected the DNA condensation and size of DNA complexes.[25] Different structures of spermine oligopolymers were studied, for example, when spermine was used as surface groups of a dendron structure to target human breast carcinoma cells (MDA-MB-231) and murine myoblast cells (C2C12). Spermine-decorated dendrons were able to transfect DNA to cells only in the presence of chloroquine which enables the endosomol escape. Since blank spermine is completely protonated at physiological pH, it is possible that these dendritic structures have only a limited proton sponge effect. It was concluded that dendritic spermine derivatives act more similarly to polylysine and not like proton sponge polymers, such as PAMAM or PEI.[11b]

In this study, spermine units were polymerized to synthesize different chemical structures of oligospermines described as linear bisspermine, linear tetraspermine and dendritic tetraspermine. These cationic polymers were used to condense siRNA molecules in the form of polyplexes (Figure 1). Oligospermine/siRNA polyplexes were characterized and evaluated as non-viral carriers for condensation, stability, transfection of siRNA and gene knockdown in H1299 human non-small cell lung carcinoma cells. The aim of this study was to identify a suitable oligospermine architecture for siRNA delivery.

2.3. Experimental

2.3.1 Materials

Linear bisspermine (MW 1299.40), linear tetraspermine (MW 2581.82), and dendritic tetratspermine (MW 2625.87) were synthesized as described below. Lipofectamine 2000[TM] (LF), SYBR® Gold dye, and (3-(4,5-dimethylthiazol-2-yl)-2,5-diphenyltetrazolium bromide (MTT) were purchased from Invitrogen (Carlsbad, CA). Polyethylenimine (PEI, MW 5 kDa) was

obtained from BASF (Lupasol®, Cologne, Germany). Dicer substrate double-stranded siRNA (DsiRNA) targeting firefly luciferase gene (FLUC siRNA, 25/27mer), human glyceraldehyde 3-phosphate dehydrogenase (hGAPDH) gene, nonspecific control (siNegCon) DsiRNA as well as Alexa Fluor®-488 labeled siRNA were bought from Integrated DNA Technologies (IDT, Coralville, Iowa). RPMI-1640 medium (1x) with 2.05 mM L-glutamine, HyClone™ trypsin, penicillin/streptomycin, 4-(2(hydroxyethyl)-1-piperazine ethanesulfonic acid (HEPES), and SurePrep™ TrueTotal™ RNA purification kits were purchased from Thermo Fisher Scientific (Waltham, MA). Dulbecco's Phosphate Buffered Saline (PBS), Fetal Bovine Serum (FBS) Heat Inactivated, D-(+)-Glucose, sodium bicarbonate, sodium pyruvate, 2-mercaptoethanol, dimethyl sulfoxide Hybri-Max™ (DMSO, ≥99.7%), ethylenediaminetetraacetic acid (EDTA, 99.4%-100.06%), trypan blue (0.4%, sterile filtered) and luciferin solution were bought from Sigma-Aldrich (St. Louis, MO). Hs_GAPDH_primers and Hs_β-actin-primers were purchased from Qiagen (Valencia, CA). Brilliant III SYBR Green QRT-PCR Master Mix was bought from Agilent (Santa Clara, CA). And DNAse I reaction buffer and DNase/RNase free water were purchased from ZYMO RESEARCH (Irvine, CA).

2.3.2 Synthesis of Oligospermines

Three different polycatonic-based oligospermines namely, linear bisspermines, linear tetraspermines and dendritic tetraspermines were successfully synthesized as described previously.[26] Briefly. the process involved 1) the synthesis of the monomer I MPBBSP (monoprotected bis-boc spermine), 2) the synthesis of the reactive intermediates of 2-arm and 4-arm linker, and 3) the conjugation of monomer I to the linkers to get respective protected oligospermines. Deprotection of boc groups yielded oligospermines as salts of trifluroacetic acid

that were used for biological characterization. All compounds synthesized were characterized using NMR, MS/MALDI and HPLC to confirm the identity and purity. Oligospermines with different structures were screened to evaluate their efficiency as siRNA delivery carriers for the transfection of lung cancer cells.
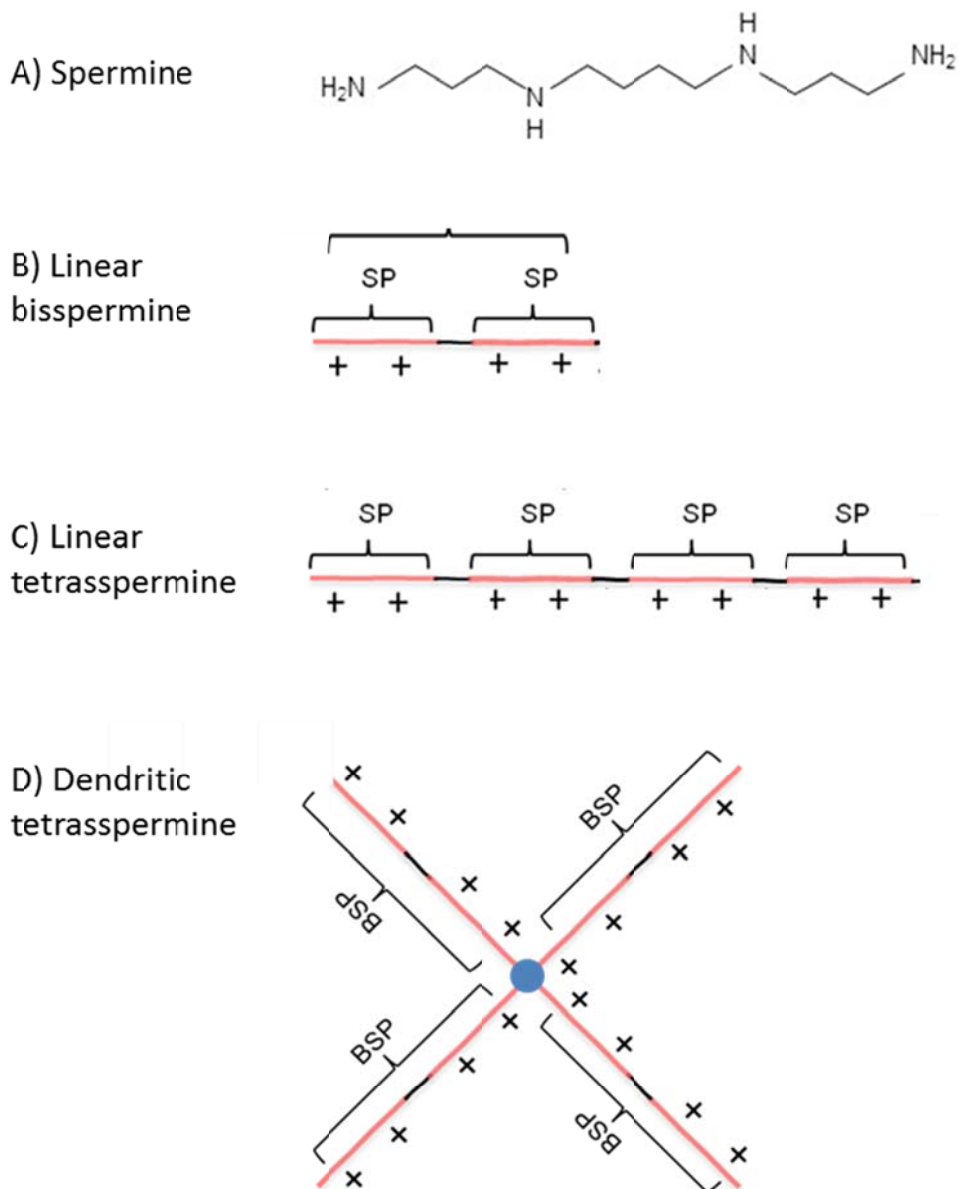
Figure 2.2. Schematic representation of oligospermines polymers with different architectures. A) Spermine B) Linear bisspermines. C) Linear tetraspermines. D) Dendritic tetraspermines.

Spermine is used as the main building block for the three polymers. SP= Spermine, BSP = bisspermine.
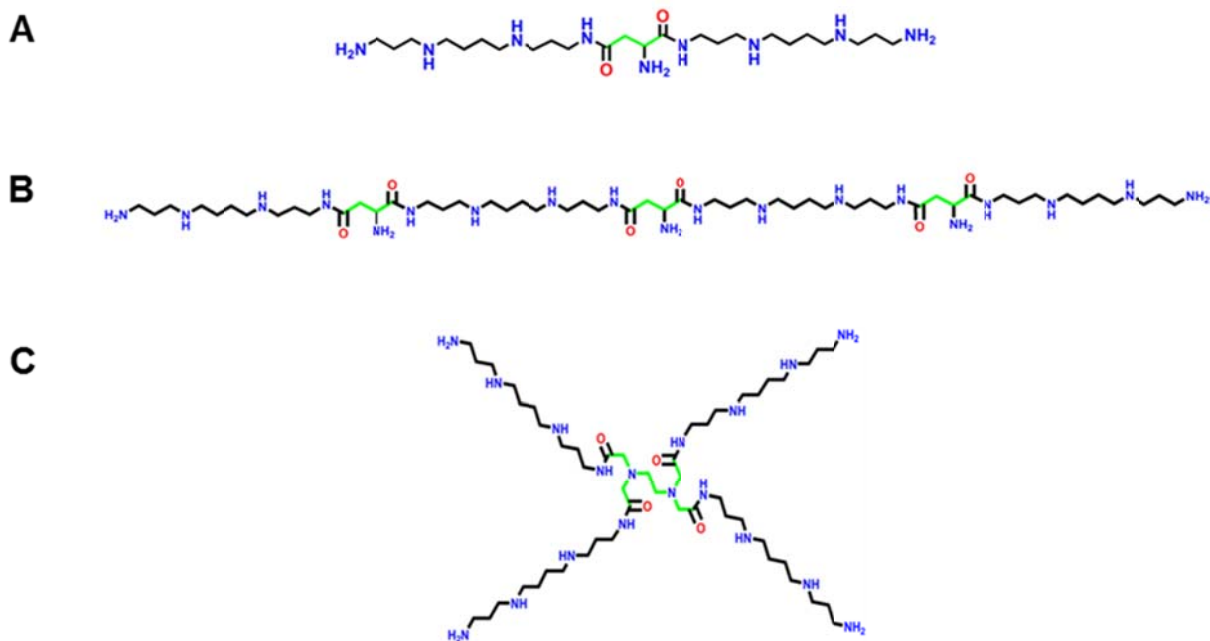
Figure 2.3. Chemical structures of A) Linear bisspermine, B) Linear tetraspermine, and C) Dendritic tetraspermine. **Preparation of oligospermines-siRNA polyplexes**

The ratio between the polymer amine groups (N) and the siRNA phosphate groups (P) in a polyplex is defined as the N/P ratio. The N/P ratio obtained after complexation was calculated based on the molecular weight, number of protonable units of the oligospermines, and number of base pairs in the siRNA duplexes. Polymer stock solutions (1 mg/ml) were diluted with 5% glucose solution and siRNA stock solutions (100 μM) were diluted with RNase free-water. All solutions used were filtered with 0.2 μm pore size syringe filters (Fisher Scientific, Waltham, MA). The amount of oligospermines required to prepare polyplexes with a specific amount of siRNA and at a specific N/P ratio was calculated as following:

m(polymer)= n(siRNA) X 52 X MW(protonable unit) X N/P   (1)

Where m is the mass of the polymer needed, (n) is the amount of siRNA used per well. The total number of nucleotides in DsiRNA is 52. N/P is the ratio between polymer amine groups and siRNA phosphate groups.

Equal volumes of polymer and siRNA solutions were mixed to form the according N/P ratio, vortexed for 30 s and incubated at room temperature for 20 minutes.

2.3.4   Size and zeta (ζ)-potential analysis

Sizes of polyplexes were evaluated by Dynamic Light Scattering (DLS) analysis. Polyplexes were prepared with 40 pmol of FLUC siRNA at N/P 2 and 10 as described above in a total volume of 350 µl. Measurements were performed with a Malvern Zetasizer Nano ZS (Malvern Instruments Inc., Westborough, MA) in quadruplicates at 25 °C using disposable cuvettes (low volume 70 µl, Brookhaven Instruments Corporation, NY, USA) for size measurements. Measurements were set up at 173º backscatter angle with 15 runs per measurement. For data analysis, the viscosity (0.88 mPa.s) and the refractive index (1.33) of water at 25ºC were used. Results are given as Z average in nm +/- standard deviations. Polyplexes were then diluted to 700 µl with 5% glucose solution before ζ-potential measurements were performed in disposable capillary cells (Malvern Instruments Inc., Westborough, MA). Results are given in mV +/- standard deviations.

2.3.5   Size and Morphology: Transmission Electron Microscopy (TEM) and Atomic Force Microscopy (AFM)

For Transmission Electron Microscopy (TEM), polyplexes were prepared as described above at N/P 2 with 40 pmol of FLUC siRNA in a total volume of 20 µl. A drop of particle

suspension was dispensed on a copper-coated grid (200-mesh) and left to dry before imaging

with a transmission electron microscope (JEOL 2010 TEM). Several representative images were

taken for each sample at different magnifications. Atomic force microscopy (AFM) was

performed using a Pico LE Atomic Force Microscope (Molecular Imaging, Agilent

Technologies, Santa Clara, CA). Polyplex suspensions were freshly prepared as described above.

A drop was incubated on a freshly cleaved mica surface for 5 minutes and rinsed with deionized

water to remove excess liquid. Samples were allowed to dry at room temperature and imaged in

contact mode using a Si_3Ni_4 V-shaped cantilever.

2.3.6 SiRNA condensation efficiency and stability against polyanions in neutral and acidic conditions: SYBR® gold dye binding assays and heparin competition assays

SYBR® Gold assays were used to evaluate the capacity of the oligospermines to condense

siRNA at various N/P ratios (0 to 20). SYBR® Gold dye intercalates only with free and

accessible siRNA and does not fluoresce if the siRNA is condensed and protected by a

polycation. In a FluoroNunc™ 96-well white polystyrene plate (Nunc, Thermo Fisher Scientific,

Waltham, MA), 50 pmol of FLUC siRNA per well in 50 μl was complexed with the according

amount of oligospermine in the same volume to obtain the corresponding N/P ratios in a total

volume of 100 μl of 5% glucose solution. PEI (5 kDa) was used for comparison. Formulations

were incubated at room temperature for 20 minutes. A 4x SYBR® Gold solution (30 μl) was

added to each well and incubated in the dark for 10 minutes. Fluorescence was measured at 495

nm/537 nm excitation and emission wave lengths on a Synergy 2 Multi-Mode microplate reader

(BioTek Instruments, Winooski, VT). For heparin assays, polyplexes were prepared at N/P 2 as

described above. In addition, experiments were performed in presence of two different media to

compare the stability of the polyplexes at different pH and ionic strengths. The media were 5% glucose solution (pH 7.4) and sodium acetate buffer (pH 4.5). For the heparin assays, a master solution of heparin was prepared (0.1 IU/μL). Serial dilutions of heparin were then prepared (0-1 IU/well) and added to the wells (10 μl/well). Subsequently, a 4x SYBR® Gold solution (30 μl/well) was added and incubated for 10 minutes. After different incubation times with heparin (20 minutes, 1, 2 and 3 hours) at 25ºC, fluorescence was measured on a Synergy 2 Multi-Mode microplate reader (BioTek Instruments, Winooski, VT) at 495 nm/537 nm excitation and emission wave lengths. Measurements were performed in triplicates. The relative stability of polyplexes was determined by normalizing the fluorescence intensity of the intercalating SYBR® gold dye to SYBR® gold only (0%) and SYBR® gold with free siRNA (100%). Results are shown as mean values +/- standard deviation and analyzed by Graph Pad Prism5.0 software (GraphPad Software, La Jolla, USA).

2.3.7   Cell culture

NCI-H1299/LUC cells are derived from a human non-small cell lung carcinoma cell line (ATCC®) and transfected to stably expressing the reporter gene luciferase.[27] H1299/LUC represents an established model for gene knock down studies as shown previously.[27-28] Cells were cultured and grown in RPMI-1640 cell culture medium (Thermo Scientific Hyclone, Pittsburgh, PA) supplemented by sodium pyruvate (1 mM), HEPES (10 mM), 10% fetal bovine serum (Thermo Scientific Hyclone, Pittsburgh, PA), and 1% penicillin/streptomycin. Cells were grown in 75 cm^2 cell culture flasks (Thermo Scientific, Waltham, MA) at 37 °C and 5% CO_2 and sub-cultured until approximately 90% confluence with changing fresh culture medium every 2-3 days.

2.3.8   Cytotoxicity of polyplexes: MTT assay

H1299/LUC cells were seeded in a 96-well plate (Thermo Scientific, Waltham, MA) with 10,000 cells per well in 100 μl of growth medium and incubated for 24 hours at 37 °C and 5% CO_2 in a HERAcell 150i CO_2 incubator (Thermo Scientific, Waltham, MA). Oligospermines with varying concentrations (2-1000 μg/ml) were added to the cells in fresh media and incubated for 24 hours at 37 °C and 5% CO_2. Sterile filtered-MTT solution (5 mg/ml) was added to the cells (10 μl/well) and incubated for 4 hours at 37 °C and 5% CO_2. Water-soluble MTT is enzymatically converted to insoluble formazan particles by metabolically active mitochondria.[29] Subsequently, the cell culture media was removed, and DMSO (200 μl/well, Sigma-Aldrich, St. Louis, MO) was added and incubated at room temperature for 10 minutes to solubilize the formazan particles. The optical absorbance was measured at 540 nm on a Synergy 2 Multi-Mode microplate reader (BioTek Instruments, Winooski, VT). The percentage of cell viability is measured as the ratio between the absorbance of a sample and the untreated control cells. Results are shown as the mean value +/- standard deviation of triplicates.

2.3.9   Quantification of cellular uptake by flow cytomtery

H1299/LUC cells were seeded in 24-well plate (Corning Incorporated, Corning, NY) with a density of 200,000 cells per well and incubated for 24 hours at 37 °C and 5% CO_2. Polyplexes were freshly prepared as described above with 40 pmol of AlexaFluor488-labeled siRNA at N/P ratio 2 and 10. Negative controls included untreated control cells. PEI (5 kDa) was used as a positive control for comparison. Cells were transfected for 4 hours with 100 μl of cell culture medium and 100 μl of polyplexes, after which growth medium was added to a total volume of

500 μl, and cells were incubated for another 20 hours. Trypan blue quenching was used to extinguish the extracellular fluorescence caused by polyplex binding and to confirm the internalization of siRNA in the cells. Trypan blue 0.4% (100 μl per well), a dye that quenches the extracellular fluorescence,[30] was added to the samples for 5 minutes before trypsinizing the cells. Results were compared to those obtained with cells that did not undergo trypan blue staining. Cells were rinsed with 1X PBS buffer supplemented with 2 mM EDTA, treated with trypsin and incubated at 37 °C and 5% CO_2 for 3-4 minutes to detach the cells. Fresh medium (400 μl) was added to each well to deactivate the trypsin. Samples were transferred to microcentrifuge tubes (Seal-Rite, USA Scientific, Orlando, FL) and centrifuged at 400 g for 5 minutes. Samples were washed twice with 1X PBS with 2 mM EDTA. Fluorescence was quantified by flow cytometry on an LSR II (BD Biosciences, San Jose, CA) after staining with 4',6-diamidino-2-phenylindole (DAPI) for dead cells. Cell fluorescence was measured with excitation at 488 nm and the emission filter set to a 530/30 bandpass. Cell gating and data analysis was performed using FACSDiVa™ (BD Biosciences, San Jose, CA) software. Measurements were performed in triplicates; 10,000 viable cells each were gated and analyzed. Mean fluorescence intensity (MFI) results are given as the mean value of three independent measurements. Data analysis was performed by Graph Pad Prism5.0 software (GraphPad Software, La Jolla, CA).

2.3.10 RNA knockdown measured by qRT-PCR

In 6-well plates (Corning Incorporated, Corning, NY), H1299/LUC cells were seeded with a density of 500,000 cells per well and incubated for 24 hours at 37 °C and 5% CO_2. Polyplexes were prepared with 200 pmol of hGAPDH siRNA at N/P 2 in a total volume of 100 μl and added to 1 ml of cell culture medium per well. LF (0.5 μL/10 pmol of siRNA) was used as a positive

transfection control. Cells were transfected with samples in fresh medium and incubated for 4 hours. After 4 hours of incubation, medium was added to a total volume of 3 ml, and cells were allowed to incubate for an additional 20 hours. Subsequently, cells were washed with 1X PBS and lysed with lysis buffer (SurePrep TrueTotal™ RNA Purification Kit (Fisher BioReagents, Fisher Scientific, Waltham, MA). Total RNA was then isolated from cells according to the manufacturer's protocol with supplementary DNase I digestion and reverse transcribed to cDNA and amplified in a one-step protocol using Brilliant III SYBR Green QRT-PCR Master Mix . Hs_GAPDH-primers primers were used to quantify the gene expression of hGAPDH. Hs_β-actin-primers were employed as a standard to evaluate the relative gene expression of the two genes. Serial dilutions of total RNA of untreated cells were performed to plot calibration curves for GAPDH and β-actin mRNA levels. Measurements were performed on a Stratagene Mx 3005P (Agilent Technologies, Santa Clara, CA). Ct values were analyzed with the MxPro software (Mx 3005P version). Results were shown as mean values +/- standard deviation of triplicates and analyzed by Graph Pad Prism5.0 software (GraphPad Software, La Jolla, CA).

2.3.11 Protein knockdown measured in reporter gene assays

H1299/LUC cells were seeded at a density of 25,000 cells per well in a 24-well plates (Corning Incorporated, Corning, NY) and incubated at 37 °C and 5% CO_2 for 24 hours before transfection. Cells were transfected with polyplexes with 40 pmol FLUC siRNA or nonspecific control DsiRNA at N/P 2 and allowed to incubate for 4 hours. Commercially available LF 2000™ was used as a positive control. After 4 hours of incubation, medium was added to a total volume of 500 µl and allowed to incubate for an additional 44 hours. Cells were washed with 1X PBS and lysed with cell culture lysis reagent (CCLR 1X, 100 µl/well, Promega, Fisher Scientific,

Waltham, MA) for 10 minutes. Cell lysates were then transferred to microcentrifuge tubes and centrifuged at 15,000 g for 5 minutes. Luciferase expression was quantified by mechanical injection of 50 μl luciferase assay buffer, containing 10 mM luciferin, into each well containing 20 μL of cell lysate using a Synergy 2 Multi-Mode microplate reader (BioTek Instruments, Winooski, VT). Relative light units (RLU) were measured as the mean value of gene expression relative to untreated cells with full expression (100%) +/- standard deviation of triplicates. Data was statistically analyzed using Graph Pad Prism5.0 software (GraphPad Software, La Jolla, CA).

2.4. Results and discussion

2.4.1 Synthesis of oligospermines

Spermine monomers were covalently coupled to yield three different polymers with different amounts of spermine units and distinct geometrical structures. The three polymers tested here are linear bisspermine, linear tetraspermine, and dendritic tetraspermine. The nomenclature of the polymers was based on the structure and number of spermine monomers. Oligospermine polymers were characterized by NMR and purified by HPLC. Molecular weights of the polymers were obtained by Mass Spectrometry for linear bisspermines (MW 1299.40), linear tetraspermines (MW 2581.82) and dendritic tetratspermines (MW 2625.87). The different architectures of the oligospermines were chosen to obtain differences in the charge distribution over the different structures. Our aim was to compare the siRNA polyplex formation of linear and dendritic structures with different cationic charge densities. At neutral pH (7.4) of the intra- and extracellular environment, it is expected that only the primary amines are protonated,

whereas only a small portion of the secondary amines are protonated.[31] The linear tetraspermine has the highest number of secondary amines compared to the other two oligospermines suggesting the ability of this polymer to act as a "proton sponge" at the acidic pH of the endo-lysosomal compartment.[32] The structure of linear tetraspermines possesses multiple spermine units in a linear arrangement which enables cross-linking of single oligospermine molecules. Cross-linked polymers have been reported to better interact with negatively charged regions of nucleic acids and can therefore yield enhanced transfection efficiencies.[33]

Dendritic structures are also very attractive as gene and drug delivery systems since they can be flexible structures with a multitude of end groups. The latter can be exploited to attach ligands, which opens various opportunities for cell-specific targeting. Due to their structure, dendrimers are believed to be more accessible for electrostatic interaction with RNA.[34] In flexible dendrimers, the amines located within the inner structure are accessible for protonation which results in an increased "proton sponge effect"[35] and consequently better transfection efficiency.[34]

2.4.2   Size and zeta (ζ)-potential analysis

To achieve efficient transfection, polyplexes must be well-characterized and reproducible. Many of the physico-chemical properties of polyplexes determine if they can overcome intracellular and extracellular barriers.[36]. Their size is an important factor for intracellular uptake and transfection. Some reports indicated that particles with a size below 150 nm are required for uptake in lung cells by endocytosis.[37]. However, other reports described that spermine-based delivery systems with a larger size have good transfection efficiency in vivo and are suitable for lung cancer gene therapy.[21a] The ability of oligospermines to condense siRNA and form polyplexes with defined structures was therefore evaluated here. Polyplexes prepared with 40

pmol of FLUC siRNA at N/P 2, 5, and 10 were compared in terms of hydrodynamic diameters and zeta-potentials. The change of size and zeta potential of polyplexes as a function of carrier/siRNA ratio was examined to determine a suitable N/P ratio for further investigations. All three oligospermines were able to condense siRNA into particles of sizes from 198.7 to 423.1 nm in diameter (Figure 2.4A). All polyplexes at N/P 5 were at least slightly larger than those at N/P 2, which is in line with an earlier report that described N/P ratio dependent trends in sizes of siRNA polyplexes.[38] Interestingly, both linear oligospermines showed an increase in size with increasing N/P ratios. Apparently, these polymers wrapped around the siRNA efficiently at an N/P ratio as low as 2 and then formed further layers of polymer on the surface of the polyplex. Another indication that supports this hypothesis is the increase of the zeta potential for the linear tetraspermine polyplexes with increasing N/P ratio (Figure 2.4B). Although linear bisspermine/siRNA polyplexes did not show a significant change in the zeta potential when increasing the N/P ratio, the zeta potentials of linear tetraspermine polyplexes increased from 1.5 mV to 10.6 mV and 12.7 mV for N/P 2, 5, and 10, respectively.

The dendritic tetraspermine, however formed polyplexes with decreased size at N/P 10 (225.4 in diameter nm and 17.6 mV). This behavior can be explained by its intertwining structure that causes not all amines of the tetraspermine to be available for electrostatic interaction with siRNA at low N/P ratios. The comparably high zeta potentials these polyplexes bear also support the idea of positively charged dendrimer arms that are unable to be neutralized by the interaction with phosphates.[39] However, these relatively high zeta potentials could possibly mediate cytotoxicity.[40] Zeta potentials of dendritic tetraspermines polyplexes increased with increasing N/P ratios. Comparing polyplexes of linear and dendritic tetraspermines, the zeta potential of the

linear tetraspermine polyplexes were lower than that of the dendritic tetraspermine polyplexes at all of the tested N/P ratios (2, 5 and 10, Figure 2.4B).

The surface charge of polyplexes is a significant factor for transfection efficiency of the polymer. Other studies have shown the ability of spermine-based polymers to neutralize the negative charge of nucleic acids to yield an overall neutralized to slightly positive charge suitable for interaction with the negatively charged cell membrane.[13] In our study, all oligospermines polyplexes were positively charged (Figure 2.4B).

Another prerequisite for successful and reproducible transfection, especially in vivo, is a narrow size distribution of the polyplexes [39]. The polydispersity expressed as the polydispersity index (PDI) was low for polyplexes formed with the linear bisspermine (0.14<PDI< 0.3) compared to those formulated with the linear tetraspermine (0.26<PDI<0.34) and dendritic tetraspermine (0.22 <PDI<0.36, Table SI 1). The broader size distribution of the polyplexes obtained with the tetraspermines can be interpreted as a result of interaction between one longer polycationic polymer with more than one siRNA molecule, which can cause coalescence of the polyplexes.[39] Many physical and biological parameters such as the molecular weight play an important role in determining the efficiency of a polymer to condense and deliver siRNA,.[41] Linear tetraspermines (MW 2581.82) and dendritic tetraspermines (MW 2625.87) naturally have a higher molecular weight compared to linear bisspermines (MW 1299.40), which affects the ability of the polymers to interact with siRNA and to form polyplexes. As reflected by the size and zeta potential data shown in Figure 2.4, the structure of the polymer also plays a very important role regarding the ability of an oligospermine to interact electrostatically with siRNA.

Based on these results, the linear tetraspermine/siRNA polyplexes seemed to be the most favorable with the smallest size at N/P 2 (198.7± 22 nm) and a slightly positive zeta potential (1.54 mV). These characteristics are caused by (i) a favorable number of positively charged spermine units (4 units), and (ii) the linear structure which seems to be important for efficient interaction with siRNA and to yield a low positive close to neutral surface charge that facilitates the crossing of the particle across the negatively charged cell membrane barrier. Polyplexes at N/P 2 with hydrodynamic diameters of 253.4± 26.3 nm for linear bisspermine polyplexes, 198.7± 22 nm for linear tetraspermine polyplexes, and 311.5±18.5 nm for dendritic tetraspermine polyplexes were therefore selected for further experiments.
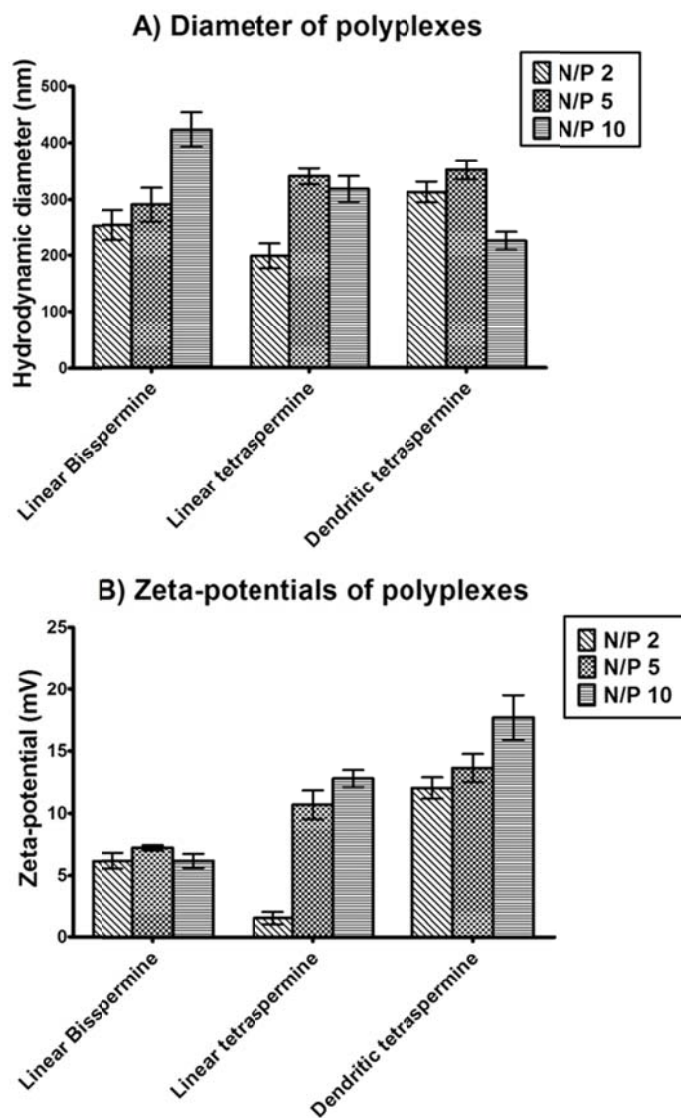
Figure 2.4. A) Hydrodynamic diameters and B) zeta potential values of siRNA polyplexes made with the linear bisspermine, linear tetraspermine, and dendritic tetraspermine at N/P 2, 5, and 10 at room temperature. Glucose solution 5% was used as suspension medium.

2.4.3 Size and morphology: Transmission Electron Microscopy (TEM) and Atomic Force Microscopy (AFM)

The morphologies and sizes of the different polyplexes at N/P 2 were imaged by AFM (Figure 2.5). The sizes of the polyplexes estimated from the AFM images were 24-73 nm for linear bisspermine polyplexes, 101-348 nm for linear tetraspermine polyplexes, and 202-480 nm for polyplexes made with the dendritic tetraspermine. The differences between the sizes obtained by DLS compared to the AFM images can be explained by the different processes used to prepare the samples for DLS or AFM. The hydrodynamic diameters were determined in a suspension of the particles while the particles were dried for AFM. It is possible that polyplexes coalesced during the drying step. Additionally, the broad size distribution of the polyplexes shown by the imaging technique and confirmed by the polydispersity measurements (PDI) can explain why the Z average of the hydrodynamic diameters does not reflect the sizes measured by AFM. Most importantly, AFM images showed different morphologies of oligospermines polyplexes as a result of the different chemical architectures of the polymers used. Both linear oligospermines formed spherical particles, while the dendritic tetraspermine complexes show less defined morphology. These observations strengthen the hypothesis that linear oligospermines wrap around siRNA and condense it efficiently, whereas not all arms of the dendritic tetraspermine are involved in siRNA condensation, as shown in the fuzzy morphology of the polyplexes.

TEM showed electron-dense areas in the polyplexes which could be the siRNA and the presence of very small particles (about 40 nm) in all polyplex formulations besides larger particles of 440 nm, 330 nm, and 189 nm for linear bisspermine, linear tetraspermine and

dendritic tetraspermine polyplexes, respectively (Figure SI 1). AFM confirmed such small polyplexes (about 40 nm). This presence of small particles could explain the rather broad size distribution of the formulations.
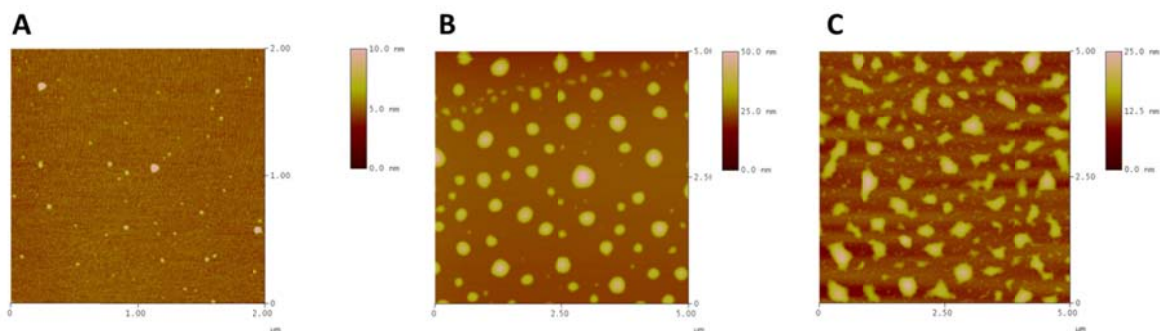
Figure 2.5. AFM images of polyplexes at N/P 2 with the A) linear bisspermine, B) linear tetraspermine, and the C) dendritic tetraspermine showing different morphologies.

2.4.4   SiRNA condensation efficiency and stability against polyanions in neutral and acidic conditions: SYBR® Gold dye binding assays and heparin competition assays

Among all the omnipresent cellular polyamines, spermines are more efficient in condensing and stabilizing DNA than spermidine and putrescine,[42] Spermine-based delivery systems condense DNA molecules by electrostatic interactions.[43] Therefore, SYBR®-Gold assays were employed to compare the ability of different oligospermines to condense siRNA at various N/P ratios.[44] In this assay, free or unbound siRNA is accessible to the intercalating dye SYBR-Gold® and is subsequently quantified based on the fluorescence emitted. Results were compared to low molecular weight PEI (5 kDa) as a control. As expected, all the polyplexes assayed were able to condense siRNA more efficiently with increasing N/P ratio (Figure 2.6). At higher N/P ratios, the net positive charge of the polyplexes was shown to increase, which is

reflected by increasing zeta potentials (Figure 1). With the rise of the zeta potential, the electrostatic interaction is enhanced, followed by higher condensation. All oligospermines were able to completely condense siRNA at N/P 2 and higher, whereas complete condensation of siRNA was only achieved at N/P 5 and higher for low molecular weight PEI. These results indicate that oligospermines tend to bind siRNA with higher affinity than PEI at low N/P ratios. Noticeably, linear bisspermine/siRNA polyplexes at N/P 2 showed relatively low condensation of siRNA compared to the other two oligospermines. This observation can be explained by the low molecular weight and short chain length of the bisspermine compared to the tetraspermines. The fact that the condensation efficiency did not increase for the bisspermine by increasing the N/P ratio additionally corroborates the observation of almost constant zeta potentials. Polyplexes with N/P 2 ratio were selected for further experiments based on their small size and overall good siRNA condensation.
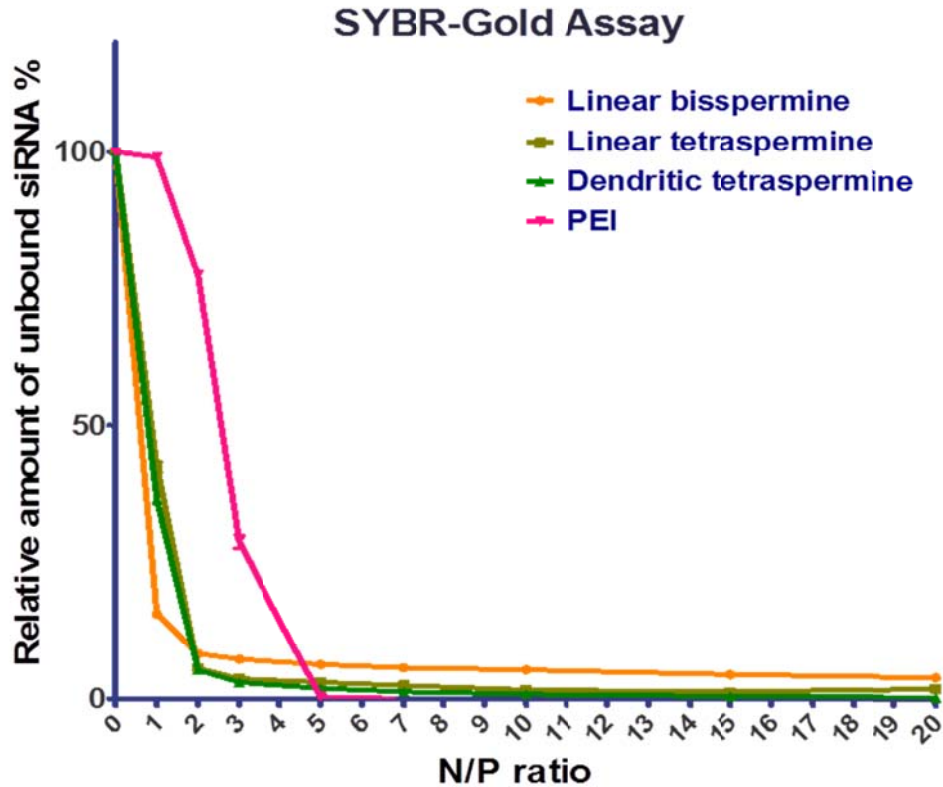
Figure 2.6. Condensation efficiency of oligospermines polyplexes measured by SYBR® Gold intercalation of siRNA at increasing N/P ratios. Results are given as average of n=3 +/- S.D.

Stability of cationic polyplexes is important for determining their efficiency as non-viral vectors. Their stability is influenced by the presence of competing anions[45] in the cell membrane[46] or in serum.[27] Heparin assays were therefore performed to confirm the ability of oligospermines to protect the siRNA in the presence of polyanions under physiologically relevant conditions. Different pH conditions were chosen to mimic the neutral (7.4) or acidic (4.5) environment of the cytoplasm and endo-lysosomes, respectively. As expected, the stability of all polyplexes decreased with increasing heparin concentration. The amount of siRNA released from the polyplexes increased rapidly as a function of heparin concentration. However, oligospermine polyplexes maintained higher stability profiles than PEI (5 kDa) polyplexes

against heparin competition, especially at low concentrations of heparin (Figure 4). It is important to note that the release profile from low molecular weight PEI complexes needs to be seen in the context of its poor condensation at N/P 2. As shown in Figure 3, at N/P 2, 75% of the siRNA is not yet condensed by 5 kDa PEI. It is not surprising, therefore, that the same amount of siRNA (75%) is found to be accessible for intercalation even in the absence of heparin. The remaining 25% of the siRNA are consequently very easily released from the complexes as shown in Figure 4.

At neutral pH, less than 75% of the siRNA was released from the oligospermine complexes even at the highest heparin concentration (Figure 2.7A). Since a balance between complexation and decomplexation is necessary to release siRNA in the cytosol for efficient incorporation to the RNA induced silencing complex (RISC), the release profiles at lysosomal pH were tested also. At acidic pH, many amines, especially in PEI, which are not protonated at pH 7.4, were charged leading to an increase of the complexation efficiency. However, siRNA was easily released from PEI complexes at comparably low heparin concentrations at acidic pH also. In comparison, oligospermine complexes displayed better stability again. In the acidic environment, the tetraspermine complexes released comparable amounts of siRNA as PEI at high heparin concentrations. Only the bisspermine lacked efficient decomplexation properties.
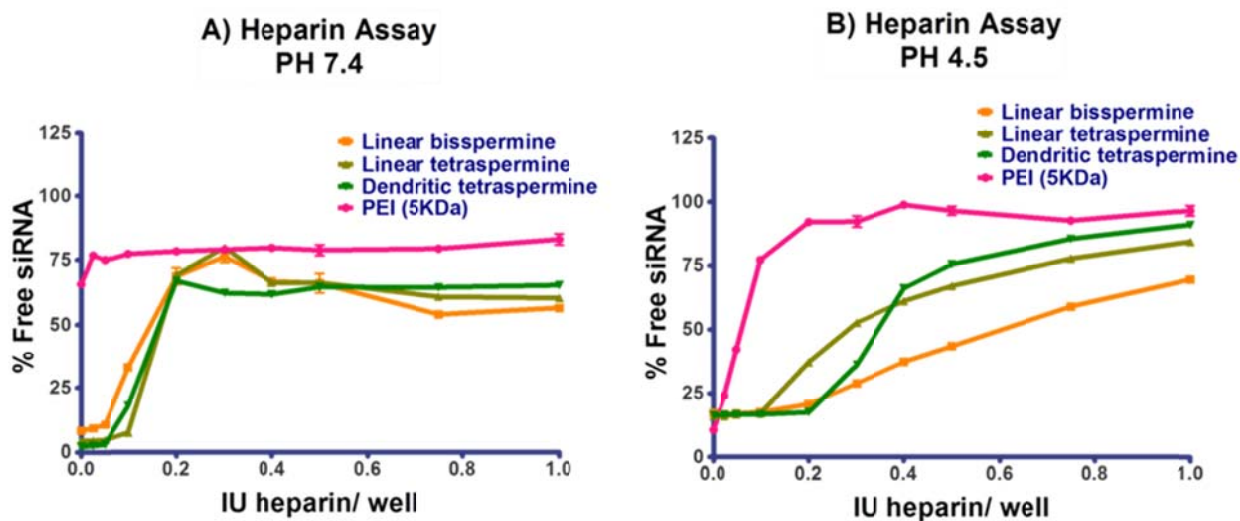
Figure 2.7. Release profiles of siRNA from oligospermines polyplexes (N/P 2, 50 pmol/well) compared to PEI as a function of heparin concentration at A) pH 7.4 and B) pH 4.5. Results are given as mean normalized fluorescence (n=3) +/− S.D.

To study the development of the polyplexes stability against heparin over time, heparin stability assays were performed for each polyplex after different incubation periods (20 minutes, 1 hour, 2 hours and 3 hours) with heparin at both pH 7.4 and pH 4.5 (Supplementary Information). At pH 7.4, all polyplexes showed a slight increase of siRNA release over time. The strongest effects were observed for the linear spermine polyplexes. These differences can be explained by the structural differences of the oligospermines and their different interaction with siRNA. While it is hypothesized that the linear oligospermines wrap around the siRNA and are efficiently neutralized, as reflected by rather low zeta potentials, not all amines of the dendritic oligospermine seem to be involved in the interaction with siRNA. It can therefore be understood that an excess of heparin binds to positively charged parts of the dendritic oligospermine before it displaces siRNA from a complex. Prolonged incubation of high concentrations of heparin with

polyplexes made of linear spermines, however, results in more quantitative competition with siRNA and thus release of the latter.

2.4.5 Polymer cytotoxicity: MTT assay

The formulation of non-viral vectors of cationic polymers and anionic nucleic acids is constrained by the compromise of high transfection efficiency which is often times only achieved at the price of high cytotoxicity.[47] Using cationic polymers with high molecular weight and charge density can protect the resulting polyplex from destabilization by natural cellular polyanions. The trade off, however, is that these positive charges can interact with cell membranes, inhibit crucial biological processes and lead to cytotoxic effects. [40] MTT assays were therefore used here to evaluate the cytotoxic effect of three cationic oligospermine polymers on H1299/LUC cells after 24 hours of incubation with the polymers. Results are presented as percentage of cell viability compared to untreated control cells. As expected, the cytotoxicity of oligospermines increased with increasing polymer concentration. Moreover, increasing the cationic charge of the polymer by increasing the number of spermine moieties also increased the cytotoxicity. Linear tetraspermines and dendritic tetraspermines showed a higher toxicity at higher concentrations when compared to linear bisspermines. This trend is due to the presence of a higher number of positively charged groups at neutral pH in the linear tetraspermine (13 positively charged groups) and dendritic tetraspermine (14 positively charged groups) compared to linear bisspermine (7 positively charged groups). The dendritic tetraspermine polymer was even more toxic than the linear tetraspermine at high concentrations (0.5-1 mg/ml) which may be due to its structure. In conclusion, all oligospermines affected the cell viability significantly less than PEI (5 kDa, IC50=3.63 µg/ml) and commercially available

LF 2000TM (IC50=41.41 µg/ml). At the corresponding polymer concentrations in polyplexes used in the following experiments, the cell viability was at least 83% after treatment with linear bisspermine, 88% with linear tetraspermine, and 77.3% with dendritic tetraspermine (Figure 2.8). It is important to note that the positive charge of the polymers is neutralized after polyplex formation with siRNA, so the viability shown here after treatment with polymer only is the assumption of a "worst case scenario".

MTT Assay
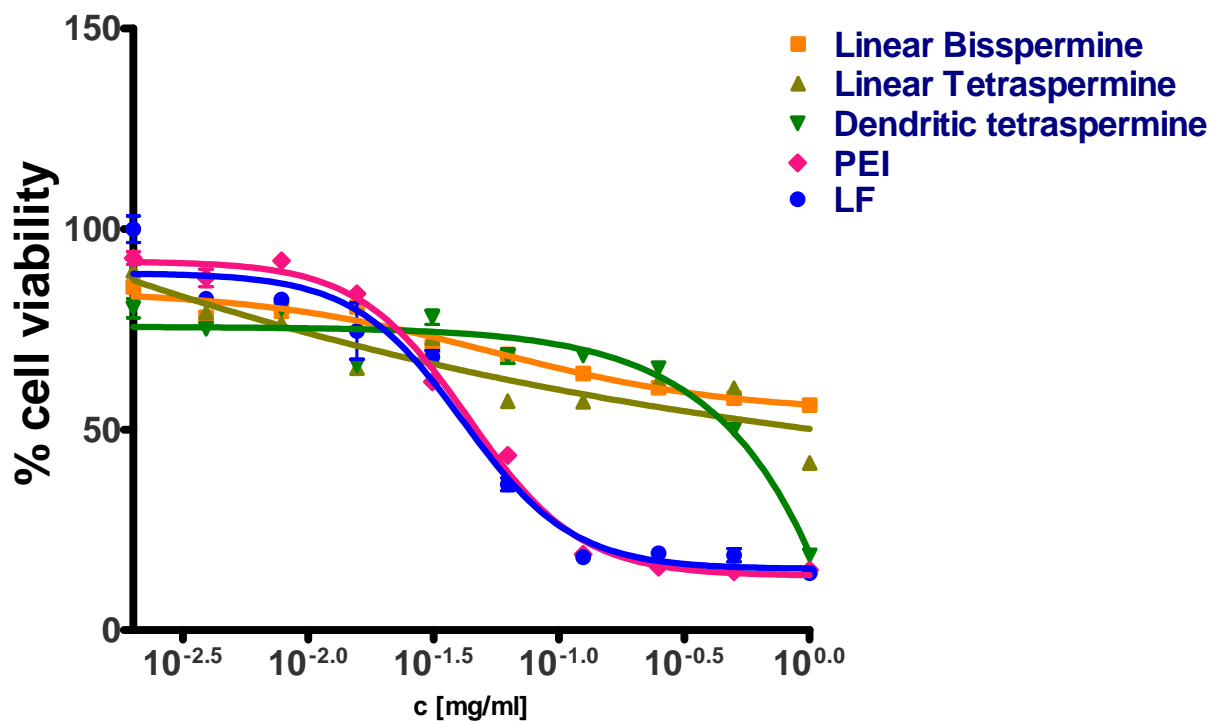
Linear Bisspermine	0.05367
Linear Tetraspermine	~ 6.648e-008
Dendritic tetraspermine	~ 32.86
PEI	0.04363
LF	0.04141

Figure 2.8. Cytotoxicity profiles of oligospermine polymers obtained by MTT assays. Percentages of cell viability of H1299/LUC cells are shown as a function of increasing polymer concentration after 24 hours of polymer incubation. The table shows the IC50 concentrations of the polymers in mg/ml.

2.4.6 Quantification of cellular uptake by flow cytomtery

Cellular uptake was quantified by flow cytometry and compared to PEI (5 kDa) as a positive control and untreated cells as a negative control. Polyplexes with 40 pmol of AlexaFluor488-labeled siRNA at N/P 2 and 10 were compared. Additionally, trypan blue 0.4% was used on the cells to quench the extracellular fluorescence associated with polyplexes that bind to the surface but are not internalized. The results were compared to untreated cells. Overall, trypan blue-treated cells showed slightly lower mean fluorescence intensities compared to cells that did not undergo quenching of bound polyplexes. This indicates that a small fraction of the siRNA polyplexes were attached to the cell membrane but are not taken up intracellularly. Among the oligospermine polyplexes, the highest cellular uptake was achieved by polyplexes made of linear tetraspermine/AlexaFluor488-siRNA at N/P 2 (no trypan blue-treatment) (Figure 2.9). These results are surprising because linear tetraspermine polyplexes were almost neutral at N/P 2 (1.54±0.5 mV), whereas dendritic tetraspermine polyplexes had a more cationic zeta potential (12±0.85 mV). For polymers such as PEI, an increase of the zeta potential which is obtained by increasing the N/P ratio is expected to mediate stronger siRNA delivery. This trend was confirmed here. However, PEI polyplexes at high N/P ratios are known to cause toxicity and off-target effects in transfected cells.[48] While the siRNA delivery by oligospermine polyplexes was comparable to PEI at N/P 2, an increase of the N/P ratio to 10 did not increase their efficiency. Linear tetraspermine polyplexes at N/P 2 were found to have the smallest hydrodynamic diameters, however. It is possible that this parameter is favorable for uptake and crossing of the barrier of the cell membrane. Additionally, the spherical morphology of the linear

oligospermine complexes compared to the fuzzy morphology of the dendritic tetraspermine polyplexes could have beneficially affected their internalization.
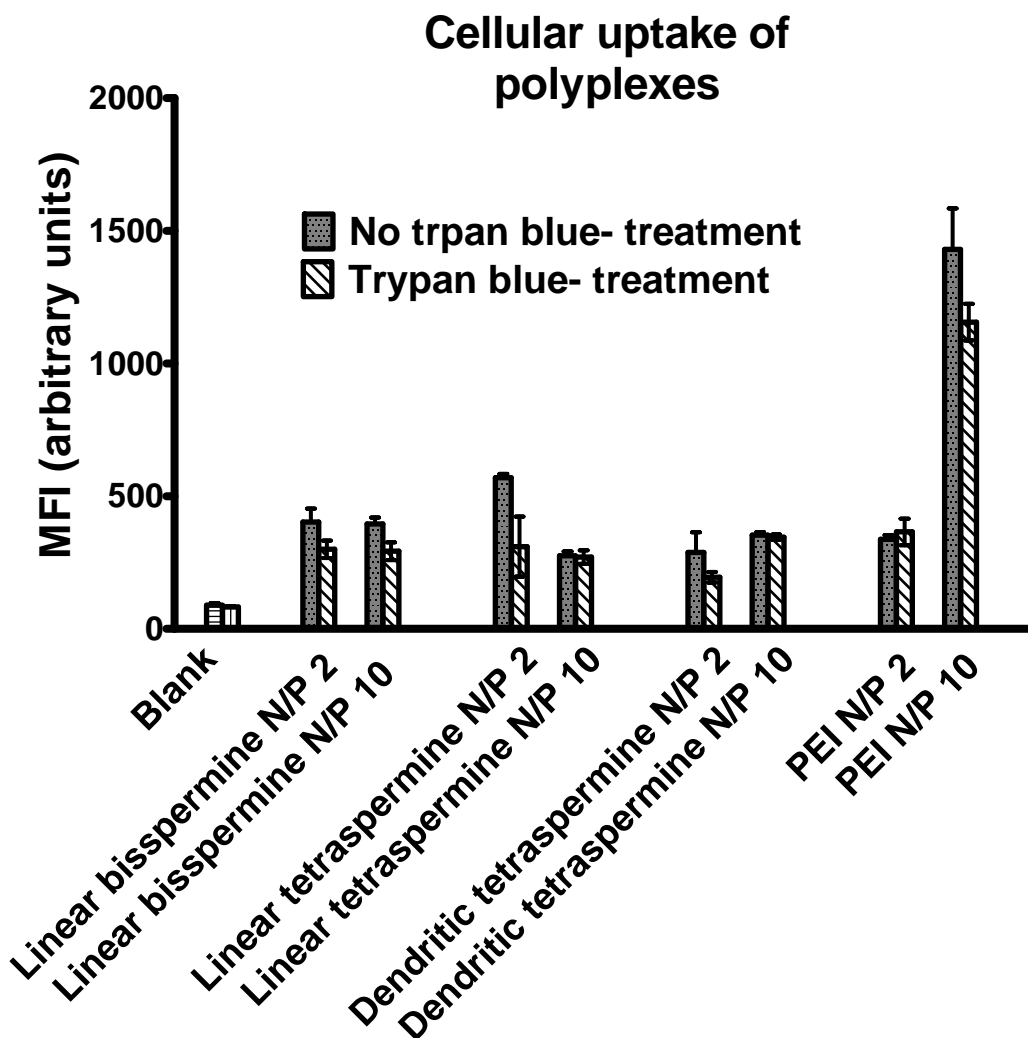
Figure 2.9. Flow cytometry measurements showing the uptake of polyplexes made of AlexaFluor-488 labeled siRNA and linear bisspermine, linear or dendritic tetraspermine. Mean fluorescence intensities were quantified in H1299/LUC cells after 24 hours incubation with polyplexes prepared at N/P 2 and 10. Trypan blue treatment is performed to quench the extracellular binding of siRNA polyplexes to the cell. Cells treated with trypan blue showed decreased mean fluorescence intensities.

2.4.7 RNA knock down measured by qRT-PCR

Real-time PCR was performed to quantify the knock down on the mRNA level mediated by polyplexes made of GADPH siRNA (200 pmol/well) and oligospermines at N/P 2. All oligospermines were used to form polyplexes with negative control siRNA (siNC) also. Linear bisspermine/siRNA polyplexes did not show gene silencing. This can be attributed to the incomplete siRNA release from the polyplex in the endo-lysolomal compartment as shown in Figure 4B. The most efficient oligospermine candidate was the linear tetraspermine, which is in line with the results of polyplexes size, zeta potentials, and flow cytometry. Linear tetraspermine polyplexes were shown to significantly downregulate the RNA expression more effectively than dendritic tetraspermines (54.6±17.3% vs. 75.1±1.5% residual GAPDH expression) (Figure 2.10). The dendritic structures showed less RNA knock down compared to the linear tetraspermine structure which could be explained by its less efficient uptake into the cells. In addition, the lack of secondary amines in the dendritic structure contributes to the lack of the "proton sponge effect".[35] Comparing the results of the three oligospermine polyplex formulations, we conclude that the difference in the architecture of the polymer strongly affected the efficiency of siRNA delivery to H1299/LUC cells. The linear tetraspermine structure is favored for successful siRNA delivery in lung cancer cells.

Transfection Efficiency
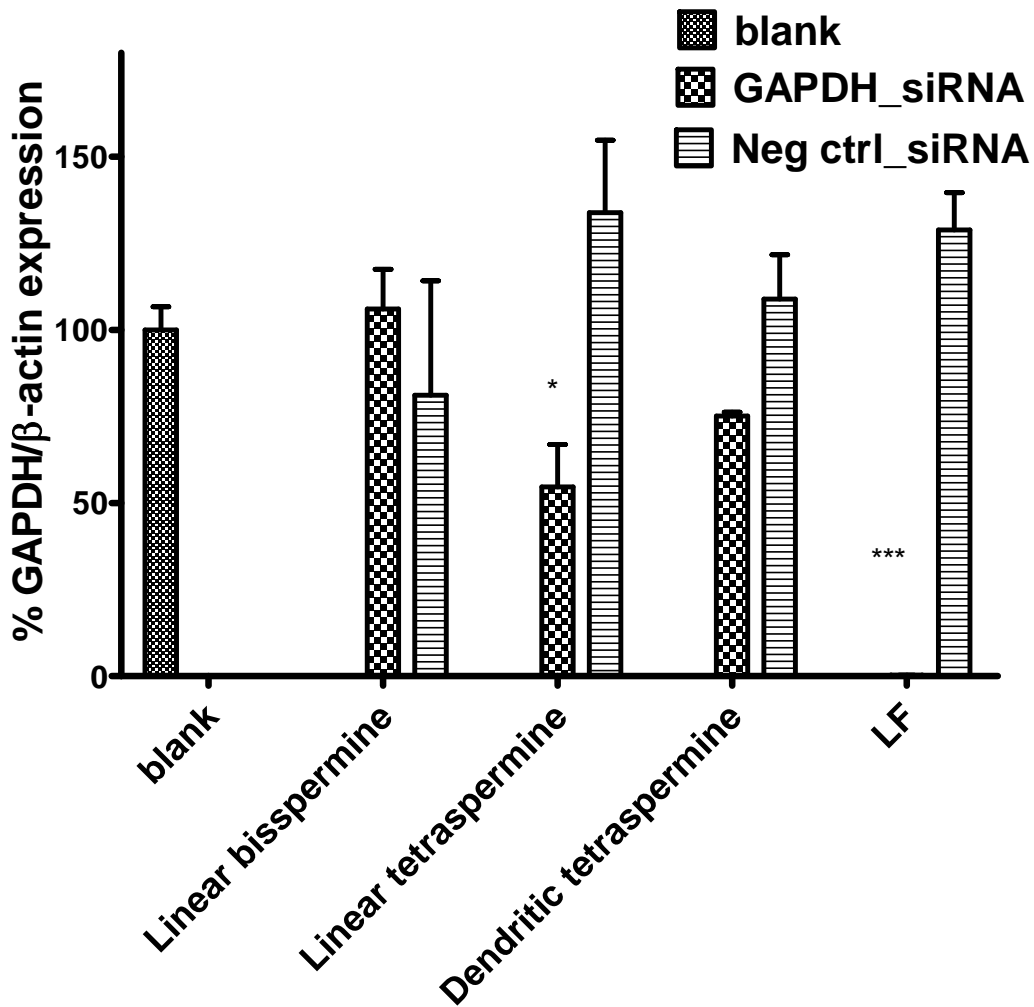
Figure 2.10. Transfection efficiency in vitro (H1299/LUC cells) of polyplexes at N/P 2 on the mRNA level measured by qRT-PCR. Hs_GAPDH-primers were used to quantify hGAPDH gene expression. Hs_β-actin-primers were employed as a standard to evaluate the relative gene expression of the two genes. Polyplexes made of GADPH siRNA and linear tetraspermine showed the best knock down compared to dendritic tetraspermine (54.6% vs. 75.1% residual GAPDH expression) and linear bisspermine polyplexes (no knock down).

2.4.8   Protein knockdown measured in reporter gene assays

At pH 4.5, the secondary amines are protonated leading to a strong buffering capacity inside the endosomes and thus a further influx of hydrochloric acid and water leading eventually to endosomal rupture. This event is believed to release endocytosed polyplexes and to support their endosomal escape into the cytosol.[31] The silencing efficiency of the luciferase protein expression in H1299/LUC cells induced by oligospermines polyplexes at N/P 2 was evaluated after transfection with 40 pmol of anti-LUC siRNA after 48 hours of incubation. The results were normalized to the relative expression of untreated cells and compared to commercially available LF 2000™. LF was used in many studies as a positive control for siRNA mediated knock down efficiency.[49] As in the mRNA knock down experiments, negative control siRNA (siNC) was also used with all oligospermines and LF. Linear tetraspermine/siRNA polyplexes showed the best knock down effect of luciferase expression compared to the other 2 oligospermines (Figure 2.11), which is in agreement with the RT-PCR results. The dendritic tetraspermine and LF showed higher cytotoxic effects than the other polymers which can be explained by the cytotoxicity results shown in Figure 7. These results suggest that not only did the oligospermine architecture affect the interaction of the protonated portions of the polymer with the phosphate groups of siRNA, but these different siRNA complexation behaviors also lead to different efficiency of gene knock down. Linear bisspermine polyplexes were taken up by the cell but, showed neither knock down on the mRNA nor the protein level. This is attributed to the lack of amines in the short chain length and low molecular weight of the bisspermine structure which does not condense siRNA as quantitatively as the tetraspermines (Figure 2.3.) and also does not efficiently decomplex (Figure 2.7). Our results are in line with other reports in

which Eliyahu et al. compared two chemically-modified spermine-based delivery systems for DNA delivery in terms of the number of spermine moieties and the distribution of charge density on the polymer backbone. In their study, a low and a high sperminated polymer were examined. The low sperminated polymer showed 56% less spermine per weight and 28% less primary amines than the high sperminated polymer. The low sperminated polymer was less efficient in neutralizing the negative groups of the nucleic acids and hence showed lower transfection efficiency compared to the high sperminated polymer.[31] Another study of cationic spermine conjugates with different polysaccharides showed efficient in vitro transfection with high spermine content (2000 nmol/mg).[31] In vivo experiments showed that chemically-modified dextran-spermine polyplexes successfully transfected mice with low toxicity and good tolerability when combined intramuscular and intranasal administration was performed.[33, 50] However, for efficient transfection, high positive zeta potential of the polyplex and large DNA doses were necessary.[50] Dendritic structures have been described to be more accessible for electrostatic interaction with RNA.[34] This is the case if the structurally inner amines are available for protonation which then also enhances the "proton sponge effect",[35] the endosomal escape, and the transfection efficiency.[34] However, our results showed that the amines in short dendritic structure are not all available for interaction with siRNA. In comparison with short linear structures, short dendrimers are more rigid. The protonated amines in the dendritic structure were thus not neutralized which increased the cytotoxicity of the polyplexes. The polyplexes made with the dendritic structure did not show strong uptake or gene knock down efficiency which may be due to the larger sizes at N/P 2 compared to the other two polymers or the less spherical morphology. Therefore, the structural architecture of dendritic tetraspermine was associated with increased cytotoxicity and decreased transfection efficiency.
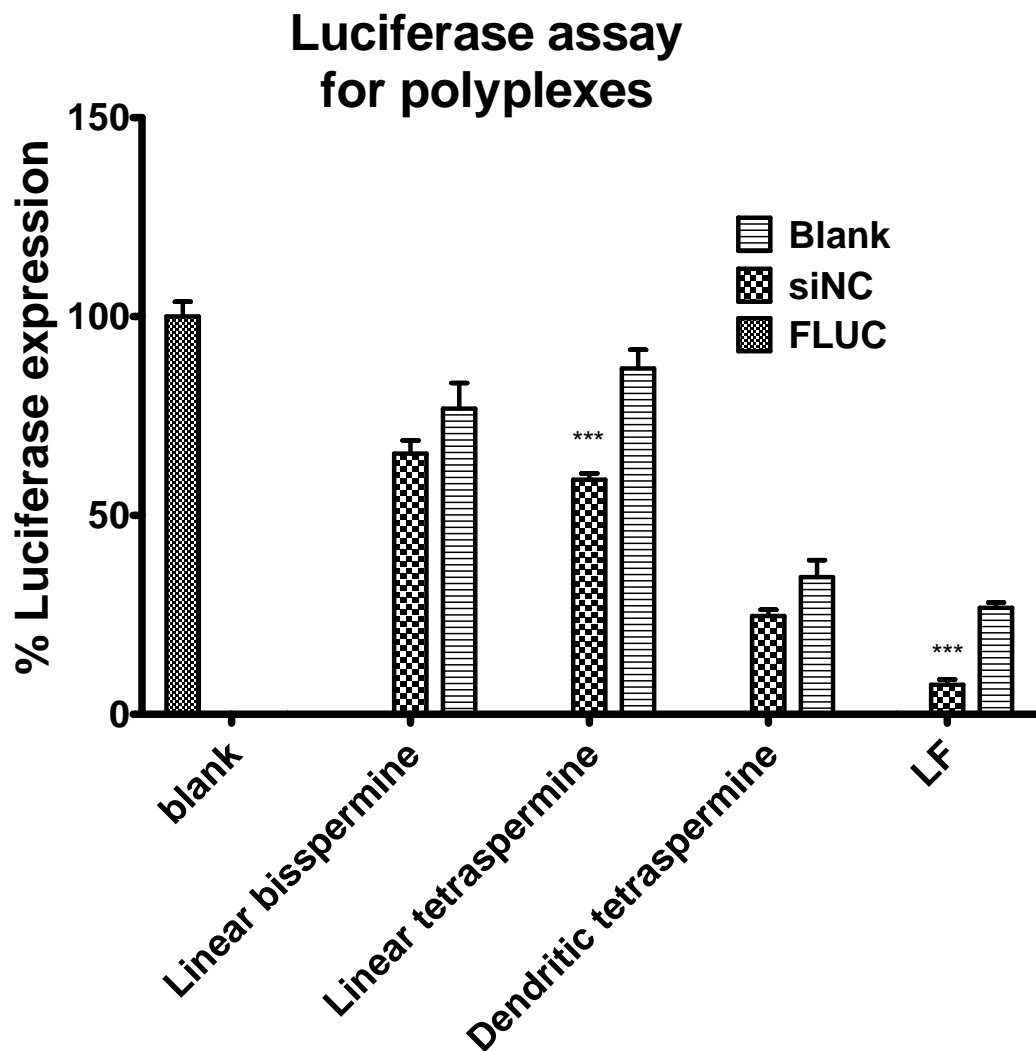
Figure 2.11. Silencing efficiency of firefly luciferase expression in H1299/LUC cells by oligospermine polyplexes with FLUC siRNA or non-specific control siRNA at N/P 2 after 48 hours of transfection. The relative gene silencing was normalized to blank untreated cells. Results are the mean value of triplicates +/- S.D.

2.5.   Conclusion

We highlighted the importance of the structure-activity relationship (SAR) of cationic oligospermines and its strong impact on siRNA delivery efficiency. The complexation and

decomplexation of siRNA and the carrier's ability to escape the degradation in lysosomes are two main factors in determining the polymer's transfection efficiency. The spatial availability of the positively charged amines in the polymer plays an important role for its electrostatic interaction with RNA and thus the shielding and protecting of siRNA. Therefore, the oligospermine architecture was shown to affect the transfection efficiency of polyplexes formed with siRNA. Consequently, an optimization of the used polymer is necessary. This can be achieved in many ways. Here, we investigated the effect of using different numbers of spermine monomers. In addition, we examined the effect of two different geometrical structures, namely linear and dendritic oligospermines. We found that tetramers of spermine are required to provide the adequate positive charge for both uptake and buffering effect for endosomal escape. From the comparison of linear bisspermines and linear tetraspermines, we found that increasing the number of spermines and charge density within the polymer enhanced the transfection efficiency at minimal toxicity. The linear structure is preferred over the dendritic structure, because the former seems to interact more efficiently with siRNA as not all amines of the latter are available for siRNA condensation leading to a more positively charged surface charge. Showing more efficient charge neutralization, the linear tetraspermine polyplexes are less cytotoxic and were shown to be more efficiently transfected into lung carcinoma cells (H1299/LUC). Therefore, we conclude that linear tetraspermines are very promising siRNA delivery systems. To enhance their intracellular uptake, coupling of targeting ligands is currently investigated.

Supplementary Information contains polydispersity values, TEM images, and the temporal development of siRNA release at pH 4.5. This material is available free of charge via the Internet at http://pubs.acs.org.

2.6. Acknowledgments

2.7. References

1. Zamore, P. D.; Tuschl, T.; Sharp, P. A.; Bartel, D. P., RNAi: double-stranded RNA directs the ATP-dependent cleavage of mRNA at 21 to 23 nucleotide intervals. *Cell* **2000,** *101* (1), 25-33.

2. Fire, A.; Xu, S.; Montgomery, M. K.; Kostas, S. A.; Driver, S. E.; Mello, C. C., Potent and specific genetic interference by double-stranded RNA in Caenorhabditis elegans. *Nature* **1998,** *391* (6669), 806-11.

3. (a) McManus, M. T.; Sharp, P. A., Gene silencing in mammals by small interfering RNAs. *Nature Reviews Genetics* **2002,** *3* (10), 737-747; (b) Lam, J. K.-W.; Liang, W.; Chan, H.-K., Pulmonary delivery of therapeutic siRNA. *Advanced Drug Delivery Reviews* **2012,** *64* (1), 1-15.

4. Elbashir, S., M. ; Harborth, J.; Lendeckel, W.; Yalcin, A.; Weber, K.; Tuschl, T., Duplexes of 21-nucleotide RNAs mediate RNA interference in cultured mammalian cells. *Nature* **2001,** *411* (6836), 494-498.

5. http://www.clinicaltrials.gov/ The US National Institutes of Health. ClinicalTrials.gov.

6. Check, E., Harmful potential of viral vectors fuels doubts over gene therapy. *Nature* **2003,** *423* (6940), 573-574.

7. Zhou, J.; Shum, K. T.; Burnett, J. C.; Rossi, J. J., Nanoparticle-Based Delivery of RNAi Therapeutics: Progress and Challenges. *Pharmaceuticals (Basel)* **2013,** *6* (1), 85-107.

8.   (a) Behr, J. P.; Demeneix, B.; Loeffler, J. P.; Perez-Mutul, J., Efficient gene transfer into mammalian primary endocrine cells with lipopolyamine-coated DNA. *Proc Natl Acad Sci U S A* **1989,** *86* (18), 6982-6; (b) Du, Z.; Chen, M.; He, Q.; Zhou, Y.; Jin, T., Polymerized spermine as a novel polycationic nucleic acid carrier system. *International Journal of Pharmaceutics* **2012,** *434* (1–2), 437-443.

9.   (a) Eliyahu, H.; Siani, S.; Azzam, T.; Domb, A. J.; Barenholz, Y., Relationships between chemical composition, physical properties and transfection efficiency of polysaccharide-spermine conjugates. *Biomaterials* **2006,** *27* (8), 1646-55; (b) Jiang, H. L.; Lim, H. T.; Kim, Y. K.; Arote, R.; Shin, J. Y.; Kwon, J. T.; Kim, J. E.; Kim, J. H.; Kim, D.; Chae, C.; Nah, J. W.; Choi, Y. J.; Cho, C. S.; Cho, M. H., Chitosan-graft-spermine as a gene carrier in vitro and in vivo. *European Journal of Pharmaceutics and Biopharmaceutics* **2011,** *77* (1), 36-42; (c) Allen, J. C., Biochemistry of the polyamines. *Cell Biochemistry and Function* **1983,** *1* (3), 131-140.

10.   Tabor, C. W.; Tabor, H., Polyamines. *Annu Rev Biochem* **1984,** *53*, 749-90.

11.   (a) Shim, M. S.; Kwon, Y. J., Dual mode polyspermine with tunable degradability for plasmid DNA and siRNA delivery. *Biomaterials* **2011,** *32* (16), 4009-4020; (b) Hardy, J. G.; Kostiainen, M. A.; Smith, D. K.; Gabrielson, N. P.; Pack, D. W., Dendrons with spermine surface groups as potential building blocks for nonviral vectors in gene therapy. *Bioconjug Chem* **2006,** *17* (1), 172-8.

12.   Fischer, W.; Brissault, B.; Prevost, S.; Kopaczynska, M.; Andreou, I.; Janosch, A.; Gradzielski, M.; Haag, R., Synthesis of linear polyamines with different amine spacings and their ability to form dsDNA/siRNA complexes suitable for transfection. *Macromol Biosci* **2010,** *10* (9), 1073-83.

13.   Duan, S. Y.; Ge, X. M.; Lu, N.; Wu, F.; Yuan, W.; Jin, T., Synthetic polyspermine imidazole-4, 5-amide as an efficient and cytotoxicity-free gene delivery system. *Int J Nanomedicine* **2012,** *7*, 3813-22.

14.   Kwon, Y. J., Before and after endosomal escape: roles of stimuli-converting siRNA/polymer interactions in determining gene silencing efficiency. *Acc Chem Res* **2012,** *45* (7), 1077-88.

15.   Jere, D.; Kim, J. E.; Arote, R.; Jiang, H. L.; Kim, Y. K.; Choi, Y. J.; Yun, C. H.; Cho, M. H.; Cho, C. S., Akt1 silencing efficiencies in lung cancer cells by sh/si/ssiRNA transfection using a reductable polyspermine carrier. *Biomaterials* **2009,** *30* (8), 1635-1647.

16.   Jere, D.; Kim, T. H.; Arote, R.; Jiang, H. L.; Cho, M. H.; Nah, J. W.; Cho, N. S., A poly(β-amino ester) of spermine and poly(ethylene glycol) diacrylate as a gene carrier. 2007; Vol. 342-343, pp 425-428.

17.   (a) Shim, M. S.; Kwon, Y. J., Dual mode polyspermine with tunable degradability for plasmid DNA and siRNA delivery. *Biomaterials* **2011,** *32* (16), 4009-20; (b) Jere, D.; Kim, J. E.; Arote, R.; Jiang, H. L.; Kim, Y. K.; Choi, Y. J.; Yun, C. H.; Cho, M. H.; Cho, C. S., Akt1 silencing efficiencies in lung cancer cells by sh/si/ssiRNA transfection using a reductable polyspermine carrier. *Biomaterials* **2009,** *30* (8), 1635-47.

18.   Blagbrough, I. S.; Geall, A. J.; Neal, A. P., Polyamines and novel polyamine conjugates interact with DNA in ways that can be exploited in non-viral gene therapy. *Biochem Soc Trans* **2003,** *31* (2), 397-406.

19.   Chen, Y.-Z.; Ruan, G.-X.; Yao, X.-L.; Li, L.-M.; Hu, Y.; Tabata, Y.; Gao, J.-Q., Co-transfection Gene Delivery of Dendritic Cells Induced Effective Lymph Node Targeting and Anti-tumor Vaccination. *Pharm Res* **2013,** *30* (6), 1502-1512.

20.   (a) Maslov, M. A.; Kabilova, T. O.; Petukhov, I. A.; Morozova, N. G.; Serebrennikova, G. A.; Vlassov, V. V.; Zenkova, M. A., Novel cholesterol spermine conjugates provide efficient cellular delivery of plasmid DNA and small interfering RNA. *J Control Release* **2012,** *160* (2), 182-93; (b) Metwally, A. A.; Blagbrough, I. S., Self-Assembled Lipoplexes of Short Interfering RNA (siRNA) Using Spermine-Based Fatty Acid Amide Guanidines: Effect on Gene Silencing Efficiency. *Pharmaceutics* **2011,** *3* (3), 406-424; (c) Xu, R.; Wang, X.; Lu, Z.-R., Intracellular

siRNA delivery with novel spermine based surfactants. *Chin. Sci. Bull.* **2012,** *57* (31), 3979-3984; (d) Metwally, A. A.; Reelfs, O.; Pourzand, C.; Blagbrough, I. S., Efficient Silencing of EGFP Reporter Gene with siRNA Delivered by Asymmetrical N(4),N(9)-Diacyl Spermines. *Mol Pharm* **2012**.

21.   (a) Jiang, H.-L.; Hong, S.-H.; Kim, Y.-K.; Islam, M. A.; Kim, H.-J.; Choi, Y.-J.; Nah, J.-W.; Lee, K.-H.; Han, K.-W.; Chae, C.; Cho, C.-S.; Cho, M.-H., Aerosol delivery of spermine-based poly(amino ester)/Akt1 shRNA complexes for lung cancer gene therapy. *International Journal of Pharmaceutics* **2011,** *420* (2), 256-265; (b) Hong, S. H.; Kim, J. E.; Kim, Y. K.; Minai-Tehrani, A.; Shin, J. Y.; Kang, B.; Kim, H. J.; Cho, C. S.; Chae, C.; Jiang, H. L.; Cho, M. H., Suppression of lung cancer progression by biocompatible glycerol triacrylate-spermine-mediated delivery of shAkt1. *Int J Nanomedicine* **2012,** *7*, 2293-306.

22.   Kim, Y. K.; Cho, C. S.; Cho, M. H.; Jiang, H. L., Spermine-alt-poly(ethylene glycol) polyspermine as a safe and efficient aerosol gene carrier for lung cancer therapy. *J Biomed Mater Res A* **2013**.

23.   Soltan, M.; Ghonaim, H.; Sadek, M.; Kull, M. A.; El-aziz, L.; Blagbrough, I., Design and Synthesis of N 4,N 9-Disubstituted Spermines for Non-viral siRNA Delivery – Structure-Activity Relationship Studies of siFection Efficiency Versus Toxicity. *Pharm Res* **2009,** *26* (2), 286-295.

24.   Duan, S.; Yuan, W.; Wu, F.; Jin, T., Polyspermine Imidazole-4,5-imine, a Chemically Dynamic and Biologically Responsive Carrier System for Intracellular Delivery of siRNA. *Angewandte Chemie International Edition* **2012,** *51* (32), 7938-7941.

25.   Vijayanathan, V.; Thomas, T.; Shirahata, A.; Thomas, T. J., DNA Condensation by Polyamines: A Laser Light Scattering Study of Structural Effects†. *Biochemistry* **2001,** *40* (45), 13644-13651.

26.   Kolhatkhar, R., **in preparation**.

27.   Merkel, O. M.; Librizzi, D.; Pfestroff, A.; Schurrat, T.; Buyens, K.; Sanders, N. N.; De Smedt, S. C.; Behe, M.; Kissel, T., Stability of siRNA polyplexes from poly(ethylenimine) and

poly(ethylenimine)-g-poly(ethylene glycol) under in vivo conditions: effects on pharmacokinetics and biodistribution measured by Fluorescence Fluctuation Spectroscopy and Single Photon Emission Computed Tomography (SPECT) imaging. *J Control Release* **2009,** *138* (2), 148-59.

28.   Merkel, O. M.; Beyerle, A.; Beckmann, B. M.; Zheng, M.; Hartmann, R. K.; Stoger, T.; Kissel, T. H., Polymer-related off-target effects in non-viral siRNA delivery. *Biomaterials* **2011,** *32* (9), 2388-98.

29.   Liu, Y.; Peterson, D. A.; Kimura, H.; Schubert, D., Mechanism of cellular 3-(4,5-dimethylthiazol-2-yl)-2,5-diphenyltetrazolium bromide (MTT) reduction. *J Neurochem* **1997,** *69* (2), 581-93.

30.   (a) Germershaus, O.; Mao, S.; Sitterberg, J.; Bakowsky, U.; Kissel, T., Gene delivery using chitosan, trimethyl chitosan or polyethylenglycol-graft-trimethyl chitosan block copolymers: Establishment of structure–activity relationships in vitro. *Journal of Controlled Release* **2008,** *125* (2), 145-154; (b) Innes, N. P. T.; Ogden, G. R., A technique for the study of endocytosis in human oral epithelial cells. *Archives of Oral Biology* **1999,** *44* (6), 519-523.

31.   Eliyahu, H.; Siani, S.; Azzam, T.; Domb, A. J.; Barenholz, Y., Relationships between chemical composition, physical properties and transfection efficiency of polysaccharide-spermine conjugates. *Biomaterials* **2006,** *27* (8), 1646-1655.

32.   Boussif, O.; Lezoualc'h, F.; Zanta, M. A.; Mergny, M. D.; Scherman, D.; Demeneix, B.; Behr, J. P., A versatile vector for gene and oligonucleotide transfer into cells in culture and in vivo: polyethylenimine. *Proc Natl Acad Sci U S A* **1995,** *92* (16), 7297-301.

33.   Eliyahu, H.; Joseph, A.; Schillemans, J. P.; Azzam, T.; Domb, A. J.; Barenholz, Y., Characterization and in vivo performance of dextran–spermine polyplexes and DOTAP/cholesterol lipoplexes administered locally and systemically. *Biomaterials* **2007,** *28* (14), 2339-2349.

34.   Posocco, P.; Laurini, E.; Dal Col, V.; Marson, D.; Karatasos, K.; Fermeglia, M.; Pricl, S., Tell me something I do not know. Multiscale molecular modeling of dendrimer/ dendron organization and self-assembly in gene therapy. *Curr Med Chem* **2012,** *19* (29), 5062-87.

35.   Sonawane, N. D.; Szoka, F. C., Jr.; Verkman, A. S., Chloride accumulation and swelling in endosomes enhances DNA transfer by polyamine-DNA polyplexes. *J Biol Chem* **2003,** *278* (45), 44826-31.

36.   Wolff, J. A.; Rozema, D. B., Breaking the bonds: Non-viral vectors become chemically dynamic. *Molecular Therapy* **2008,** *16* (1), 8-15.

37.   (a) Lebhardt, T.; Roesler, S.; Beck-Broichsitter, M.; Kissel, T., Polymeric nanocarriers for drug delivery to the lung. *Journal of Drug Delivery Science and Technology* **2010,** *20* (3), 171-180; (b) De Smedt, S. C.; Demeester, J.; Hennink, W. E., Cationic polymer based gene delivery systems. *Pharm Res* **2000,** *17* (2), 113-26.

38.   Zheng, M.; Pavan, G. M.; Neeb, M.; Schaper, A. K.; Danani, A.; Klebe, G.; Merkel, O. M.; Kissel, T., Targeting the Blind Spot of Polycationic Nanocarrier-Based siRNA Delivery. *ACS Nano* **2012,** *6* (11), 9447-9454.

39.   Merkel, O. M.; Zheng, M.; Mintzer, M. A.; Pavan, G. M.; Librizzi, D.; Maly, M.; Hoffken, H.; Danani, A.; Simanek, E. E.; Kissel, T., Molecular modeling and in vivo imaging can identify successful flexible triazine dendrimer-based siRNA delivery systems. *J Control Release* **2011,** *153* (1), 23-33.

40.   Mastrobattista, E.; Hennink, W. E., Polymers for gene delivery: Charged for success. *Nat Mater* **2012,** *11* (1), 10-2.

41.   Ahmed, M.; Narain, R., The effect of polymer architecture, composition, and molecular weight on the properties of glycopolymer-based non-viral gene delivery systems. *Biomaterials* **2011,** *32* (22), 5279-90.

42.   Wilson, R. W.; Bloomfield, V. A., Counterion-induced condesation of deoxyribonucleic acid. a light-scattering study. *Biochemistry* **1979,** *18* (11), 2192-6.

43.   Kurzbach, D.; Velte, C.; Arnold, P.; Kizilsavas, G.; Hinderberger, D., DNA condensation with spermine dendrimers: interactions in solution, charge inversion, and morphology control. *Soft Matter* **2011,** *7* (14), 6695-6704.

44.   Merkel, O. M.; Beyerle, A.; Librizzi, D.; Pfestroff, A.; Behr, T. M.; Sproat, B.; Barth, P. J.; Kissel, T., Nonviral siRNA delivery to the lung: investigation of PEG-PEI polyplexes and their in vivo performance. *Mol Pharm* **2009,** *6* (4), 1246-60.

45.   Izumrudov, V. A.; Bronich, T. K.; Novikova, M. B.; Zezin, A. B.; Kabanov, V. A., Substitution reactions in ternary systems of macromolecules. *Polymer Science U.S.S.R.* **1982,** *24* (2), 367-378.

46.   Bolcato-Bellemin, A. L.; Bonnet, M. E.; Creusat, G.; Erbacher, P.; Behr, J. P., Sticky overhangs enhance siRNA-mediated gene silencing. *Proc Natl Acad Sci U S A* **2007,** *104* (41), 16050-5.

47.   (a) Li, S. D.; Huang, L., Non-viral is superior to viral gene delivery. *J Control Release* **2007,** *123* (3), 181-3; (b) Mintzer, M. A.; Simanek, E. E., Nonviral vectors for gene delivery. *Chem Rev* **2009,** *109* (2), 259-302.

48.   D'Emanuele, A.; Attwood, D., Dendrimer-drug interactions. *Adv Drug Deliv Rev* **2005,** *57* (15), 2147-62.

49.   Liu, Y.; Samsonova, O.; Sproat, B.; Merkel, O.; Kissel, T., Biophysical characterization of hyper-branched polyethylenimine-graft-polycaprolactone-block-mono-methoxyl-poly(ethylene glycol) copolymers (hy-PEI-PCL-mPEG) for siRNA delivery. *J Control Release* **2011,** *153* (3), 262-8.

50.   Eliyahu, H.; Joseph, A.; Azzam, T.; Barenholz, Y.; Domb, A. J., Dextran–spermine-based polyplexes—Evaluation of transgene expression and of local and systemic toxicity in mice. *Biomaterials* **2006,** *27* (8), 1636-1645.

2.8. Supplementory information

Table SI 2.1: Polydispersity (PDI) values of oligospermines polyplexes at different N/P ratios

Polymer used in polyplex	N/P ratio	PDI
Linear bisspermine	2	0.301
	5	0.293
	10	0.141
Linear tetraspermine	2	0.26
	5	0.29
	10	0.34
Dendritic tetraspermine	2	0.36
	5	0.35
	10	0.22
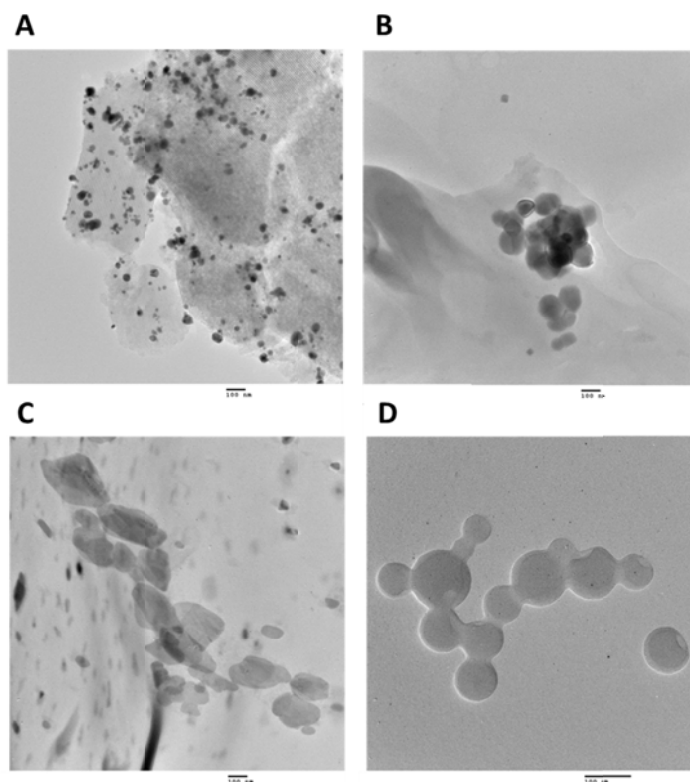
Figure SI 1: TEM images of polyplexes at N/P 2 with the A) linear bisspermine, B) linear tetraspermine, and the C) dendritic tetraspermine showing different morphologies and average

sizes of 440 nm, 330 nm, and 189 nm respectively. D) Small spherical particles of size about 40 nm were confirmed by both TEM and AFM images in all oligospermine polyplexes.
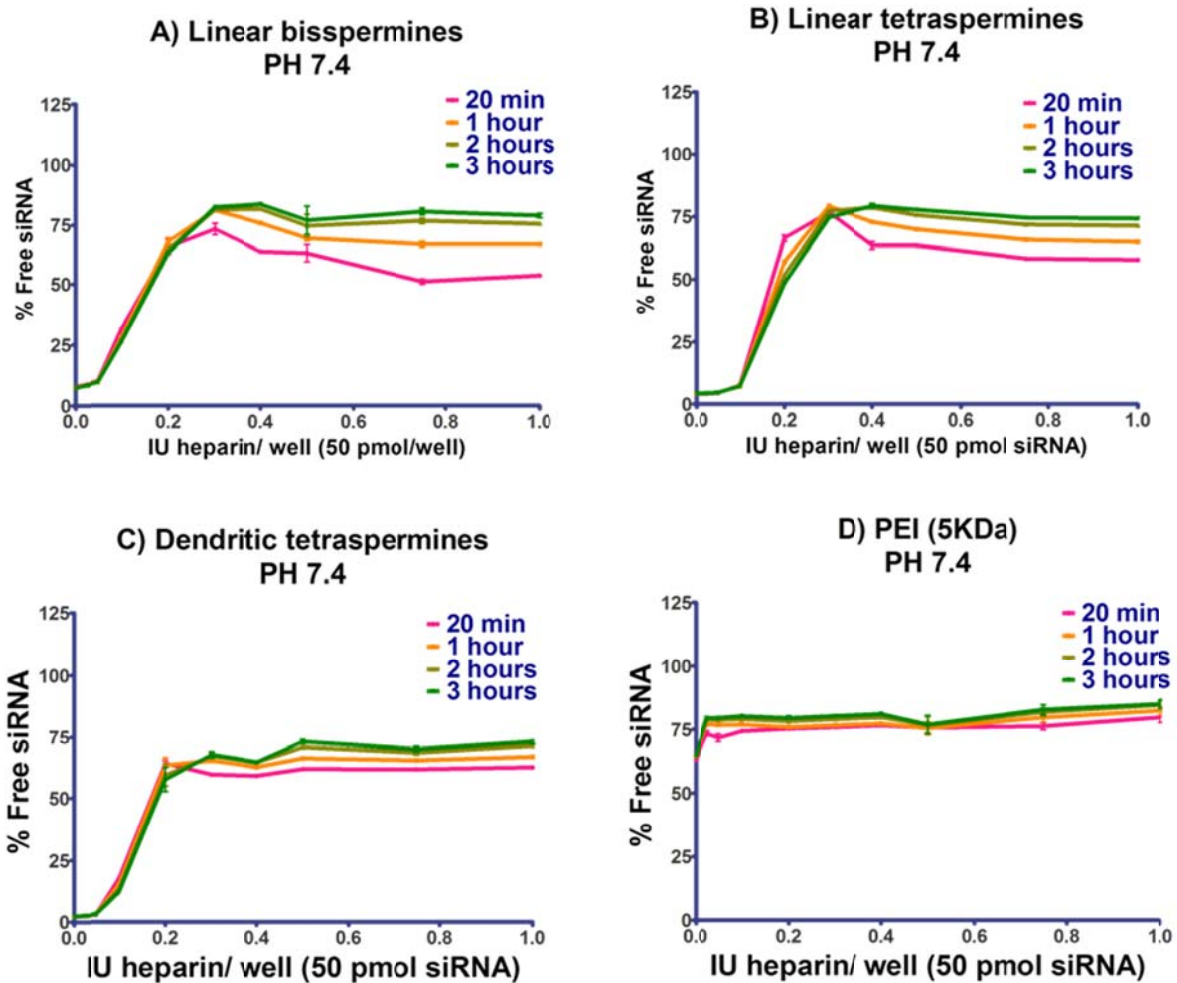
Figure SI 2. Development of the stability profiles against heparin polyanions for polyplexes with A) linear bisspermine, B) linear tetraspermine, C) dendritic tetraspermine, and D) 5 kDa PEI at pH 7.4 after 20 minutes, 1 hour, 2 hours and 3 hours of incubation of the polyplexes with increasing concentrations of heparin. All oligospermine polyplexes showed a slight increase of released siRNA over time at pH 7.4.

At pH 7.4, linear bisspermine polyplexes showed significant increase in siRNA release ($p < 0.0001$) over time compared to insignificant increases with other polymers (Figure SI 2). At pH 4.5, polyplexes made with the linear bisspermine and linear tetraspermine showed

significantly decreased siRNA release (p<0.0001) over time which indicates a dynamic rearrangement of the polyplexes in presence of heparin. On the other hand, polyplexes made with the dendritic tetraspermine and PEI (5 kDa) showed significantly increased siRNA release (p<0.0001) over time (Figure SI 3). These results showed higher stability of polyplexes in neutral medium than in acidic medium.
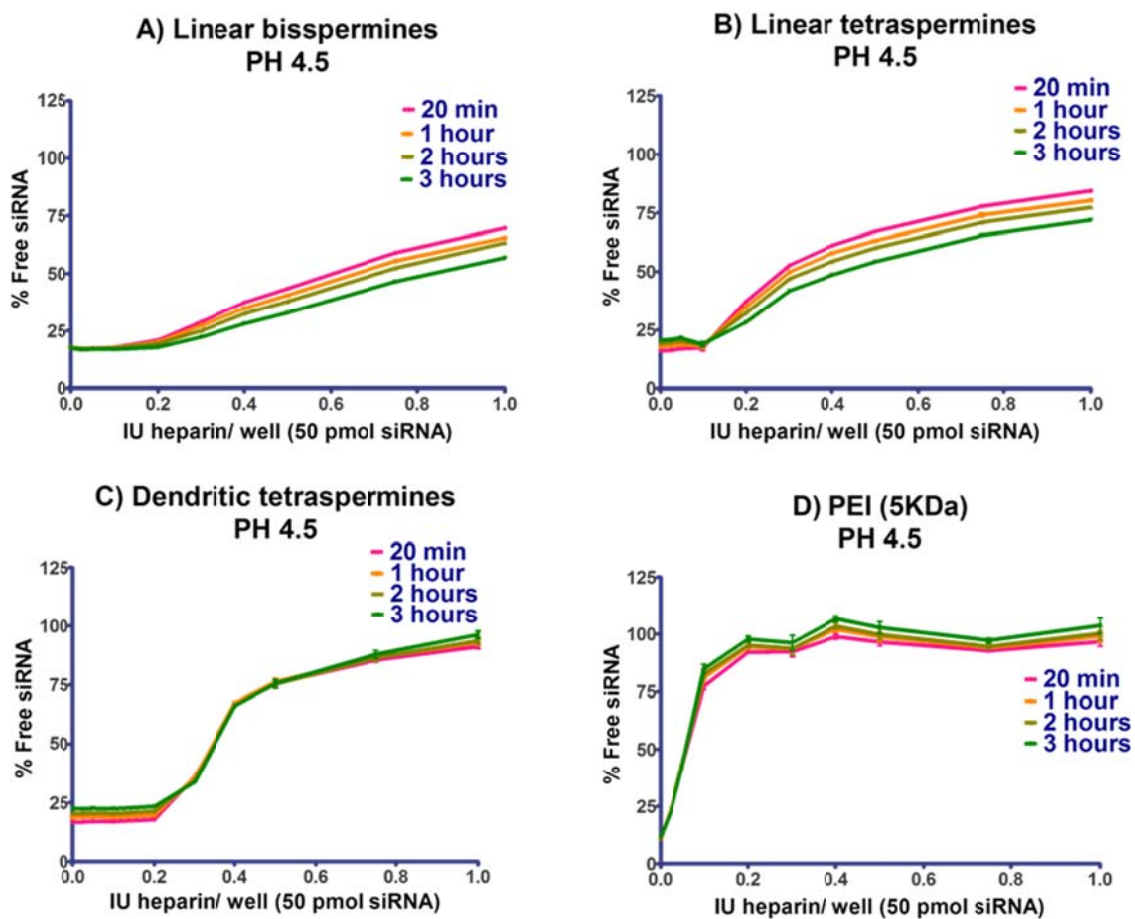
Figure SI 3. Development of the stability profiles against heparin polyanions for polyplexes with A) linear bisspermine, B) linear tetraspermine, C) dendritic tetraspermine, and D) 5 kDa PEI at pH 4.5 after 20 minutes, 1 hour, 2 hours and 3 hours of incubation of the polyplexes with increasing concentrations of heparin. For polyplexes with linear bisspermine and linear tetraspermine, the release of siRNA decreased over the time of incubation. In polyplexes with dendritic tetraspermine and PEI (5 kDa), the release of siRNA slightly increased over time at pH 4.5.

Chapter 3. Nanoimprinting of topographical and 3D cell culture scaffolds

3.1. Abstract

The extracellular matrix exhibits several nanostructures such as fibres, filaments, nanopores, and ridges which can be mimicked by topographical and three dimensional substrates for cell and tissue culture for an environment closer to *in vivo* conditions. This review summarises and discusses a growing number of reports employing nanoimprint lithography (NIL) to obtain such scaffolds. The different NIL methods as well as their advantages and disadvantages are described and special attention is paid to cell culture applications. We discuss the impact of materials, nanotopography, size, geometry, fabrication method, and cell type on growth guidance and differentiation. We present examples of cell guidance, inhibition of cell growth, cell pinning, and engineering of 3D cell sheets or spheroids. As currently applications are limited and not systematically compared for various cell types, this review only suggests promising substrates for particular applications. The outlook proposes possible directions in which this field may proceed from here.

Keywords: Nanoimprint lithography, scaffold, substrate, cell culture, cell guidance

- This article reviews different techniques of Nanoimprint lithography (NIL) and their applications as cell substrates and suggests promising applications.

3.2. Introduction

Bio-mimicking the natural environment of the cell has attracted great interest. The extracellular matrix (ECM) of the cell exhibits several nanostructures such as fibres, filaments, nanopores and ridges [1-5]. The cell interacts chemically and topographically with the ECM components, thus regulates cell responses like motility, differentiation and proliferation, and many more. [6-10]. Understanding the morphology and topography of the cells is crucial for biological, medical and bioengineering research applications. Many techniques have been presented in the literature, which aim to mimic the ECM by developing topographical nanostructured scaffolds, in contrast to petri dishes. Among the preparation techniques, nanoimprinting lithography is a rather new one which attracted much attention recently. Nanoimprinting technology has many promising applications in the areas of biosensors, tissue engineering [11], DNA mapping as well as electronics. Nanoimprinting techniques have advanced to build topographical and even three dimensional 3D substrates which are a critical for ex-vivo cell and tissue culturing.

The conventional in vitro 2D cell culture does not mimic the cell environment in vivo in terms of the nanostructure pattern and topography as well as the 3D existence. Nano-sized substrates can be obtained by a variety of conventional technologies such as electron beam lithography [12] or holograpy lithography [13]. Non-lithographic techniques that also yield nano-scale cell culture substrates are emulsion freeze-drying [14, 15] but are not discussed here. However, the aforementioned technologies have some limitations and drawbacks. As early as 1911, Harrison showed that topography plays an important role in the cell behaviour on fibres of a spider's web [16]. Many research groups used nanoimpriting techniques to study such effects.

Extensive reviews discussed the effects of surface nanotopography and bio-interfacial interaction, which is the interface between the cell and other fabricated material, on cell behavior in terms of motility [17], alignment [18], adhesion [19, 20], migration [21], differentiation [22], proliferation [23], nerve regeneration [24] and others [25-29]. Much distinctive behaviour was observed for cells cultured on nanopatterns versus micro patterns, especially in anchorage-dependant cells like neural cells including the dynamics of its membrane, elongation of axonal fibers to reach its specific targets, the growth pathway, and the cytoskeletal rearrangement that regulates the directional cell motility. Results vary according to the cell type, topography nanostructuctures and culture conditions [30]. The methodology applied for scaffold alignment also affects the alignment of cells with the nanotopography. Chaurey *et al*. described that fibroblasts oriented similarly on electrospun vs. nanoimprinted scaffolds for fiber larger than 100 nm. However, cell alignment was more efficient on sub-100 nm nanoimprinted fibers [31]. The reason for these differences in cell behaviour is that many peptides which are ECM components (such as laminin [32] and fibronectin) exist in nanoscale. Generally, nanopatterned structures on substrate surface were shown to induce cells to change morphology, alignment and adhesion compared to flat surfaces [33]. Dalby and coworkers cultured fibroblasts on 13 nm islands. Fibroblasts were found to have an increased cell attachment and spreading compared to a planar surface which were reflected by up-regulation of specific proliferative genes [33]. Later on, the same group used nanotopograhy as a non-invasive tool to understand the mechanism the mechano-transduction cascade of gene expression in fibroblasts [34].

Wieringa *et al*. studied the effect of nanotopography effect on F11 a root-ganglion derived cell line in terms of cell contact guidance. Contact guidance is the induced effect of the

anisotropic topographic structures on the cell regarding the alignment and migration in the direction of the topographies [35]. F11 is an established model for studying cytoskeletal rearrangement, plasticity [36] and differentiation [37]. Wieringa *et al.* presented the F1 cell line as a potential peripheral sensory neuron model for nanotopographical guidance [38]. Substrates with two different ridge dimensions of 500 nm and 2000 nm and a constant groove width of 500 nm were used to culture the cells. Another factor, the percentage of fetal bovine serum (FBS) in culture media was considered. In regards to the neurite guidance, no difference was shown between patterned and flat surface when cultured with 1% FBS. In contrast, when cells were cultured with 10% FBS, it was shown that the patterned surfaces induced the cell alignment with a trend of decreasing neurite alignment with increasing ridge width.   This supports the hypothesis that the cell alignment on nano-patterns occurs differently than on flat unpatterned surfaces and thus might influence the reliability of other aspects such as nerve regeneration. It also suggests that sometimes, a set of culture conditions can control the cell response rather than only one condition. A different report by Lee *et al.* describes osteoblast-like cells cultured on nano-thin polymer films on which nanopillar features were imprinted with a favourable size of 200 nm. This process changed the contact angle of the thin film and the surface property from hydrophilic to hydrophobic. When cells were cultured on hydrophobic nanopillar surface, they showed poor spreading and adhesion, which might be due to the deprived adhesion on top of the nanopillars. This represents therefore a cell substrate model that resists the cell adhesion and spreading. Additionally, it was found that the most important factor in terms of the contact angle of the nanopillar with the plastic thin film is the temperature of imprinting and de-molding of the nanostructures and not the imprinting time [39].

However, the mechanism of cell response corresponding to different nanopatterns remains unclear [40, 41]. Typically, it is a trial and error approach to examine the response of the cell towards a substrate nanopattern. So far, the literature provides reference to such patterns with specific cell lines. Over the last decades, many fabrication methods, inspired by the nature of ECM have been investigated. Some of them are novel techniques. Others are established fabrication methods that are modified to overcome one or more drawback of an established method. In this review, we describe basic nanoimprint lithography techniques that can be applied for patterning of topographical and three dimensional scaffolds for cell and tissue culture and we discuss the applications and possible future developments.

- Nanotopography significantly affects cell behaviour. In order to mimic the *in vivo* conditions of the cell growth, it is necessary to consider the patterns and topography of the extracellular matrix (ECM) nanostructures and to incorporate them in the proposed cell substrate.

3.3. Nanoimprint lithography (NIL)

Nanoimprint lithography [42] is a top-down nano-patterning technique with sub-100 nm high resolution and high throughput at low cost. NIL methods are classified as thermoplastic (T-NIL) and ultra-violet nanoimprint lithography (UV-NIL) methods [43, 44]. Additionally, variants to those two techniques exist. Nano-patterns can be formed on different substrates such as glass plates, silicon wafers, flexible polymer resists and non-planar substrates [45]. NIL exhibits many advantages over other conventional optical lithographic techniques that depend on electron beam scattering or light diffraction since NIL adapts a different concept which is causing a uniform mechanical deformation onto the substrates [42]. In NIL, mechanical

embossing is applied on the resists that later serves as a replica of the original pattern. Using this technique allows for avoiding the limitations associated by electron beam scattering and light diffraction such as the lower resolution [46, 47]. Moreover, NIL demonstrated ultrahigh resolution shortly after its introduction [48]. However, NIL is associated with various etching and deposition processes [49], which increase the time and the cost of the process. Therefore NIL is not suitable for commercial large- scale production, however, on the lab-scale, it has many advantages and applications [50].

- Nanoimprint lithography (NIL) presents many advantages over other conventional techniques. NIL methods can be subdivided into thermal, ultraviolet and variant NIL techniques.

3.4.   Thermoplastic NIL (T-NIL)

NIL, first introduced by Chou *et al* in 1995 [42] was called "hot embossing", and then developed to what we now understand as NIL. In the thermoplastic NIL (T-NIL), as shown in Figure 3.1, a fine layer of a thermoplastic polymer is deposited on a substrate which is a silicon wafer and is spin coated to form the surface of the imprint resist. A hard mould, usually made of silicon, with pre-patterned nanostructures is embossed in the resist surface by a thermo-mechanical single step under pressure to stamp the desired nanostructures of the mould into the polymer resist. The thermoplastic polymer temperature is elevated above its glass transition temperature (T_g) to facilitate the flow of the polymer into the nanocavities of the hard mould [51-54]. Consequently, the temperature of the polymer is lowered below T_g to freeze and solidify the replicated patterns and to detach the mould, thus leaving the pattern on the substrate [52]. Only

two years after this initial report, sub-10 nm structures as small as 6 nm were constructed [48]. The high imprinting temperature well above T_g and the high pressure (50-100 bar) represent the main limitations of the T-NIL technique [55], in addition to the mechanical strain involved. At this high temperature, the polymer exists in a viscous liquid form under pressure, and thereby can occupy the cavities of the mould. The main principle of NIL is based on squeeze flow of a sandwiched viscoelastic material between a substrate and a mould. Many attempts to overcome these limitations were reported, such as room temperature NIL [56-58] and low pressure nanoimprint lithography [59].
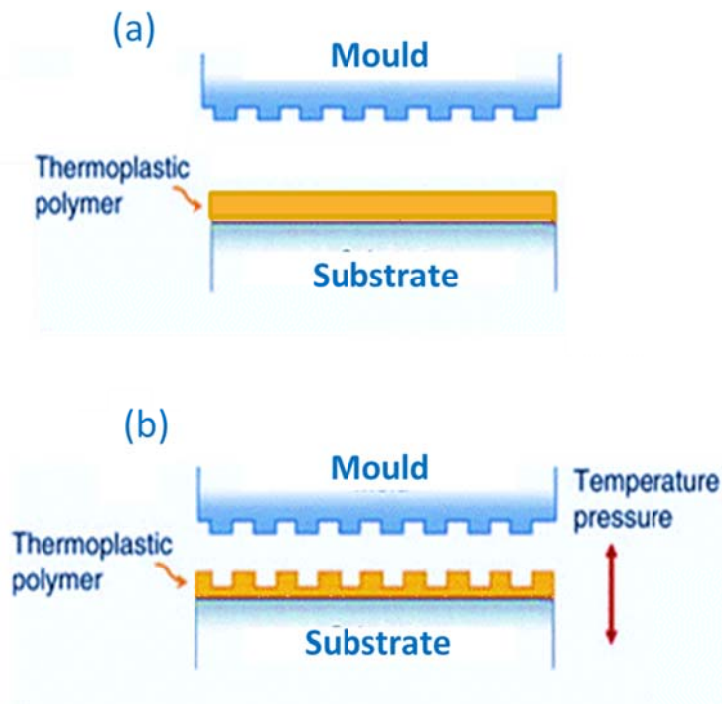
Figure 3.1: Schematic illustration of thermal NIL. (a) A fine layer of a thermo-plastic polymer is deposited and spin-coated on the substrate, a silicon wafer. (b) A hard mould, usually made of silicon, contains pre-patterned nanostructures and is mechanically embossed into the thin polymer film at high pressure (50-100 bar). The temperature of the polymer is raised above T_g for a few minutes to allow the flow of the polymer resist into the mould cavities. Then the temperature is lowered to solidify the patterns. The mould is detached to leave the pattern on the

substrate. A thin residual layer that is originally left on purpose to avoid the direct contact between the substrate and the hard mould is then removed by reactive ion etching (RIE). Adapted from [11]
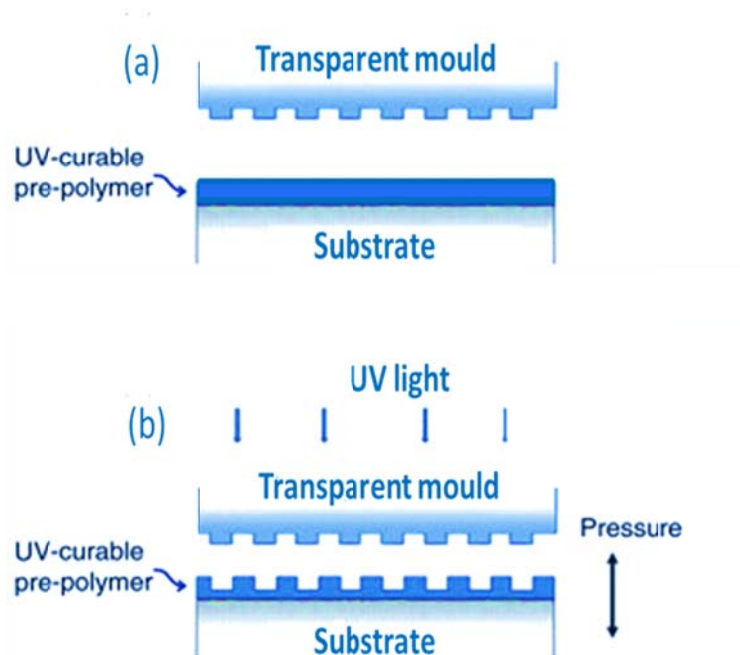
Figure 3.2: Schematic illustration of UV NIL. (a) The substrate is coated by a UV-curable liquid polymer resist. (b) A transparent mould (quartz glass) is pressed into the substrate. The imprinted nanostructures are cured by UV-radiation applied to cross-link the polymer resist and to facilitate pattern formation on the substrate at room temperature and under reduced pressure (0-5 bar). Subsequently, the mould is released leaving the imprinted structures on the substrate. Adapted from [11]

The resist used is a key in the process; usually a polymer curable upon heat or UV-exposure is used. The material of the resist can be chosen depending on the adhesion desired between the resist and the template [60]. Variable materials can be used with different properties. Regarding the mould manufacture, a hard mould is typically fabricated by electron beam lithography, focused ion-beam etching and dry etching techniques [61], or a variety of other

innovative techniques to yield a high nano-sized resolution [62]. Many reviews on types of moulds, resists and conditions of the NIL process [47, 63-65] and commercially available imprint moulds [66] have been published. Generally, the considerations for the mould fabrication include the hardness, thermal expansion coefficient and compatibility. Variable parameters such as the chemical, physical patterning and mechanical aspects as well as the interface interaction and its effect on mould filling and the de-moulding process [67-69] play an important role in NIL.

- Thermal nanoimprint lithography (T-NIL) relies on the mechanical embossing of a mould into a thermoplastic resist. Main limitations are the high temperature and pressure applied.

3.5.   Ultra-violet NIL

Ultra-violet nanoimprint lithography (Figure 3.2) is performed by coating the substrate surface with a UV-curable liquid resist. An optically-transparent mould is used to press into the substrate, and then UV radiation is applied to solidify the resist. It provides several advantages, such as reduced cycle time, lower cost, as well as polymerisation at room temperature [44]. All these factors yield to the success of UV-NIL. However, it is difficult to replicate patterns with high aspect ratio and high density with UV-NIL. This is due to the high force needed to remove the pattern formed from the mould. In an attempt to overcome this challenge, an anti-reflective glassy carbon mould was used to aid in the release of the pattern from the mould. Results showed that the force of release is dependent on the surface area of the mould [70].

Strong and significant advances have improved the nanoimprinting process throughout the years. Step–and-flash imprint lithography (SFIL) is one of them. In this technique, a monomer of

low viscosity is deposited as drops by ink jet printing without spin coating. The template is then lowered to a contact point with the resist. The resist flows to fill in the gaps between the substrate and the template topographies by the capillarity effect. Subsequently, UV irradiation is applied to cause polymerisation. The lowest possible pressure (<0.02 atm) among all other techniques is used in SFIL. The drop injection renders SFIL useful for patterning on non-planar surfaces [71]. Step and flash imprint lithography (SFIL) is a good example for an optimised automated operation with reduced defects and contamination [72]. The alignment accuracy is about 10 nm [73]. Glangchai *et al*. used SFIL to form nanoparticles with uniform 50 nm size and shape using macromers. These nanoparticles are enzymatically-triggered to release an encapsulated drug. This novel incorporation of nanoimprinting represents a high-throughput technique with a precise control of the nanoparticles size. SFIL requires neither high temperature nor exposure of UV radiation for a long time. SFIL showed many advantages such as the high accuracy of alignment and uniformity. Besides, it can be used to imprint over a pre-patterned resist. This property suggests that SFIL can perform multi-layering of resists and form 3D scaffolds [74].

Other developments have been studied to improve the conditions of NIL. The air cushion technique used to enhance the uniformity of the applied force was shown to increase the yield as well [75]. Other developments were the incorporation of a biological sample as a template in the process [76], reduction of temperature and pressure applied [77], polymerisation at room temperature [57], and others [78-83].

- In ultraviolet NIL, a transparent mould is pressed into a photoresist, and then UV radiation is applied to harden the resist at room temperature. Limitations are the difficulty to obtain patterns with high density and high aspect ratio.

3.6. NIL variants

Other variants of NIL emerged, such as step and stamp nanoimprint lithography SSIL [84-87], NIL using wafer stamps [88-90], electro-chemical nanoimprint lithography, reverse nanoimprint lithography [55], substrate conformal imprint lithography, ultrasonic NIL, roll-to-roll NIL, and laser assisted direct imprint reverse imprint lithography [63, 64].

Electrochemical nanoimprinting involves using a mould fabricated from a solid electrolyte or superionic conductor. When the mould contacts the substrate, a voltage is applied to initiate electrochemical etching that dissolves the metals in the mould. Metal ions formed by electrochemical etching are then transferred from the film to the mould. A complementary pattern to the mould with sizes of 50 to 500 nm on metal silver surface are formed [91]. A continuous roll-to-roll NIL (R2RNIL) technique can imprint nanostructures with high-throughput and speed. Ahn *et al*. demonstrated a roll-to-plate imprinting (R2PIL) on a rigid substrate as well as R2RNIL on a flexible web to transfer nano-gratings in a large area of 4 inch wide with high-throughput. The continuity of the technique provides a uniform applied pressure on the resists [92]. Continuous UV roll NIL technology was also described [93].

Molecular imprints Inc. introduced the jet and flash imprint lithography[TM] (J-FIL[TM], 2009) which is used to design a nanopattern layer-to-layer alignment in semiconductor and memory devices with high resolution, extendible to sub-10 nm resolution and low cost production. Low

viscosity imprint fluids are used, of which a drop is dispensed in a controlled-on-demand-manner depending on the template pattern desired. These two properties, the adaptive material dispensing and the low viscosity nanoimprint fluids results in control of the residual layer with dimension uniformity. This technique is performed at room temperature and uniform low pressure, which is advantageous. Furthermore, the transparent template used in J-FIL^{TM} is a key to yield a high resolution layer-to-layer alignment.

- Many variants of NIL have developed to either provide different parameters and advantages or to avoid specific limitations of established techniques.

3.7. Reverse nanoimprint lithography

Reverse nanoimprint lithography (RNIL) [55, 94] is a relatively recent technique that inherits the concept of conventional NIL and adapts advantages over it. In conventional NIL, the substrate is spin-coated by a polymer layer before being stamped by a hard mould to deform the polymer film and to create thickness contrast. Hence, high temperature and pressure are needed, typically at least 70°C above T_g and pressure of 10 MPa [95-97]. Noticeably, in the reverse nanoimprinting technique (RNIL), the liquid polymer resist is poured into the mould with no pressure applied, spin-coated and cured by thermal application. Hence, a replica of the mould pattern is formed in the polymer resist, then peeled off and transmitted to the substrate at appropriate pressure and temperature as shown in Figure 3 [11]. This advantage allows for the usage of substrates which are hard to be spin-coated with a polymer, for example flexible polymer substrates [55]. Also the reduction of temperature and pressure compared to T-NIL shortens the time of the imprinting and eases the change of the pattern upon cooling [98]. The

consequentially transffered pattern is used as a substrate for cell culture or as a negative mould

for a new nano-imprinting process which allows for enhancing the durability of the original

mould.
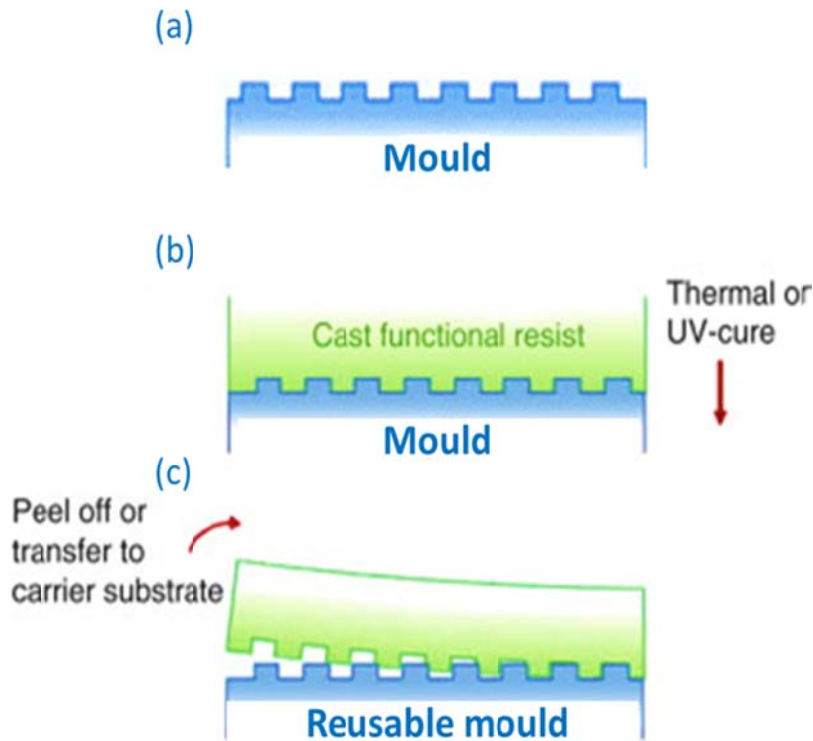
Figure 3.3: Schematic illustration of **r**everse nanoimprint lithography (RNIL) (a) A mould with desired nano-features is used. (b) The liquid resist is poured into the mould structures without pressure. The resist is spin-coated and cured by thermal or UV cross-linking. (c) The cured resist is peeled off and transferred to either a substrate or to pre-patterned resists to form topographical substrates for cell cultures. The resulting substrate can be directly used as a cell substrate or it can be used as a negative mould for another imprinting process and can hence increase the durability of the master mould. Adapted from [11]

Huang *et al*. successfully transferred the patterns from the mould to the substrate by three

different modes i.e. inking, embossing, and whole-layer transfer. This was done by controlling

both the temperature and the surface planarisation of the polymer resist. The surface

planarisation is characterised by the average peak-to-valley height of the coated resist. The solution used for spin-coating is the parameter that most strongly controls the thickness of the layer. By adjusting the degree of surface planarisation after spin-coating, pattern transfer can be accomplished in the inking and whole-layer transfer modes at temperatures and pressures as low as 30 °C below T_g and 1 MPa, respectively, which is significantly beneficial. At this lower temperature, the pattern transfer was found to be strongly dependant on the planarisation degree. If the polymer coating is non-planarised on the mould, the protruded areas only will be transferred to the substrate, resulting in so called inking pattern transfer. But if the polymer is planarised, then the entire polymer coat is transferred to the substrate which is called whole-layer transfer. The nature of these two modes only requires minimal dislocation of the polymer film which renders RNIL less prone to polymer flow problems [55].

To reduce the high temperature and pressure requirements, Borzenko *et al*. modified the conventional NIL by applying the polymer bonding method. In this method, the polymer is applied on both the mould and the substrate to facilitate their bonding at reduced temperature and pressure. A specific treatment is used to leave the polymer on the substrate only after cooling. However, this method leaves a thick residue layer after the imprinting which complicates the subsequent transfer steps [99, 100].

- Reverse nanoimprint lithography (RNIL) is similar to T-NIL; however the thermoplastic resist is applied on the mould rather than the substrate. RNIL provides opportunities to use a variety of flexible polymer substrates which are difficult to be covered with a polymer.

3.8.   Reverse UV-NIL

In this method, a liquid UV- curable polymer resist is dispensed in a mould which is spin-coated, and then cured by UV- cross-linking to form the desired nano-patterned structures. The patterned resist can either be transferred to a substrate to act as a functional cell culture substrate or can be transferred to a pre-patterned resist to build up a three-dimensional (3D) scaffold [11]. Combining RNIL with UV-NIL enables 3D structuring at reduced temperature and pressure. Hu *et al*. fabricated micro and nanostructures of an adhesive material, SU-8, at 50 °C, 1MPa and 1s of UV exposure. SU-8 is a commonly used epoxy-based negative photoresist. It is highly transparent in the UV-range which renders it ideal for imaging. Gratings of sizes from 100 nm to 1 μm were formed. This process was repeated to yield cavities and channels with sizes ranging from 400 nm to 10 μm [98]. The 3D patterning of nanoimprinted substrates is the first step in the development of nanoimprinted cell culture scaffolds.

- Reverse ultra violet NIL is related to UV-NIL; however the photoresist is applied on the mould rather than the substrate.

3.9.   Combination of NIL with other techniques for cell culture applications

Many research groups combined both types of NIL with other methodologies to optimise the results. One of the alternative competitive methods is microcontact printing (μCP) which is a lithographic method. It is an inking approach in which an elastomeric stamp is used with self-assembled monolayers (SAMS) which acts as the ink. Consequently, The SAMS are transferred to the substrate for further characterisation and processing of the chemical surface [101]. Hu *et al*. reported the fabrication of a hybrid environment of nano and micro structures using soft UV-NIL, photolithography, reactive ion etch (RIE) techniques as well as micro-contact printing

(µCP) [102]. The formed nanopatterns were used to grow Hela cells. Results showed alignment, elongation as well as preferential localisation of cells at the nanolines formed. Another example for the combination of techniques is that of laser interference lithography (LIL) and UV-NIL. Although LIL is a simple, quick and easy method to fabricate nanopatterns, it has some limitations, namely the non-selectivity of produced patterns and difficulty of size restriction of maximum and minimum structures. On the other hand, fabricating master stamps by NIL is costly. In order to reduce the costs, LILL is used to fabricate the master stamp, subsequently, NIL is performed to form replicas used as cell substrates. Combining both techniques is advantageous to limit the non-selectivity of LIL as well [103]. Therefore, Lee *et al.* used LIL to fabricate a master stamp where a quartz wafer was coated with a photoresist of 1 µm thickness. Two series of laser exposures were performed at the interference state. The sample was rotated by 90 degrees before the second exposure. The photoresist was hard-baked to develop the patterns. These nano-patterns were then transferred by a reactive ion etching (RIE) process onto a quartz wafer coated with a Cr layer. At this point, a negative replica is produced. A further RIE process was performed onto a quartz substrate to obtain a positive replica. The produced replicas are used as substrates for cell culture. Two patterns were obtained, i.e. a dense pattern and a scarce pattern. Patterns 1 and 2 are nanopillars round in shape, 123.3 and 130.1 nm in diameter, 200 and 500 nm in height, with an interval of 163.6 and 438.7 nm, respectively. The ratio percentage between pattern area and unit surface area of original flat surface was ~14.5 for pattern 1 and ~4.1 for pattern 2. Human osteoblasts (hFOB1.19) were cultured on the two patterns as well as on a flat control surface. Cells on scarce patterns showed good adaptation to the pattern and filopodial extension with high directionality. Cells on dense patterns showed filopodia with different turning points that indicated difficulty in finding the pathway of

migration. The authors concluded that the contact guidance is dependent on the ratio of the pattern surface area to the pattern interval [104]. Rajput *et al.* recently used nanoholes with a gradient array of relative spacing ratios on a fused silica layer to form nanoneedles structures. Using nanoimprinting, the negative replica of the nanoholes was extracted by a polymer layer, on which silica was placed to form nano-needles. The pattern varied from 10 μm to 50 μm in one micron increments in both orthogonal directions in a spatial 2D gradient array. When fibroblasts were cultured on nanoneedles, an enhancement in cell adhesion was observed compared to flat silica surface which is due to the interaction between ECM components and nanoneedles, and prevention of cell aggregate formation [105].

As described in the introduction, the mechanism of cell response to different nanopatterns had been poorly understood before the emerging of NIL. Cells cultured on hydrophobic nanopillar surfaces had shown poor spreading and adhesion [39]. Later, the role of the type of nanotopography in guidance and cell spreading was investigated in 2010 by Hu *et al.* The authors used nanoimprinting followed by demould-induced feature elongation to obtain nanopillar topographies with pillars larger than the mold depth. After seeding human foreskin fibroblasts on nanopillar topographies with 150 nm, ~700 nm, or 1 μm in height, these cells also spread poorly on both the hydrophobic and hydrophilic nanopillar surfaces due to the restricted area at the tops of the pillars which did not suffice for the formation of micron-scale focal adhesions between the cells and the surfaces. The authors therefore suggested nanopillar topographies for surfaces on which cell spreading needs to be avoided [106].

In a study by Xie at al., on the contrary, nanopillar arrays were used to pin the position of neurons and to serve for better cell attachment. Similarly, as in the report described above, the

nanopillar dimensions were 150 nm in diameter, and 1 μm in height. However, Si and SiO2 nanopillar substrates on platinum and quartz material were chosen for biocompatibility. After pinning the neurons to the nanopillars, the authors observed inhibited migration of the cell body. However, axons and dendrites were observed to freely grow and elongate into the surrounding area [107]. It becomes clear that on a similar nanotopography, different cell types can behave very differently, and that the substrate material plays an important role also.

Another example for the fact that the combination of two parameters, rather than one [38], namely topography and culturing time, can significantly change the cellular alignment fibroblasts was reported by Loesberg *et al*. The authors determined the orientation angle of cells by measuring the angle between the direction of the grooves and the direction of cell growth which was determined by the maximum cell diameter to determine cell orientation. Loesberg *et al*. found that fibroblasts seeded on nanogrooved polystyrene (PS) substrates had aligned with the nanotopography of the substrates after only 4 h if the grooves were at least 100 nm wide and 75 nm deep. Contact guidance reflected in fibroblasts orientation according to the grooves was even observed in only 35 nm deep grooves 24 h after cell seeding. The authors therefore concluded that the grove depth is the most determining parameter, although interdependence with culture time becomes obvious [108]. This is in contrast with a value reported by Dalby *et al*., who showed that lamellapodia and filopodia still show interaction with random nano islands as shallow as 10 nm [33].

Nanotopographical substrates were also used to investigate nuclear deformation in human mesenchymal stem cells as it is known that nanoscale features can initiate cell-matrix adhesion signals that, mediated by the cytoskeletal network, are transduced to the nucleus. Chalut *et al*.

therefore used a combination of soft lithography and T-NIL to obtain nanograted poly(dimethylsiloxan) (PDMS) and PS substrates which were coated with collagen for cell culture purposes. The authors were able to show by fluorescence microscopy and live cell imaging that nuclei of stem cells oriented and extended along the axis of the grating if grown for 48 h on nanograted the PDMS or PS substrates. They also found that the mechanical properties of the substrate were an important parameter as shown by more rapid nuclei elongation on the stiffer PS substrates [109].

Johansson *et al*. also found that sympathetic and sensory ganglia cultured close to nano-printed patterns in polymethylmethacrylate (PMMA)-covered silicon chips showed axonal outgrowth on ridge edges and elevations only tone week. The authors used electron beam lithography (EBL) and T-NIL to fabricate PMMA-covered silicon wafers and fast Fourier transform (FFT) analysis in order to quantify the alignment of the axonal outgrowth of ganglia. They described that axons were guided by nanoimprinted polymer patterns of at least 100 nm and concluded that the ratio of axon diameter and groove width was the major determinant affecting axonal guidance [110].

Crouch *et al*. directly imprinted tissue culture polystyrene (TCPS) with gratings of various pitches and depths using T-NIL after preparing their molds by UV contact photolithography and inductively coupled plasma (ICP) etching. To obtain 3D collagen-like structures with nano- and microstructures, they used double-imprinting. Human foreskin fibroblasts were seeded on the substrates and fixed 24 h later and found to align and elongate efficiently at increased aspect ratios of the nonpattern width and depth. Although they found that the aspect ratio can describe

the cell behaviour, they also acknowledged that differences in cell types, culture conditions, and structure variation makes predictions difficult [111].

Although by far the most studies investigating cell guidance on nanotopographies have employed fibroblasts, other reports describe the growth of cells such as mesenchymal stem cells [109], neurons [107, 110, 112], astrocytes [113] or cardiac aorta endothelial cells [114] on nanoimprinted substrates. In a study investigating astrocyte reactivity, Ereifej *et al.* used UV-NIL and pre-made reflective holographic-grated molds to obtain poly(methyl methacrylate) (PMMA) patterned substrates with either a period of 3600 grooves/mm or 1800 grooves/mm. The authors found that C6 rat astrocytoma cells seeded on the differently nanopatterened and non-patterened substrates showed less protein adsorption, less cell adhesion, proliferation, and viability if seeded on the 3600 nanopattern surface. They concluded that this particular nanopattern could be beneficial for the fabrication of neural electrodes to avoid glial scarring and astrogliosis after microelectrode implanation [113].

Similarly, Baranes *et al.* demonstrated that leech neurons growing on nano-scale line-pattern ridges develop more simplified neuronal branching tree [112]. Their observations that small filopodia attach to the nano-ridges which guides the neuronal growth direction is in line with findings by Johansson *et al.* described above [110].

In another example of neuronal cell culturing on nanoimprinted substrates, the impact of topographical noise, such as protein aggregates [115], and cellular debris [116], on the guided growth of neuritis was investigated. Tonazzini *et al.* used T-NIL to produce noisy nanogratings of 500 nm ridge and 500 nm grooves. Different substrates with variable percentage of noise and

cell-dependant directionality were fabricated. Differentiating neuronal PC12 cells were cultured on the patterned substrates, and observed for alignment and guidance. Results showed that the loss of neurite guidance is not linear to increasing the topographical noise. It is rather a threshold effect that is associated with the spatial arrangement and the focal adhesion (FA) maturation. Lastly, an antineoplastic drug, that promotes cell contractility, nocodazole, stimulated aligned FA maturation when incorporated in the scaffold and hence boosted the alignment. This suggests that using specific drugs can modulate the cell culture conditions and cellular growth on cell substrates [117].

In 2009, Idota *et al*. used graft-polymerisation with an electron beam (EB) lithography system to fabricate temperature-responsive micrometer and nanometer-patterned poly(N-isopropylacrylamide) (PIPAAm) layers with a 200 nm line-width. The authors found that fibroblasts and cardiac aorta endothelial cells growth was guided by the pattern orientation at temperatures above the lower critical solution temperature (LCST) but detached, shrunk and folded along the pattern below the LCST. It was concluded that this nano-scale system may allow engineering of functional 3D cell sheets or spheroids [114].

Table 3.1: Classification of nanoabrication methods in terms of type of energy sources. For each method, important characteristics, polymer used, advantages and disadvanatages are summerised.

Source of Energy	Technique	Important Characteristics	Advantages	Disadvantages	References
Thermal	**Thermal NIL (T-NIL)**	Physical deformation of thermoplastic polymer above T_g	High resolution. High throughput. Low cost.	High temperature High pressure (50-100 bar)	[42] [48] [118]

				Simple set-up. Short procedure.	Mechanical tension	
	Reverse NIL (RNIL)	Thermal cure is applied to liquid resist. Pattern is formed on mould then transferred to substrate.		Possible for substrates that are not suitable for spin-coating and those with surface topographies. Short process. No external pressure.	Pattern transfer can be challenging	[47, 51]
Optical	**Ultraviolet NIL (UV NIL)**	UV curable polymer resist dispensed and spin-coated on substrate.		Room temperature. Low pressure (0-5 bar). Short process. Low cost.	Hard to replicate patterns with high density and high aspect ratio. Difficult to release pattern from mould.	[44] [118]
	Reverse UV NIL	UV curable liquid resist. Pattern is formed on mould then transferred to substrate.		Enables 3D patterning by repeating the process. Reduced temperature. Reduced pressure.	Pattern transfer can be challenging.	[98]
Chemical	**Microcontact printing (µCP)**	Pattern transfer to a substrate through relative difference		Simple. Low cost. Versatile.	Stamp deformation during removal from template.	[101, 119-121]

		between surface energies.	Elastomeric stamps afford sufficient mechanical strength to print 500 nm structures.	Lower resolution of patterning and decreased reproducibility. Contamination with uncured fragments. Swelling of stamps by organic solvents.	
Electrical	**Electro-chemical deposition**	Electrochemical oxidation/reduction between conductive and ionic interfaces.	Yields highly accurate structures.	Only applicable to conductive or ionic materials.	[91] [122, 123]

- Combining more than one nanoimprint technique as well as other distinct methods can account for optimising the resultant patterns and eliminate undesired fabrication steps. Most cell culture substrates were fabricated through a combination of methods, and substrates that promote cell guidance, that pin cells to a certain area, that inhibit cell adhesion, or that allow for the growth of spheroids are discussed.

3.10. 3D patterning

In reality, the fabrication process of a 3D environment can be expensive and complicated. Several conventional techniques can construct complex 3D nanoscaffolds, classified as lithographic and non-lithographic techniques. Lithographic techniques include electron beam lithography [124] and soft lithography [125], capillary force lithography [126, 127], polymer

transfer printing, decal-transfer lithography [128], and ion projection lithography as reviewed [129, 130]. NIL can be used to build 3D substrates with inter-connected material using single lithography by either direct nanoimprint lithography over pre-patterned resists or by vertical layer-to-layer stacking of resists, shown in Figure 3.4 [94, 131].
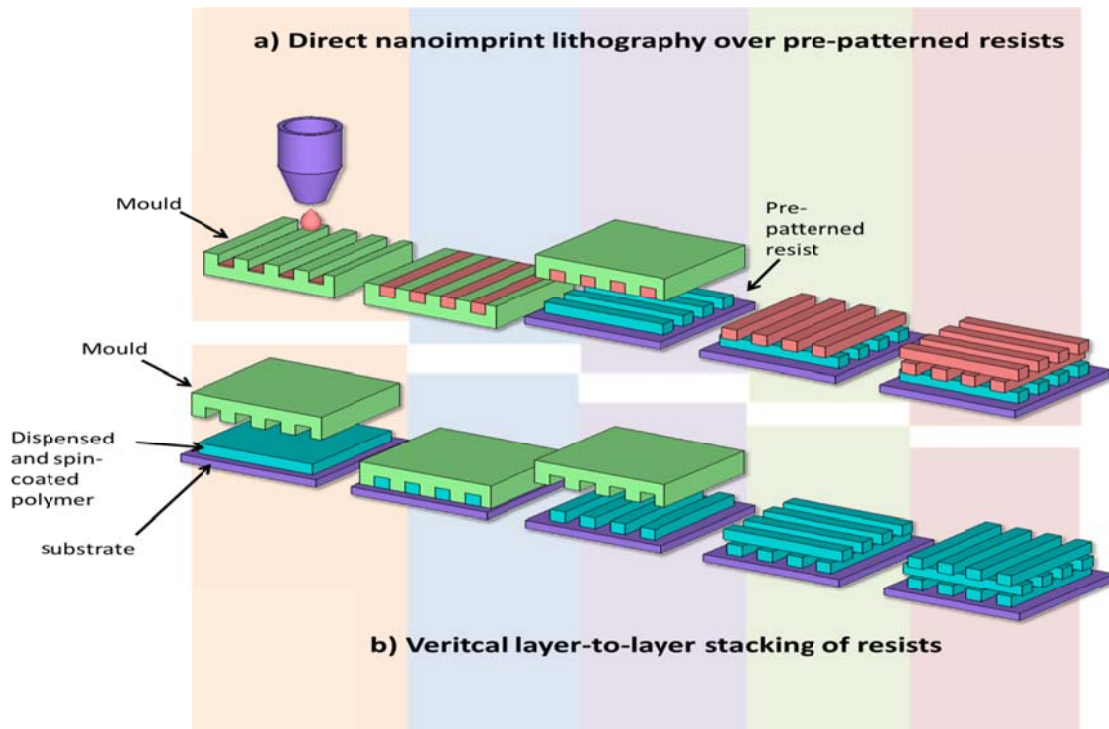
Figure 3.4: 3D Patterning a) Direct nanoimprint lithography over pre-patterned resists. A polymer resist is dispensed in the mould to occupy the spaces between the mould cavities. The mould is thermally or UV cured to fabricate a nanopattern. This mould contacts a substrate with pre-patterned nanostructures to detach and transfer the secondary patterned resist from the mould to the substrate. A two-level pattern is formed. This process is repeated to form the desired 3D environment. b) Vertical layer-to- layer stacking of resists. A polymer resist is dispensed and spin-coated on a substrate. A mould is embossed into the resist. Thermal or UV cure takes place to form a nanopattern. The mould is released leaving the pattern on the substrate. This process is repeated to yield another layer of pattern which is transferred and stacked on the previous layer. This process continues with the number of layers essential to form a spatial arrangement for 3D growth of cells. Adapted from [132, 133]

In vivo, cells are exposed to physical directional cascade signals due to their existence in a 3D environment with certain topographical noise as discussed above [115, 116]. For example, cell guidance is also significantly altered if cells are cultured on a 3D scaffold with more than one type of cells. One example for cross-talk between two different filopodia populations was reported by Jang *et al*. The authors provided a 3D model to understand the guidance mechanism induced by artificial nanotopographies resembling ECM cues in neuronal cells. They used two different populations of filopodia at the growth cone. UV-NIL was used to fabricate arrays of parallel ridges (350 nm wide and 350 nm high, separated by grooves of 1, 2, 3, 5 times 350 nm width increments). Laminin, an ECM protein, was presented on a line nanopattern. The neurite outgrowth was shown to be oriented along the line pattern and the neurite length increased. Neurite outgrowth is a conventional behavior of the growth cone involving the two populations of the filopodia. The authors described the cross-talk between the two filopodia populations which regulated the sensing mechanism of nanotopographical stimuli. This cross-talk happens by the integration of the signals originating from the two populations but was not observed on a non-topographical substrate [134].

Three dimensional moulds can be used in NIL for direct 3D patterning. Li *et al*. used 3D moulds in a single-NIL-step. Moulds were fabricated by a single step electron beam lithography and reactive ion etching (RIE), then imprinted in polymer templates to yield three dimensional metal T-gates and air–bridge structures of sub 40 nm size [135]. The availability of 3D patterning stamps can allow for more opportunities and can reduce the cost of the process. Stamps are fabricated by various techniques, mostly electron beam techniques [136] [137], focused ion-beam (FIB) milling [138-140], focused ion-beam etching [141, 142] and two photon

polymerisation [143, 144]. Other advances have developed to overcome the challenges of 3D mould fabrication [145, 146].

Reverse nanoimprint can be used to construct multi-layer 3D nanostructures as described before [94]. Tavakkoli *et al.* used RNIL to fabricate a uniform nanostructured discrete-track recording media at a 50 nm track pitch in order to increase the current capacity of the magnetic hard disk recording media [147]. This study revealed even more advantages of RNIL over conventional NIL, such as the speed of the imprinting process, and a thinner residual layer.

Multi-layered nanostructures can be built by layer-by-layer stacking of nanostructured layers via reverse nanoimprinting which does not require a planarisation layer and therefore is a desired technique. Multi-layering has recently been reviewed elsewhere [148, 149]. Multi-layering by UV curable resists [150] avoids the formation of unfavourable residual layers and takes place at relatively low temperature and pressure compared to T-NIL. On the other hand, it is not easy to detach the cured structures which are used as templates later in the process. In distinction, thermally curable resists are easily detached, however one limitation to this technique is the relatively high temperature involved in the pattern transfer step near the glass transition temperature T_g of the resist which may cause the flowing and deformation of the bottom layer. To overcome this problem, two moulds with different silane treatment can be used to stack the two layers [151]. To overcome the high temperature limitation, Bao *et al.* used reverse thermal nanoimprinting with reduced T_g to stack three different polymers [94], however this methodology is limited in the type of polymers that can be used and in number of polymer layers that can be stacked. Therefore it was necessary to develop a technique to stack multilayers from one polymer.

Hu *et al.* used a simple NIL method to imprint 3D nanostructures on the widely used tissue culture polystyrene plates (TCPS). The process started by traditional NIL to imprint the first layer; however the second step was performed at a reduced temperature and pressure to avoid disturbance of the first layer. The second imprint was repeated for multiple layers to fabricate a 3D scaffold with 350 nm to 10 μm gratings to study the effects of nano versus micro-patterns. Bovine pulmonary artery smooth cells (SMCs) were cultured on both patterns. Cell alignment and elongation was significantly higher in cells cultured on nano-patterns [152].

Following a similar strategy, Yoshii *et al.* developed 3D nano-culture plates (NCPs) by imprinting into resinous inorganic sheets that were used to culture tumour cells. Tumour cells grown on NCPs formed cell aggregates and attached to the nano-imprinted scaffold via the elongated lamellipodia. Consequently, these tumour cells produced multi-cellular spheroids which resemble in *vivo* tumour conditions. All these properties were lacking in cells grown on non-patterned scaffolds. Also it was found that 17 genes were overexpressed in cells grown on NCPs, including hypoxia-induced factors target genes and genes relevant to intracellular interaction and multicellular organisation [153].

Yew *et al.* used a single polymeric material to fabricate double and three-layer residual-free nanostructures using reverse T-NIL [133]. A one dimensional grafting with ridges around 250 nm width and 200 nm depth was transferred from the mould to the substrate in an orthogonal arrangement. Using a single material ensured avoiding another bonding material and the need for a planarisation layer. The stacking of the layers occurred at the T_g. On the other hand, some limitations occurred, such as a 30% compression in the lower layers to guarantee good adhesion

between them; however, by optimizing the fabrication conditions, such as the pressure, the compression can be avoided.

Nakajima *et al*. fabricated multi–layers by applying a differential temperature between the lower layer (below T_g) and the upper layer (above T_g) [154]. Another recent technique, named reverse contact UV NIL, was developed by Kehagias *et al*. in 2007, which is a combination of nanoimprint lithography and contact printing lithography. The main purpose of combining these two techniques is to obtain 3D wood-pile like nanostructures and to transfer this pattern with no residual layers. This technique avoided the undesired etching processes that are typically necessary to remove the residual layer [155]. In 2013, Han *et al*. used RNIL to fabricate 3D nanostructures with a UV curable resin and a resin of dispersed zinc oxide (ZnO) nanoparticles [131]. The UV-curable resin was transferred from a silicon stamp to a substrate as a 2D dual-sided pattern layer. In this transfer step, a diluted UV-glue was used to increase the adhesion force between the pattern layer and the substrate without generating a thick residual layer. A ZnO dual side patterned layer was also fabricated. ZnO nanoparticles of 40 nm in size were used as a higher refractive index material to increase the photonic effect. After repeating these RNIL steps and stacking the 2D layers, a 3D structure was obtained. Haitainen *et al*. used T-NIL to linearly pattern micro gratings on top of nano pre-patterned structures [85]. Then step and stamp nanoimprint lithography (SSIL) was used to regulate the positioning and angle of the stamp rotation.

Inclined nanoimprint lithography (INIL) is another technique used to develop 3D nanostructures in a single-imprinting step without the need to use a 3D template or multiple steps. In INIL, a polymer with an anisotropic dewetting phenomenon is used where the

inclination angle controls the degree of anisotropy. An INIL apparatus induces a zero inclination angle leading to asymmetry in the polymer flow path, resulting in 3D nanopatterns with different heights [156].

Despite recent progress in nanoimprinting and the development of many new techniques and combinations of techniques, overall, more research is needed to optimise the nanoimprinted 3D moulds, substrates, and products as cell culture scaffolds. In summary, multi-layering of NIL resists offers many advantages; however, the development of new instruments including multi-layer aligners is required for such improvement.

- Three dimensional cell (3D) substrates provide conditions closer to the *in vivo* environment and can be obtained by either direct nanoimprint lithography over pre-patterned resists or by vertical layer-to-layer stacking of resists. Only very few reports in the literature are available so far.

3.11. Concerns

Addressing the concerns associated with NIL is a step forward towards its success. One challenge is the template wear, which was addressed by Kumar *et al*. They showed that nanomoulding of the template, performed by metallic glasses as amorphous metals can yield sub 100 nm patterns at a reduced cost of the template [157]. Another solution presented was a programmable re-usable template to reduce the cost of templates and avoid template wear [73]. Another concern is that NIL processes rely on other lithographic techniques such as electron-beam lithography or focused ion beam patterning to fabricate the mould with high resolution.

However some self-assembled structures for templates were established by NIL at a high resolution of sub 10 nm scale [158].
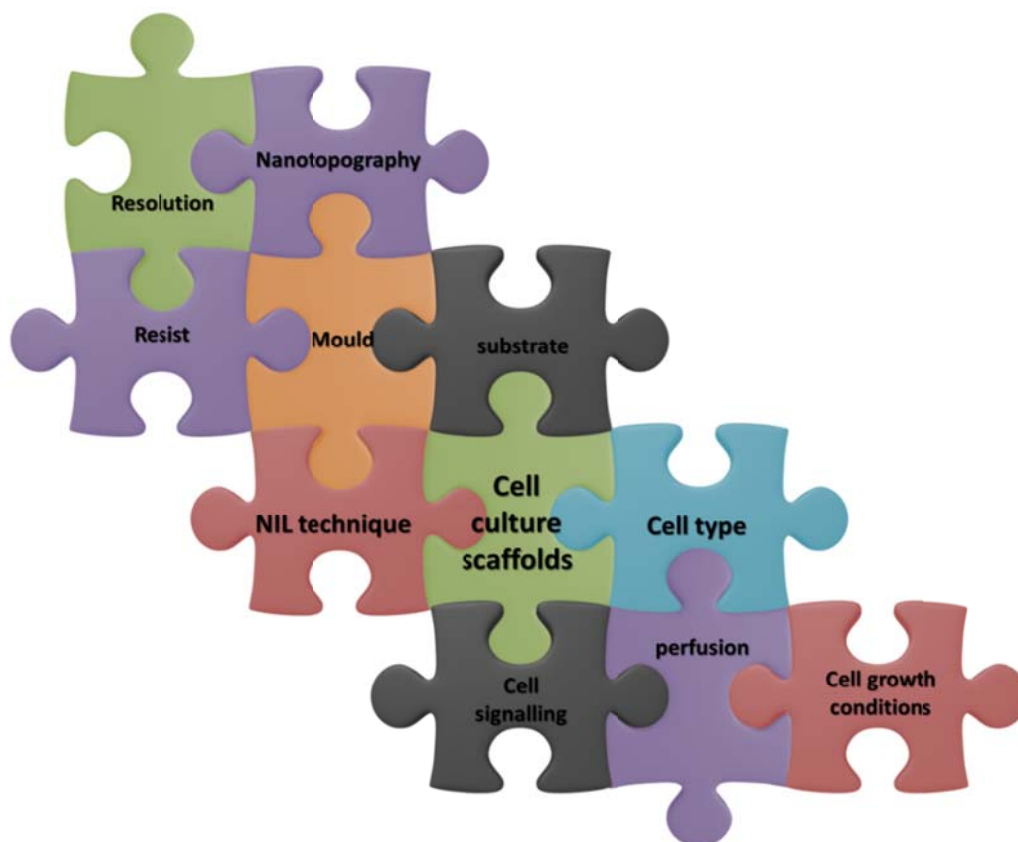
Figure 3.5: Parameters involved in the design of cell substrate. Fabrication aspects include the composition of mould, resist and substrate, size of nanostructures, texture, wettability, rigidity, as well as the method used, etc. Fabrication aspects highly influence the resolution and cost of method. Biological aspects include the cell type and its inter-facial interaction with the substrate. After given cells are cultured on substrate, many other cell behavioural factors are counted in, like cell growth conditions, cell migration, alignment, growth, signaling, etc   All those parameters are inter-connected, hence they should be all considered in the optimisation of the design process. Understanding these parameters can determine which technique is best to be used.

Here, we report on several approaches to use nanoimprinted scaffolds for cell culture. However, the optimisation of scaffolds for cell and tissue culture involves not only the NIL

technique, resist, mould and substrate, but also needs to take into consideration the biological parameters such as the cell type, cell signalling, perfusion, and many other factors involved. As shown in Figure 3.5, a multitude of factors interplays with each other.

- Optimising NIL parameters by reducing the template wear, cost and increasing the resolution is necessary for an effective technique.

3.12. Applications

Nanoimprint lithography is regularly applied in the area of nanofluidics [159] which studies the complex fluid behaviour confined to nanostructures. A modified nano-imprint technique was described to develop nanofluidic devices with specific dimensions [160, 161]. In another approach, the fabrication of an extremely long (1.5 cm) fluidic channels with sub-20 nm diameter by nano-imprinting mould fabrication is useful in developing biochemical sensors with higher sensitivity [162]. This report, however, highlights several studies in which nano-imprinted scaffold were used in cell culture and showed to mimic the natural environment of cells significantly better than a cell culture flask.

- Nanoimprint lithography (NIL) is applied in diverse and broad research fields, i.e. studying cell response to substrates, nanofludics, and biochemical sensors.

3.13. Conclusion

Nanoimprinting lithography represents a useful tool to imprint 3D scaffolds due to the high precision, well controllability and unique flexibility. Different geometries with a wide range of polymers including biodegradable and biocompatible polymers can be modified to meet the

needs of the fabrication process and the yielded scaffold. It is certain that the research undertaken so far to examine the effects of substrate properties on cell responses enhanced our comprehension. Certainly, topography affected cell morphology, cytoskeletal rearrangement, adhesion, differentiation, proliferation and gene expression. Not only the surface features, but also the cell type greatly influences the results. With this knowledge in mind, we can tailor cellular responses and better implement them to bio-mimic the natural conditions of cell culture. There is, therefore, a definite need to discover which substrate topography; each cell type favourably grows on. To attain a highly functional scaffold, many fabrication parameters are important as reviewed here, which provides a wealth of possibilities. However at this point, there is no up-front answer to the question of how to optimize topographical scaffolds for cell cultures. So far, a trial-and-error approach has been followed, which intrinsically limits the outcomes to what is achievable instead of what is desired.

- Many NIL techniques exist, with variable advantages and disadvantages to suit the used material, fabrication steps and desired substrate. Hybridisation of techniques allows for more options.

3.14. Outlook

It becomes obvious that the applications for nanoimprinted scaffolds are very broad. However, also the choice of techniques for nanoimprinting and the variety of materials are vastly diverse. With this review, we give an overview of previous and possible nanoimprinting technique as well as their advantages and disadvantages that partially pose limitations on combinations of a technique with a certain material. New combinations of techniques and

materials, however, may also develop as more research is performed. So far, applications are still limited and very experimental, but an increase in model development, correlation of factors and results for a better prediction of successful models, as well as a strong increase in publications describing nanoimprinted cell and tissue culture models is expected.

We believe research in this field is advancing in two main directions. The first one would be the optimisation of the polymer and scaffold properties. The second one could involve integrating more ECM components into the cell culture conditions, i.e. proteins, lipids, glucosamines, and others. Cells interact with ECM via transmembrane receptors called integrins which link the ECM to molecular complexes that bind to actin filaments [163]. Interactions mediated by integrins regulate cell adhesion, differentiation, migration and metastasis [164, 165]. Different integrins interact with different ECM ligands. The amino acid sequence RGD (Arg-Gly-Asp) is the main adhesive site in the fibronectin binding region [165-167]. Including transmembrane ligands in cell culture substrates could augment our understanding of various ligand-receptor interactions as described by Schvartzman et al. Their study showed that spreading of mouse fibroblasts increased when at least four sites of ligands were placed within 60 nm or less with no dependency on density [168]. Similar studies with nanoimprinted substrates including receptor proteins or ligands could give insights into interactions of cells with different receptors. Besides, 3D models would be a step towards mimicking the natural conditions of cell growth, but it is anticipated that research will move further towards a complete organ scaffold model. One example could be a lung model, designed and manufactured by nanoimprinting with detailed structures that can possibly be used in the future for transplantation as well as a research model. So far, nanoimprinting has not been employed to fabricate such a

model. However, a sophisticated *in vitro* lung tissue model on a microchip was produced by a technique called microfabrication to reconstitute the human-alveolar capillary interface. This device showed similar structural, functional and mechanical properties to alveolar capillary interface of human lung. It also showed similar physiological effects to nanoparticle absorption as in mouse lung [169]. Such an approach could possibly be followed by NIL techniques. Although a nanostructured organ model is not yet feasible, we believe that this is the ultimate goal in the next years. Developing such macromodels with massive complexity requires the consideration of critical concerns such as the coordinated arrangement of different cell and tissue types in a particular architecture, the vascularization of tissues, and biosafety [171]. Therefore novel solutions are needed to handle those complex macromodels [172]. Also, we expect that in the future cell culture substrates will be further customised based on the properties of the proposed cell line or tissue, such as the morphology, rigidity, perfusion, and many other factors. Examples are cortical bone tissues with concentric cylindrical structure, spongy bone tissues with spongy-like structure [173], skeletal muscles with cylindrical muscle fibers, longitudinally aligned to each other [174], and cardiac muscle cells with a leaflet–like morphology [175].

- Nano-imprinted cell substrates hold great potential in diverse fields. More work is needed to optimise and enrich these applications and to customise the proposed substrate.

3.15.   Acknowledgements

3.16. References

1. Benjamin Geiger, Spatz JP, Bershadsky AD: Environmental sensing through focal adhesions. *Nature Reviews Molecular Cell Biology* 10, 21-33 (2009).

2. Shekaran A, Garcia AJ: Nanoscale engineering of extracellular matrix-mimetic bioadhesive surfaces and implants for tissue engineering. *Biochimica et Biophysica Acta (BBA) - General Subjects* 1810(3), 350-360 (2011).

3. Waldeck HM, Kao WJ: *2.207 - Extracellular Matrix: Inspired Biomaterials*. In: *Comprehensive Biomaterials*, Editor-in-Chief: paul D (Ed.^(Eds). Elsevier, Oxford 113-126 (2011).

4. Abrams GA, Goodman SL, Nealey PF, Franco M, Murphy CJ: Nanoscale topography of the basement membrane underlying the corneal epithelium of the rhesus macaque. *Cell Tissue Res* 299(1), 39-46 (2000).

5. Abrams GA, Bentley E, Nealey PF, Murphy CJ: Electron microscopy of the canine corneal basement membranes. *Cells Tissues Organs* 170(4), 251-257 (2002).

6. Ross AM, Jiang Z, Bastmeyer M, Lahann J: Physical Aspects of Cell Culture Substrates: Topography, Roughness, and Elasticity. *Small* 8(3), 336-355 (2012).

7. Chandra P, Lai K, Sung H-J, Murthy NS, Kohn J: UV laser-ablated surface textures as potential regulator of cellular response. *Biointerphases* 5(2), 53-59 (2010).

8. Bettinger CJ, Langer R, Borenstein JT: Engineering Substrate Topography at the Micro- and Nanoscale to Control Cell Function. *Angewandte Chemie International Edition* 48(30), 5406-5415 (2009).

9. Stevens MM, George JH: Exploring and Engineering the Cell Surface Interface. *Science* 310(5751), 1135-1138 (2005).

10.   Hill RT, Chilkoti A: *Chapter I.2.13 - Surface Patterning*. In: *Biomaterials Science (Third Edition)*, Buddy DR,Allan SH,Frederick JS,Jack E. Lemonsa2 - Buddy D. Ratner ASHFJS,Jack EL (Ed.^(Eds). Academic Press, 276-301 (2013).

11.   Li K, Morton K, Veres T, Cui B: *5.11 - Nanoimprint Lithography and Its Application in Tissue Engineering and Biosensing*. In: *Comprehensive Biotechnology (Second Edition)*, Editor-in-Chief: murray M-Y (Ed.^(Eds). Academic Press, Burlington 125-139 (2011).

12.   Bhatnagar P, Mark SS, Kim I *et al.*: Dendrimer-Scaffold-Based Electron-Beam Patterning of Biomolecules. *Advanced Materials* 18(3), 315-319 (2006).

13.   Stankevicius E, Balciunas E, Malinauskas M, Raciukaitis G, Baltriukiene D, Bukelskiene V: Holographic lithography for biomedical applications. 843312-843312 (2012).

14.   Leong MF, Rasheed MZ, Lim TC, Chian KS: In vitro cell infiltration and in vivo cell infiltration and vascularization in a fibrous, highly porous poly(D,L-lactide) scaffold fabricated by cryogenic electrospinning technique. *Journal of Biomedical Materials Research Part A* 91A(1), 231-240 (2009).

15.   Sultana N, Wang M: *Fabrication of Tissue Engineering Scaffolds Using the Emulsion Freezing/Freeze-drying Technique and Characteristics of the Scaffolds*. In: *Integrated Biomaterials in Tissue Engineering*, (Ed.^(Eds). John Wiley & Sons, Inc., 63-89 (2012).

16.   Rg. H: The culitivation of tissues in extraneous media as a method of morphogenetic study. *Anat. Rec.* 6, 181-193 (1912).

17.   Bettinger C, Borenstein JT, Tao SL: *Chapter 5 - Mechanobiological Approaches for the Control of Cell Motility*. In: *Microfluidic Cell Culture Systems*, (Ed.^(Eds). William Andrew Publishing, Oxford 105-136 (2013).

18.   Russell P, Gasiorowski JZ, Nealy PF, Murphy CJ: Response of human trabecular meshwork cells to topographic cues on the nanoscale level. *Invest Ophthalmol Vis Sci* 49(2), 629-635 (2008).

19.   Karuri NW, Liliensiek S, Teixeira AI *et al.*: Biological length scale topography enhances cell-substratum adhesion of human corneal epithelial cells. *J Cell Sci* 117(Pt 15), 3153-3164 (2004).

20.   Teixeira AI, Mckie GA, Foley JD, Bertics PJ, Nealey PF, Murphy CJ: The effect of environmental factors on the response of human corneal epithelial cells to nanoscale substrate topography. *Biomaterials* 27(21), 3945-3954 (2006).

21.   Pot SA, Liliensiek SJ, Myrna KE *et al.*: Nanoscale topography-induced modulation of fundamental cell behaviors of rabbit corneal keratocytes, fibroblasts, and myofibroblasts. *Invest Ophthalmol Vis Sci* 51(3), 1373-1381 (2010).

22.   Ankam S, Suryana M, Chan LY *et al.*: Substrate topography and size determine the fate of human embryonic stem cells to neuronal or glial lineage. *Acta Biomaterialia* 9(1), 4535-4545 (2013).

23.   Liliensiek SJ, Campbell S, Nealey PF, Murphy CJ: The scale of substratum topographic features modulates proliferation of corneal epithelial cells and corneal fibroblasts. *J Biomed Mater Res A* 79(1), 185-192 (2006).

24.   Hoffman-Kim D, Mitchel JA, Bellamkonda RV: Topography, Cell Response, and Nerve Regeneration. *Annual Review of Biomedical Engineering* 12(1), 203-231 (2010).

25.   Kim HN, Jiao A, Hwang NS *et al.*: Nanotopography-guided tissue engineering and regenerative medicine. *Advanced Drug Delivery Reviews* (0),

26.   Koegler P, Clayton A, Thissen H, Santos GNC, Kingshott P: The influence of nanostructured materials on biointerfacial interactions. *Advanced Drug Delivery Reviews* 64(15), 1820-1839 (2012).

27.   Kim DH, Provenzano PP, Smith CL, Levchenko A: Matrix nanotopography as a regulator of cell function. *J Cell Biol* 197(3), 351-360 (2012).

28.   Yim EK, Leong KW: Significance of synthetic nanostructures in dictating cellular response. *Nanomedicine* 1(1), 10-21 (2005).

29. Martínez E, Engel E, Planell JA, Samitier J: Effects of artificial micro- and nano-structured surfaces on cell behaviour. *Annals of Anatomy - Anatomischer Anzeiger* 191(1), 126-135 (2009).

30. Wen Z, Zheng JQ: Directional guidance of nerve growth cones. *Curr Opin Neurobiol* 16(1), 52-58 (2006).

31. Chaurey V, Block F, Su YH *et al.*: Nanofiber size-dependent sensitivity of fibroblast directionality to the methodology for scaffold alignment. *Acta Biomater* 8(11), 3982-3990 (2012).

32. Clark P, Britland S, Connolly P: Growth cone guidance and neuron morphology on micropatterned laminin surfaces. *J Cell Sci* 105 (Pt 1), 203-212 (1993).

33. Dalby MJ, Yarwood SJ, Riehle MO, Johnstone HJH, Affrossman S, Curtis ASG: Increasing Fibroblast Response to Materials Using Nanotopography: Morphological and Genetic Measurements of Cell Response to 13-nm-High Polymer Demixed Islands. *Experimental Cell Research* 276(1), 1-9 (2002).

34. Dalby MJ, Riehle MO, Sutherland DS, Agheli H, Curtis AS: Use of nanotopography to study mechanotransduction in fibroblasts--methods and perspectives. *Eur J Cell Biol* 83(4), 159-169 (2004).

35. Flemming RG, Murphy CJ, Abrams GA, Goodman SL, Nealey PF: Effects of synthetic micro- and nano-structured surfaces on cell behavior. *Biomaterials* 20(6), 573-588 (1999).

36. Borgesius NZ, Van Woerden GM, Buitendijk GH *et al.*: betaCaMKII plays a nonenzymatic role in hippocampal synaptic plasticity and learning by targeting alphaCaMKII to synapses. *J Neurosci* 31(28), 10141-10148 (2011).

37. Mcilvain HB, Baudy A, Sullivan K *et al.*: Pituitary adenylate cyclase-activating peptide (PACAP) induces differentiation in the neuronal F11 cell line through a PKA-dependent pathway. *Brain Research* 1077(1), 16-23 (2006).

38. Wieringa P, Tonazzini I, Micera S, Cecchini M: Nanotopography induced contact guidance of the F11 cell line during neuronal differentiation: a neuronal model cell line for tissue scaffold development. *Nanotechnology* 23(27), 275102 (2012).

39. Lee J-L, Shen Y-K, Lin Y, Chen W-R: The Nano-topology Influence of Osteoblast-like Cell on the Bio-nanostructure Thin Film by Nanoimprint *2010 International Conference on Nanotechnology and Biosensors IPCBEE* 2, (2011).

40. Dalby MJ, Riehle MO, Sutherland DS, Agheli H, Curtis ASG: Use of nanotopography to study mechanotransduction in fibroblasts – methods and perspectives. *European Journal of Cell Biology* 83(4), 159-169 (2004).

41. Biggs MJP, Richards RG, Dalby MJ: Nanotopographical modification: a regulator of cellular function through focal adhesions. *Nanomedicine: Nanotechnology, Biology and Medicine* 6(5), 619-633 (2010).

42. Chou SY, Krauss PR, Renstrom PJ: Imprint of sub-25 nm vias and trenches in polymers. *Applied Physics Letters* 67(21), 3114-3116 (1995).

43. Biswas A, Bayer IS, Biris AS, Wang T, Dervishi E, Faupel F: Advances in top–down and bottom–up surface nanofabrication: Techniques, applications & future prospects. *Advances in Colloid and Interface Science* 170(1–2), 2-27 (2012).

44. Sreenivasan SV, Choi J, Schumaker P, Xu F: *4.04 - Status of UV Imprint Lithography for Nanoscale Manufacturing*. In: *Comprehensive Nanoscience and Technology*, Editors-in-Chief: david LA,Gregory DS,Gary PW (Ed.^(Eds). Academic Press, Amsterdam 83-116 (2011).

45. Costner EA, Lin MW, Jen W-L, Willson CG: Nanoimprint Lithography Materials Development for Semiconductor Device Fabrication. *Annual Review of Materials Research* 39(1), 155-180 (2009).

46. Wagner DJ, Jayatissa AH: *Nanoimprint lithography: Review of aspects and applications*. In: 2005.

47.   Guo LJ: Nanoimprint Lithography: Methods and Material Requirements. *Advanced Materials* 19(4), 495-513 (2007).

48.   Chou SY, Krauss PR, Zhang W, Guo L, Zhuang L: Sub-10 nm imprint lithography and applications. *J. Vac. Sci. Technol. B* 6(15), (1997).

49.   Ofir Y, Moran IW, Subramani C, Carter KR, Rotello VM: Nanoimprint Lithography for Functional Three-Dimensional Patterns. *Advanced Materials* 22(32), 3608-3614 (2010).

50.   Engel Y, Schiffman JD, Goddard JM, Rotello VM: Nanomanufacturing of biomaterials. *Materials Today* 15(11), 478-485 (2012).

51.   Heidari B, Maximov I, Sarwe E-L, Montelius L: Large scale nanolithography using nanoimprint lithography. *J. Vac. Sci. Technol.* 17(6), 2961-2964 (1999).

52.   Chou SY, Krauss PR, Renstrom PJ: Imprint Lithography with 25-Nanometer Resolution. *Science* 272(5258), 85-87 (1996).

53.   Morita T, Watanabe K, Kometani R *et al.*: Three-Dimensional Nanoimprint Mold Fabrication by Focused-Ion-Beam Chemical Vapor Deposition. (2003).

54.   Hirai Y, Kanakugi K, Yamaguchi T, Yao K, Kitagawa S, Tanaka Y: Fine pattern fabrication on glass surface by imprint lithography. *Microelectronic Engineering* 67-68, 237-244 (2003).

55.   Huang XD, Bao L-R, Cheng X, Guo LJ, Pang SW, Yee AF: Reversal imprinting by transferring polymer from mold to substrate. *J. Vac. Sci. Technol.* B.20(6), 2872-2876 (2002).

56.   Lebib A, Chen Y, Cambril E *et al.*: Room-temperature and low-pressure nanoimprint lithography. *Microelectronic Engineering* 61–62(0), 371-377 (2002).

57.   Khang DY, Yoon H, Lee HH: Room-Temperature Imprint Lithography. *Advanced Materials* 13(10), 749-752 (2001).

58.   Alkaisi MM, Blaikie RJ, Mcnab SJ: Low temperature nanoimprint lithography using silicon nitride molds. *Microelectronic Engineering* 57–58(0), 367-373 (2001).

59.   Khang D-Y, Kang H, Kim T-I, Lee HH: Low-Pressure Nanoimprint Lithography. *Nano Letters* 4(4), 633-637 (2004).

60.   Guo LJ: Recent progress in nanoimprint technology and its applications. *J Phys D: Appl Phys* 37(11), R123-R141 (2004).

61.   Pang SW, Tamamura T, Nakao M, Ozawa A, Masuda H: Direct nano-printing on Al substrate using a SiC mold. *Journal of Vacuum Science & Technology B: Microelectronics and Nanometer Structures* 16(3), 1145-1149 (1998).

62.   Murphy PF, Morton KJ, Fu Z, Chou SY: Nanoimprint mold fabrication and replication by room-temperature conformal chemical vapor deposition. *Applied Physics Letters* 90(20), 203115 (2007).

63.   Hendricks NR, Carter KR: *7.13 - Nanoimprint Lithography of Polymers*. In: *Polymer Science: A Comprehensive Reference*, Editors-in-Chief: Krzysztof M,Martin M (Ed.^(Eds). Elsevier, Amsterdam 251-274 (2012).

64.   Lan H, Ding Y, Liu H: Nanoimprint Lithography: Principles, Processes and Materials. Nova Science Publishers, Incorporated, (2011).

65.   Hocheng H, Nien CC: A review of monitoring for nanoimprinting. *Journal of achievments in Materials and Manfacturing Engineering* 24(1), (2007).

66.   Maltabes JG, Mackay RS: Current overview of commercially available imprint templates and directions for future development. *Microelectronic Engineering* 83(4–9), 933-935 (2006).

67.   Heo J-C, Kim K-S, Kim K-W: A simple and novel method for the evaluation of adhesion properties between UV curable resin and stamp in UV-nanoimprint lithography (UV-NIL). *Microelectronic Engineering* 98(0), 64-69 (2012).

68.   Kim K-S, Kang J-H, Choi D-G, Kim K-W: Characterization of adhesion property between fused silica and thermoplastic polymer film in thermal nanoimprint lithography using a novel pull-off test. *Microelectronic Engineering* 88(6), 855-860 (2011).

69. Amirsadeghi A, Lee JJ, Park S: Surface adhesion and demolding force dependence on resist composition in ultraviolet nanoimprint lithography. *Applied Surface Science* 258(3), 1272-1278 (2011).

70. Taniguchi J, Kamiya Y, Ohsaki T, Sakai N: Technique for transfer of high-density, high-aspect-ratio nanoscale patterns in UV nanoimprint lithography and measurement of the release force. *Microelectronic Engineering* 87(5–8), 859-863 (2010).

71. Colburn M: Development and advantages of step-and-flash lithography. *Solid State Technology*, 44 (2001).

72. Bailey T, Choi BJ, Colburn M *et al.*: Step and flash imprint lithography: Template surface treatment and defect analysis. *Journal of Vacuum Science & Technology* 18, 3572-3577 (2000).

73. Cardinale GF, Talin AA: Programmable imprint lithography template US 7128559 B1. (US7128559 B1), (2006).

74. Glangchai LC, Caldorera-Moore M, Shi L, Roy K: Nanoimprint lithography based fabrication of shape-specific, enzymatically-triggered smart nanoparticles. *Journal of Controlled Release* 125(3), 263-272 (2008).

75. Gao H, Tan H, Zhang W, Morton K, Chou SY: Air Cushion Press for Excellent Uniformity, High Yield, and Fast Nanoimprint Across a 100 mm Field. *Nano Letters* 6(11), 2438-2441 (2006).

76. Kostovski G, White DJ, Mitchell A, Austin MW, Stoddart PR: Nanoimprinted optical fibres: Biotemplated nanostructures for SERS sensing. *Biosensors and Bioelectronics* 24(5), 1531-1535 (2009).

77. Jung GY, Ganapathiappan S, Li X *et al.*: Fabrication of molecular-electronic circuits by nanoimprint lithography at low temperatures and pressures. *Applied Physics A* 78(8), 1169-1173 (2004).

78. Kumar G, Tang HX, Schroers J: Nanomoulding with amorphous metals. *Nature* 457(7231), 868-872 (2009).

79.   Landis S, Chaix N, Gourgon C, Perret C, Leveder T: Stamp design effect on 100 nm feature size for 8 inch NanoImprint lithography. *Nanotechnology* 17(10), 2701-2709 (2006).

80.   Scheer HC, Schulz H: A contribution to the flow behaviour of thin polymer films during hot embossing lithography. *Microelectronic Engineering* 56(3–4), 311-332 (2001).

81.   Cao H, Tegenfeldt JO, Austin RH, Chou SY: Gradient nanostructures for interfacing microfluidics and nanofluidics. *Applied Physics Letters* 81(16), 3058-3060 (2002).

82.   Cao H, Yu Z, Wang J *et al.*: Fabrication of 10 nm enclosed nanofluidic channels. *Applied Physics Letters* 81(1), 174-176 (2002).

83.   Khang D-Y, Lee HH: Sub-100 nm Patterning with an Amorphous Fluoropolymer Mold. *Langmuir* 20(6), 2445-2448 (2004).

84.   Haatainen T, Ahopelto J: Pattern Transfer using Step&Stamp Imprint Lithography. *Phys. Scr* 67, 357 (2003).

85.   Haatainen T, Mäkelä T, Schleunitz A, Grenci G, Tormen M: Integration of rotated 3-D structures into pre-patterned PMMA substrate using step & stamp nanoimprint lithography. *Microelectronic Engineering* 98(0), 180-183 (2012).

86.   Haatainen T, Majander P, Riekkinen T, Ahopelto J: Nickel stamp fabrication using step & stamp imprint lithography. *Microelectronic Engineering* 83(4-9 SPEC. ISS.), 948-950 (2006).

87.   Haatainen T, Mäkelä T, Ahopelto J, Kawaguchi Y: Imprinted polymer stamps for UV-NIL. *Microelectronic Engineering* 86(11), 2293-2296 (2009).

88.   Beck M, Graczyk M, Maximov I *et al.*: Improving stamps for 10 nm level wafer scale nanoimprint lithography. *Microelectronic Engineering* 61–62(0), 441-448 (2002).

89.   Lee H, Jung G-Y: Wafer to wafer nano-imprinting lithography with monomer based thermally curable resin. *Microelectronic Engineering* 77(2), 168-174 (2005).

90.   Lee H, Jung G-Y: Full wafer scale near zero residual nano-imprinting lithography using UV curable monomer solution. *Microelectronic Engineering* 77(1), 42-47 (2005).

91.   Hsu KH, Schultz PL, Ferreira PM, Fang NX: Electrochemical Nanoimprinting with Solid-State Superionic Stamps. *Nano Letters* 7(2), 446-451 (2007).

92.   Ahn SH, Guo LJ: Large-Area Roll-to-Roll and Roll-to-Plate Nanoimprint Lithography: A Step toward High-Throughput Application of Continuous Nanoimprinting. *ACS Nano* 3(8), 2304-2310 (2009).

93.   Ahn S, Cha J, Myung H, Kim S-M, Kang S: Continuous ultraviolet roll nanoimprinting process for replicating large-scale nano- and micropatterns. *Applied Physics Letters* 89(21), 213101 (2006).

94.   Bao L-R, Cheng X, Huang XD, Guo LJ, Pang SW, Yee AF: Nanoimprinting over topography and multilayer three-dimensional printing. *J. Vacuum Sci. and Technol.* 20(6), 2881-2886 (2002).

95.   Heyderman LJ, Schift H, David C, Gobrecht J, Schweizer T: Flow behaviour of thin polymer films used for hot embossing lithography. *Microelectronic Engineering* (54), 229–245 (2000).

96.   Scheer H-C, Schulz H, Hoffmann T, Torres CMS: Problems of the nanoimprinting technique for nanometer scale pattern definition. *J. Vac. Sci. Technol.* 16(6), 3917-3921 (1998).

97.   Gottschalch F, Hoffmann T, Sotomayor Torres CM, Schulz H, Scheer H-C: Polymer issues in nanoimprinting technique. *Solid-State Electronics* 43(6), 1079-1083 (1999).

98.   Hu W, Yang B, Peng C, Pang SW: Three-dimensional SU-8 structures by reversal UV imprint. *Journal of Vacuum Science & Technology B: Microelectronics and Nanometer Structures* 24(5), 2225-2229 (2006).

99.   Borzenko T, Tormen M, Hock V, Liu J, Schmidt G, Molenkamp LW: Imprint with sharp tip stamps. *Microelectronic Engineering* 57–58(0), 389-396 (2001).

100.   Borzenko T, Tormen M, Schmidt G, Molenkamp LW, .Janssen H: Polymer bonding process for nanolithography. *Applied Physics Letters* 79(14), 2246-2248 (2001).

101.   Torres CMS: Alternative Lithography: Unleashing the Potentials of Nanotechnology. (2003).

102. Hu J, Shi J, Zhang F *et al.*: High resolution and hybrid patterning for single cell attachment. *Microelectronic Engineering* 87(5–8), 726-729 (2010).

103. Ahn S, Choi J, Kim E *et al.*: Combined laser interference and photolithography patterning of a hybrid mask mold for nanoimprint lithography. *J Nanosci Nanotechnol* 11(7), 6039-6043 (2011).

104. Lee J-W, Lee K-B, Jeon H-S, Park H-K: Effects of Surface Nano-Topography on Human Osteoblast Filopodia. *Analytical Sciences* 27(4), 369-369 (2011).

105. Rajput D, Crowder SW, Hofmeister L, Costa L, Sung H-J, Hofmeister W: Cell interaction study method using novel 3D silica nanoneedle gradient arrays. *Colloids and Surfaces B: Biointerfaces* 102(0), 111-116 (2013).

106. Hu W, Crouch AS, Miller D, Aryal M, Luebke KJ: Inhibited cell spreading on polystyrene nanopillars fabricated by nanoimprinting and in situ elongation. *Nanotechnology* 21(38), 385301 (2010).

107. Xie C, Hanson L, Xie W, Lin Z, Cui B, Cui Y: Noninvasive neuron pinning with nanopillar arrays. *Nano Lett* 10(10), 4020-4024 (2010).

108. Loesberg WA, Te Riet J, Van Delft FCMJM *et al.*: The threshold at which substrate nanogroove dimensions may influence fibroblast alignment and adhesion. *Biomaterials* 28(27), 3944-3951 (2007).

109. Chalut KJ, Kulangara K, Giacomelli MG, Wax A, Leong KW: Deformation of stem cell nuclei by nanotopographical cues. *Soft Matter* 6(8), 1675-1681 (2010).

110. Johansson F, Carlberg P, Danielsen N, Montelius L, Kanje M: Axonal outgrowth on nano-imprinted patterns. *Biomaterials* 27(8), 1251-1258 (2006).

111. Crouch AS, Miller D, Luebke KJ, Hu W: Correlation of anisotropic cell behaviors with topographic aspect ratio. *Biomaterials* 30(8), 1560-1567 (2009).

112. Baranes K, Kollmar D, Chejanovsky N, Sharoni A, Shefi O: Interactions of neurons with topographic nano cues affect branching morphology mimicking neuron-neuron interactions. *J Mol Histol* 43(4), 437-447 (2012).

113. Ereifej ES, Matthew HW, Newaz G *et al.*: Nanopatterning effects on astrocyte reactivity. *J Biomed Mater Res A* 101(6), 1743-1757 (2013).

114. Idota N, Tsukahara T, Sato K, Okano T, Kitamori T: The use of electron beam lithographic graft-polymerization on thermoresponsive polymers for regulating the directionality of cell attachment and detachment. *Biomaterials* 30(11), 2095-2101 (2009).

115. Morawski M, Brückner G, Jäger C, Seeger G, Matthews RT, Arendt T: Involvement of Perineuronal and Perisynaptic Extracellular Matrix in Alzheimer's Disease Neuropathology. *Brain Pathology* 22(4), 547-561 (2012).

116. Varga R, Eriksson M, Erdos MR *et al.*: Progressive vascular smooth muscle cell defects in a mouse model of Hutchinson–Gilford progeria syndrome. *Proceedings of the National Academy of Sciences of the United States of America* 103(9), 3250-3255 (2006).

117. Tonazzini I, Meucci S, Faraci P, Beltram F, Cecchini M: Neuronal differentiation on anisotropic substrates and the influence of nanotopographical noise on neurite contact guidance. *Biomaterials* 34(25), 6027-6036 (2013).

118. Andrea Cattoni JC, Dominique Decanini, Jian Shi and Anne-Marie Haghiri-Gosnet: Soft UV Nanoimprint Lithography: A Versatile Tool for Nanostructuration at the 20nm Scale, Recent Advances in Nanofabrication Techniques and Applications. (2011).

119. Perl A, Reinhoudt DN, Huskens J: Microcontact Printing: Limitations and Achievements. *Advanced Materials* 21(22), 2257-2268 (2009).

120. Hui CY, Jagota A, Lin YY, Kramer EJ: Constraints on Microcontact Printing Imposed by Stamp Deformation. *Langmuir* 18(4), 1394-1407 (2002).

121. Bietsch A, Michel B: Conformal contact and pattern stability of stamps used for soft lithography. *Journal of Applied Physics* 88(7), 4310-4318 (2000).

122. Abidian MR, Kim DH, Martin DC: Conducting-Polymer Nanotubes for Controlled Drug Release. *Advanced Materials* 18(4), 405-409 (2006).

123. Liang L, Liu J, Windisch JCF, Exarhos GJ, Lin Y: Direct Assembly of Large Arrays of Oriented Conducting Polymer Nanowires. *Angewandte Chemie International Edition* 41(19), 3665-3668 (2002).

124. Tennant DM, Bleier AR: *4.02 - Electron Beam Lithography of Nanostructures*. In: *Comprehensive Nanoscience and Technology*, Editors-in-Chief: david LA,Gregory DS,Gary PW (Ed.^(Eds). Academic Press, Amsterdam 35-62 (2011).

125. Lee TW, Mitrofanov O, Hsu JWP: Pattern-Transfer Fidelity in Soft Lithography: The Role of Pattern Density and Aspect Ratio. *Advanced Functional Materials* 15(10), 1683-1688 (2005).

126. Suh KY, Kim YS, Lee HH: Capillary Force Lithography. *Advanced Materials* 13(18), 1386-1389 (2001).

127. Suh KY, Jeong HE, Kim D-H, Singh RA, Yoon E-S: Capillarity-assisted fabrication of nanostructures using a less permeable mold for nanotribological applications. *Journal of Applied Physics* 100(3), 034303 (2006).

128. Kim M, Kim YS: Advancing Decal-Transfer Lithography with a Reusable PDMS-Coated Nanoscale Stamp. *Journal of the American Chemical Society* 129(37), 11304-11305 (2007).

129. Biswas A, Bayer IS, Biris AS, Wang T, Dervishi E, Faupel F: Advances in top-down and bottom-up surface nanofabrication: techniques, applications & future prospects. *Adv Colloid Interface Sci* 170(1-2), 2-27 (2012).

130. Betancourt T, Brannon-Peppas L: Micro- and nanofabrication methods in nanotechnological medical and pharmaceutical devices. *Int J Nanomedicine* 1(4), 483-495 (2006).

131. Han KS, Hong SH, Kim KI, Cho JY, Choi KW, Lee H: Fabrication of 3D nano-structures using reverse imprint lithography. *Nanotechnology* 24(4), 045304 (2013).

132. Bao LR, Cheng X, Huang XD, Guo LJ, Pang SW, Yee AF: Nanoimprinting over topography and multilayer three-dimensional printing. *J. Vacuum Sci. and Technol.* 20, 2881-2886 (2002).

133. Yew SY, Kustandi TS, Low HY, Teng JH, Liu YJ, Leong ESP: Single-material-based multilayered nanostructures fabrication via reverse thermal nanoimprinting. *Microelectronic Engineering* 88(9), 2946-2950 (2011).

134. Jang KJ, Kim MS, Feltrin D, Jeon NL, Suh KY, Pertz O: Two distinct filopodia populations at the growth cone allow to sense nanotopographical extracellular matrix cues to guide neurite outgrowth. *PLoS One* 5(12), e15966 (2010).

135. Li M, Chen L, Chou SY: Direct three-dimensional patterning using nanoimprint lithography. *Applied Physics Letters* 78(21), 3322-3324 (2001).

136. Taniguchi J, Iida M, Miyazawa T, Miyamoto I, Shinoda K: 3D imprint technology using substrate voltage change. *Applied Surface Science* 238(1-4 SPEC. ISS.), 324-330 (2004).

137. Unno N, Taniguchi J, Ide S *et al.*: Three-dimensional metal nanoimprint technique for electrode and electric probe. *J. Phys.: Conf. Ser.*, (2009).

138. Li W, Dimov S, Lalev G: Focused-ion-beam direct structuring of fused silica for fabrication of nano-imprinting templates. *Microelectronic Engineering* 84(5-8), 829-832 (2007).

139. Waid S, Wanzenboeck HD, Muehlberger M, Bertagnolli E: Optimization of 3D patterning by Ga implantation and reactive ion etching (RIE) for nanoimprint lithography (NIL) stamp fabrication. *Microelectronic Engineering* 97(0), 105-108 (2012).

140. Taniguchi J, Koga K, Kogo Y, Miyamoto I: Rapid and three-dimensional nanoimprint template fabrication technology using focused ion beam lithography. *Microelectronic Engineering* 83(4–9), 940-943 (2006).

141. Kettle J, Hoyle RT, Dimov S: Fabrication of Step-and-Flash Imprint Lithography (S-FIL) templates using XeF2 enhanced focused ion-beam etching. *Applied Physics A* 96(4), 819-825 (2009).

142. Wanzenboeck HD, Waid S, Bertagnolli E, Muehlberger M, Bergmair I, Schoeftner R: Nanoimprint lithography stamp modification utilizing focused ion beams. *J. Vac. Sci. Technol.* 27(6), 2679-2685 (2009).

143. Zhang W, Han L-H, Chen S: Integrated Two-Photon Polymerization With Nanoimprinting for Direct Digital Nanomanufacturing. *Journal of Manufacturing Science and Engineering* 132(3), 030907 (2010).

144. Abaddi MA, Sasso L, Dimaki M, Svendsen WE: Fabrication of 3D nano/microelectrodes via two-photon-polymerization. *Microelectronic Engineering* 98(0), 378-381 (2012).

145. Piaszenski G, Barth U, Rudzinski A *et al.*: 3D structures for UV-NIL template fabrication with grayscale e-beam lithography. *Microelectronic Engineering* 84(5–8), 945-948 (2007).

146. Kurihara M, Abe M, Suzuki K *et al.*: 3D structural templates for UV-NIL fabricated with gray-scale lithography. *Microelectronic Engineering* 84(5–8), 999-1002 (2007).

147. Tavakkoli A, Ranjbar M, Piramanayagam SN *et al.*: Reverse Nanpimprint Lithography for Fabrication of Nanostructures *Nanoscience and Nanotechnology Letters* 4, 835-838 (2012).

148. Seyrek E, Decher G: *7.09 - Layer-by-Layer Assembly of Multifunctional Hybrid Materials and Nanoscale Devices*. In: *Polymer Science: A Comprehensive Reference*, Editors-in-Chief: Krzysztof M,Martin M (Ed.^(Eds). Elsevier, Amsterdam 159-185 (2012).

149. Kehagias N, Reboud V, Chansin G *et al.*: Submicron three-dimensional structures fabricated by reverse contact UV nanoimprint lithography. *J. Vac. Sci. Technol.* 24(6), 3002-3005 (2006).

150. Hu W, Yang B, Peng C, Pang SW: Three-dimensional SU-8 structures by reversal UV imprint. *J. Vac. Sci. Technol* B 24, (2006).

151. Kong YP, Low HY, Pang SW, Yee AF: Duo-mold imprinting of three-dimensional polymeric structures. *Journal of Vacuum Science & Technology B: Microelectronics and Nanometer Structures* 22(6), 3251-3256 (2004).

152. Hu W, Yim EK, Reano RM, Leong KW, Pang SW: Effects of nanoimprinted patterns in tissue-culture polystyrene on cell behavior. *J Vac Sci Technol A* 23(6), 2984-2989 (2005).

153. Yoshii Y, Waki A, Yoshida K *et al.*: The use of nanoimprinted scaffolds as 3D culture models to facilitate spontaneous tumor cell migration and well-regulated spheroid formation. *Biomaterials* 32(26), 6052-6058 (2011).

154. Nakajima M, Yoshikawa T, Sogo K, Hirai Y: Fabrication of multi-layered nano-channels by reversal imprint lithography. *Microelectronic Engineering* 83(4–9), 876-879 (2006).

155. Kehagias; N, Reboud; V, Chansin; G *et al.*: Reverse-contact UV nanoimprint lithography for multilayered structure fabrication. *Nanotechnology* 18(17), 1-4 (2007).

156. Liu Z, Bucknall DG, Allen MG: Inclined nanoimprinting lithography for 3D nanopatterning. *Nanotechnology 2* 22, (2011).

157. Kumar G, Tang HX, Schroers J: Nanomoulding with amorphous metals. *Nature* 457, 868-872 (2008).

158. Shevchenko EV, Talapin DV, Kotov NA, O'brien S, Murray CB: Structural diversity in binary nanoparticle superlattices. *Nature 439*, 55-59 (2005).

159. Dumond JJ, Low HY, Rodriguez I: Isolated, sealed nanofluidic channels formed by combinatorial-mould nanoimprint lithography. *Nanotechnology* 17(8), 1975-1980 (2006).

160. Hoff JD, Cheng LJ, Meyhöfer E, Guo LJ, Hunt AJ: Nanoscale protein patterning by imprint lithography. *Nano Letters* 4(5), 853-857 (2004).

161. Wang Y, Goh SH, Bi X, Yang K-L: Replication of DNA submicron patterns by combining nanoimprint lithography and contact printing. *Journal of Colloid and Interface Science* 333(1), 188-194 (2009).

162. Liang X, Morton KJ, Austin RH, Chou SY: Single sub-20 nm wide, centimeter-long nanofluidic channel fabricated by novel nanoimprint mold fabrication and direct imprinting. *Nano Letters* 7(12), 3774-3780 (2007).

163. Burridge K, Chrzanowska-Wodnicka M: FOCAL ADHESIONS, CONTRACTILITY, AND SIGNALING. *Annual Review of Cell and Developmental Biology* 12(1), 463-519 (1996).

164. Lauffenburger DA, Horwitz AF: Cell migration: a physically integrated molecular process. *Cell* 84(3), 359-369 (1996).

165. Geiger B, Bershadsky A, Pankov R, Yamada KM: Transmembrane crosstalk between the extracellular matrix--cytoskeleton crosstalk. *Nat Rev Mol Cell Biol* 2(11), 793-805 (2001).

166. Ruoslahti E, Pierschbacher MD: New perspectives in cell adhesion: RGD and integrins. *Science* 238(4826), 491-497 (1987).

167. Ruoslahti E, Pierschbacher MD: Arg-Gly-Asp: a versatile cell recognition signal. *Cell* 44(4), 517-518 (1986).

168. Schvartzman M, Palma M, Sable J *et al.*: Nanolithographic Control of the Spatial Organization of Cellular Adhesion Receptors at the Single-Molecule Level. *Nano Letters* 11(3), 1306-1312 (2011).

169. Huh D, Matthews BD, Mammoto A, Montoya-Zavala M, Hsin HY, Ingber DE: Reconstituting Organ-Level Lung Functions on a Chip. *Science* 328(5986), 1662-1668 (2010).

170. Nyga A, Loizidou M, Emberton M, Cheema U: A novel tissue engineered three-dimensional in vitro colorectal cancer model. *Acta Biomaterialia* 9(8), 7917-7926 (2013).

171. Cheng J-X: *Research on the bio-safety of nanomaterials*. In: *Computer Science and Network Technology (ICCSNT), 2011 International Conference on*. 2011.

172. Coutinho D, Costa P, Neves N, Gomes M, Reis R: *Micro- and Nanotechnology in Tissue Engineering*. In: *Tissue Engineering*, Pallua N,Suscheck CV (Ed.^(Eds). Springer Berlin Heidelberg, 3-29 (2011).

173. Gao H: *Application of fracture mechanics concepts to hierarchical biomechanics of bone and bone-like materials*. In: *Advances in Fracture Research*, Carpinteri A,Mai Y-W,Ritchie R (Ed.^(Eds). Springer Netherlands, 101-137 (2006).

174. Sciote JJ, Morris TJ: Skeletal Muscle Function and Fibre Types: the Relationship Between Occlusal Function and the Phenotype of Jaw-closing Muscles in Human. *Journal of Orthodontics* 27(1), 15-30 (2000).

175. Severs NJ: The cardiac muscle cell. *BioEssays* 22(2), 188-199 (2000).

ABSTRACT

OLIGOSPERMINES FOR NON-VIRAL SIRNA DELIVERY

by

MAHA ELSAYED

December, 2013

Advisor: Dr. Olivia M. Merkel

Major: Pharmaceutical Sciences

Degree: Master's of Science

In this thesis, delivery systems for siRNA delivery are introduced with special attention to non-viral vectors. Many successful vectors used in vivo were reviewed. Our work focused on the effect of different architectures of oligospermine polmers on their suitability for siRNA delivery in lung cancer cells. Different archituctures showed different polyplex structures and variable transfection efficiencies. Moreover, we presented a review on nanoimprint lithography techniques with an outlook on possible biological applications in the field of gene and drug delivery.

AUTOBIOGRAPHICAL STATEMENT

MAHA ELSAYED

Maha Elsayed obtained her BSc. in Pharmacy from Misr University for Science and Technology (Egypt) in 2007. She worked as a licensed pharmacist from 2007 to 2009. In 2011, she joined Wayne State University, Department of Pharmaceutical Sciences to pursue her studies as a Master's student. She worked in Dr. Olivia M. Merkel's lab in using non-viral vectors for siRNA delivery in lung cancer cells. She worked on many delivery systems, such as nanaoparticles, micelles and polyplexes. Her main project focused on the effect of different architecture of oligospermine on its suitability for siRNA delivery in lung cancer cells. She has four publications, of which three as a first author (two are accepted, and one in preparation). During her research in Wayne State University, Maha has earned Graduate Research Assistantship (GRA) from department of Pharmaceutical Sciences in addition to Graduate Professional Scholarship (declined) in 2011.